THE INFLUENCE OF SEX-DEPENDENT VASCULAR PROPERTIES ON AORTIC HEMODYNAMICS

A Dissertation
Presented to
The Academic Faculty

by

Elizabeth Iffrig

A dissertation submitted to the Faculty of
James T. Laney School of Graduate Studies of Emory University
and
School of Engineering of Georgia Institute of Technology
in partial fulfillment of the requirements for the degree of

Doctor of Philosophy in

Biomedical Engineering

Georgia Institute of Technology
and
Emory University
December 2016

THE INFLUENCE OF SEX-DEPENDENT VASCULAR PROPERTIES ON AORTIC HEMODYNAMICS

Approved by:

Dr. W. Robert Taylor, Co-Advisor
Department of Medicine
Emory University

Dr. Jay D. Humphrey
School of Engineering & Applied Sciences
Yale University

Dr. John N. Oshinski, Co-Advisor
Department of Radiology
Emory University

Dr. Gail Peters
Department of Radiology
Emory University

Dr. Ross Ethier
Wallace H. Coulter Department of Biomedical Engineering
Georgia Institute of Technology

Dr. Alessandro Veneziani
Department of Mathematics and Computer Science
Emory University

Date Approved: November 07 ,2016

To Justin and Andrew

ACKNOWLEDGEMENTS

There are many people who are responsible for the completion and success of this dissertation. There are a few, in particular, who warrant significant attention and consideration:

First, I need to thank my husband, Andrew, and my son, Justin for being so understanding all those times mom needed to work and everyone else needed to get out of the room. They kept me sane (mostly) through the end of this part of my journey and helped me get outside when I was spending too much time in the corner of the hospital basement. Additionally I'd like to thank my mom and dad for every time they took my phone calls and reassured me that life was as unfair as I felt it to be and that I was still doing a great job in spite of the injustices (which were mostly imagined).

Next, significant credit is due to my stellar advising duo, Bob Taylor and John Oshinski. I couldn't be more grateful for the immense amount of advice and assistance they've given me not just with regards to the project presented herein, but also with respect to my personal and professional development. Their style of mentorship and focus on research is one I hope to emulate in my own future career. I can't thank them enough for supporting all the ideas I've had over the last four years while letting me find my footing as a graduate student. I (and hopefully they) look forward to many years of my calling and asking for advice and guidance.

As Bob and John were both such great mentors, it was only inevitable that they would have more great people working in their labs, all of whom I owe an immense about of gratitude. Luke served as a third mentor in many ways and with only 3 inches of

a cubicle wall separating us I'm sure I took up more of his time than he realized when he so graciously offered to help me that first time. Ali was always readily available to offer career and life advice and has become one of many lifelong colleague friends I made during my graduate school career. I will probably continue to email Adrian with questions about how to improve my code and then pretend to dismiss his help with a snarky comment about how I would have figured it out on my own anyway. Between the two labs there are too many people to count and name individually but I want to extend my thanks to every lab member with whom I overlapped. Lab meetings, conference talk preparations, and general lunch time discussions are all appreciated for the contributions to the development and execution of this project.

I need to thank each of my committee members for the support they've provided me through committee update meetings and sacrifices of their personal time to advise my research. Dr. Peters helped me to recruit most of the patients enrolled in this study who came from her own practice. Dr. Veneziani had numerous beneficial insights into the fluid mechanics element of my project and was always immensely supportive of the project's focus. Dr. Ethier can be held directly responsible for the expansion of this project beyond the focus on hemodynamics to consider the potential differences in tissue mechanics. And Dr. Humphrey really challenged me to think critically about some of my methods, encouraging me to become a better researcher.

I was fortunate to have received an American Heart Association pre-doctoral fellowship to provide financial support during my time as a graduate student and to permit me to attend and present at numerous conferences. I also received a fellowship in

my final year from the Emory University Women's Club recognizing my research and contribution to the university.

I would be remiss in failing to mention the many medical and graduate student friends and real life friends who provided me with the laughter and occasional alcohol that is necessitated by graduate school. And because at least one of the following would be upset if they didn't make it into my acknowledgements personally, I need to thank Lisa, Dwight, Chelsea, Martha, and Shruthi for everything.

Without everyone mentioned above (and the many more who went unnamed), completion of this project would not have been possible. I will be eternally indebted to each and every one of them.

TABLE OF CONTENTS

LIST OF TABLES

LIST OF FIGURES

LIST OF SYMBOLS AND ABBREVIATIONS

AAA	Abdominal Aortic Aneurysm
AI	Augmentation Index
CVD	Cardiovascular Disease
DENSE	Displacement Encoded with Stimulated Echoes
DVT	Deep Vein Thrombosis
EVAR	Endovascular Aneurysm Repair
FOV	Field of View
ICAM	Intracellular Adhesion Molecule
MCP	Macrophage Chemotactic Protein
MMP	Matrix Metalloproteinases
NOS-3	Nitric Oxide Synthase-3
OSI	Oscillatory Shear Index
PAD	Peripheral Arterial Disease
PCMR	Phase Contrast Magnetic Resonance
PWV	Pulse Wave Velocity
QISS	Quiescent Interval Single Shot
ROS	Reactive Oxygen Species
RTK	Receptor Tyrosine Kindase
SNR	Signal to Noise Ratio
TE	Echo time
TGF-β	Transforming Growth Factor β
TR	Repetition time
VCAM-1	Vascular Cell Adhesion Molecule-1
Venc	Velocity Encoding Value

WSS	Wall Shear Stress

SUMMARY

Differences in the incidence and prognosis of abdominal aortic aneurysms between men and women remain unexplained and insufficiently explored. While men are 4-5 times more likely to develop the disease, women are more likely to experience complications. Currently, screening for abdominal aortic aneurysms in women is not recommended due to the low incidence of the disease. However it remains clear that some women do develop the disease and for those who do, the consequences can be dire. Identification of risk factors beyond those classically associated with aneurysm development could be critical in improving how we care for women. We recruited healthy men and women and used MRI to quantify abdominal aortic hemodynamics to assess if men are exposed to more pro-inflammatory wall shear stress than women. We evaluated innate vascular properties that we expected to both exert control over aortic hemodynamics and to be significant different between the sexes. With this work, we showed that men and women exhibit significant differences in the hemodynamics of the abdominal aorta with men experiencing a higher degree of oscillatory shear than women. This supports the theory that early exposure to pro-inflammatory shear in men may predispose them to developing aneurysms. Additionally, we demonstrated an increase in vascular curvature of the abdominal aorta in women which was associated with an increase in the range of oscillatory shear around the circumference of the vessel. In light of the increased risk for aneurysms in patients with above the knee amputations and spinal cord injuries, we assessed differences in peripheral resistance between the sexes as mediated by uterine artery flow and measured by internal iliac artery flow oscillations. To

do this, we recruited patients with uterine fibroids and hysterectomies whom we expected to have altered uterine artery resistance profiles. In comparison with out healthy cohort, two cohorts we showed that changes in uterine physiology in these two patient groups are significantly associated with changes in aortic wall shear stress. We also demonstrated that the presence and differences in uterine flow could be detected by differences in internal iliac flow and that these differences in flow. Finally, we measured displacement and strain in the aortic wall using MRI. We demonstrated that in both sexes there is a significant difference in the primary spherical direction of peak displacement around the circumference of the aorta. Further we showed that the heterogeneity in displacement direction creates a peak circumferential strain on the lateral walls of the vessel and that this strain was higher in women than in men.

In conclusion, this work shows that both aortic hemodynamics and vessel wall properties are different between men and women. These observations may underlie the differences in risk and prognosis of aortic aneurysms and thus provide a basis for potential risk factors to be included in the screening process.

CHAPTER 1

INTRODUCTION

1.1 Women and Cardiovascular Disease

1.1.1 Awareness and a Need for Research

The belief that women are protected from cardiovascular disease (CVD) is no longer maintained in the face of statistics showing that heart disease is currently the most common cause of death among women in the United States.[1, 2]As early as 1997, only1 in 3 women in the US were aware that heart disease was the leading cause of death for their sex and the need for a campaign to increase awareness was launched by the American Heart Association and other organizations including the National Heart, Lung and Blood Institute and the Department of Health and Human Services.[3] In 2012, after 15 years of implementation, a study revealed that 50% of women over the age of 65 still did not know that heart disease was the leading cause of death for women.[4] These numbers make it readily apparent that more attention must be paid to understanding the specifics of CVD in women, particular what factors put women at risk and which protect them. At a 2010 symposium to discuss sex differences in CVD, it was universally acknowledged that there still was insufficient research dedicated to understanding the differences in how men and women develop and respond to CVD.[5]

As with many other differences in disease between men and women, hormonal control is a plausible hypothesis. Given the many transcriptional elements regulated by estrogen in the cardiovascular system, the hypothesis that estrogen is cardio-protective for women prior to menopause is worth considering.[6] However, attempts to align

estrogen levels with cardiovascular disease risk have been unsuccessful[7]. More importantly, the administration of estrogen to women following menopause fails to offer significant cardiovascular protection.[8, 9] Some studies have also demonstrated a potential additional risk with exogenous estrogen exposure following menopause, although there have been suggestions in the literature that the timing of hormone replacement therapy (HRT) must be optimized in order for it to be effective.[10] However, this remains an open question and should not be discounted when considering the biological differences in men and women and how they contribute to the risk of cardiovascular disease.

1.1.2 Abdominal Aortic Aneurysms

One cardiovascular disease in particular, abdominal aortic aneurysm (AAA), shows a substantial dichotomy in incidence between the sexes that has not yet been sufficiently explained. There is a significantly higher incidence of AAA in men when compared with women, with studies estimating an prevalence ratio of four to five times.[11] Despite the predilection for disease development in men, the outcomes are worse for women.[12] Even with "optimal" therapy, women with an AAA exhibit a higher mortality rate following both open and endovascular repair procedures.[13] While the reason for these differences in mortality is unclear, different screening protocols for women may contribute to the problem.[14, 15] The U.S. Preventative Services Task Force recommends against routine screening for AAA in women due to the low incidence.[16] It is possible that when women are diagnosed (a diagnosis based solely on size), it is too late in the disease process and the recommended interventions are insufficient. Additionally, many of the trials performed to assess the efficacy of surgical intervention enroll primarily men and thus may not be applicable to a larger female cohort.[17]

Regardless, it is clear that some women do develop AAA and those women are at higher risk for mortality in the overall AAA population. Thus it is necessary to understand why women (as a population) are at lower risk than men and potentially identify which subpopulations of women are at higher risk based as a result of currently unidentified factors. [18] Given that the role of estrogen protection from cardiovascular disease in the pre-menopausal state has been inconclusive in large scale trials, identification of female-specific risk factors could improve care and mortality of women with AAA. [19, 20] There exists, however, computational evidence that the higher incidence of rupture and mortality experienced by women could be resultant from biomechanical forces. [21]. In light of this, there is strong motivation to explore the question of pathology from a sex-dependent mechanical perspective as well.

Identifying populations of women who are at increased risk for developing AAA could provide significant improvement in how we screen women. Smoking and family history are among the top risk factors for women with AAA, similar to many other cardiovascular diseases.[12] Little work has been done, however, to look at what sex-specific properties may contribute to the increased predilection of AAA for men. One study evaluated the role of pregnancy in risk of AAA, comparing parous women with nulligravida women. The authors of that study showed that women with a history inclusive of pregnancy were at a reduced risk for developing AAA when compared with women without a prior pregnancy.[22] While the authors of this study contributed the effects to the levels of estrogen, they neglected to discuss the dramatic changes in cardiovascular biomechanics that occur with pregnancy which include a reduction in total peripheral resistance, an increase in cardiac output and an increase in uterine flow.[23] Given the lack of association demonstrated between estrogen levels and the risk of cardiovascular disease, differences in estrogen may not explain the reduction in risk as a due to pregnancy.

Thus, we believe that the role of biomechanics in the development of AAA as it relates to the differences in disease incidence between men and women is overlooked and worth further examination.

1.2 Cardiovascular Biomechanics

With the cyclical contraction of the heart to move blood into both the systemic and pulmonary circulation, there comes repeated loading of vessel walls. There are many different forces which develop in this process both from the movement of fluid and the response of the vessel tissue.[24] These biomechanical forces are known to influence vascular morphology and function in development, healthy homeostasis, and disease pathology.[25-28] Recently, researchers have begun to better understand the biological signaling pathways that sense these forces and the induction of cellular processes that can eventually result in disease.[26, 29-31] As a result, biomechanics are becoming a new avenue for quantifying CVD risk that may complement serum biomarkers and lifestyle risk factors already in use. .

1.2.1 Fluid Mechanics

As the blood passes over the endothelial surface of the vessel wall, a shearing stress is created as a result of the fluid's viscosity. One avenue of shear stress sensing is through receptor bound mechano-transducing proteins, ion channels, and structural proteins on the cell and activates intracellular pathways that influence cellular physiology as described in depth in Section 1.3.1.[32, 33] This shear stress is a product of the fluid's viscosity and the gradient of the velocity at the wall in the direction of the lumen's center. In the vascular system, a no-slip boundary condition is assumed so that at the exact location of the wall the velocity of the blood is zero. A large wall shear stress (WSS) results when there is a large gradient in the velocity from the wall towards the center of the vessel. In addition to its magnitude, the shear stress vector also has a direction. The

direction of the shear stress is in the direction of the velocity vector at the point closest to the wall, and can be in any direction orthogonal to the normal face of the vessel wall. As mentioned previously, the cyclical nature of the cardiac cycle means that the WSS vector changes both in magnitude and direction as a function of time and there are many important biological implications of how these changes affect cellular structure. [34, 35]

It was not until the 1980s that the currently accepted theory regarding low and oscillatory WSS was proposed.[36] This theory, backed by numerous in vivo and in vitro experiments and studies, states that regions of the vascular system which experience low and oscillatory wall shear stress are sites of inflammation and are at risk to develop early atherosclerotic/inflammatory vascular disease.[37-39] However this theory is challenged by conflicting evidence showing from a literature review that the association between low and oscillatory wall shear stress is not always consistent with vascular pathology changes.[40] Regardless, it is clear that the directionality and magnitude of WSS influences cellular physiology and further assessment of its role in disease development is an important direction of cardiovascular research.

1.2.2 Solid Mechanics

In addition to the shearing stress exerted by the velocity gradient of the liquid at the wall, the loading of the vessel produces both a stress (a force distributed over a deformed area) and an associated strain (change in the length of tissue in reference to an earlier time point in the cardiac cycle).[24] Each of these measurements largely depends on the specific amounts and orientations of the primary load-bearing constituents of the vessel wall, elastin and collagen, and thus will vary at all points along, around, and through the vessel wall.[41-43] In the same way that the endothelial cells are capable of responding to shear stress through mechano-transducing cellular elements (see Section 1.3.1), the vessel wall can remodel in response to these loads.[44-46] Mostly these changes result in the re-orientation, production, and degradation of collagen and elastin.

In the case of vascular disease, this remodeling becomes pathological with excessive collagen production or elastin breakdown creating an asymmetry in the vessel wall's material properties and strength.[47] In the case of AAA, this ability to remodel appropriately is thought to fail and sections of the wall begin to dilate pathologically because the components of the vessel wall can no longer withstand the imposed loads.

Much of the work to date to quantify these stresses or strains in vessels is done ex vivo where the tissue can measured both in a completely unloaded state and then under a variety of loaded conditions.[48, 49] In the human body, however, it is not possible to measure the vessel in a truly non-loaded (or even non-stressed) state. Consequently, we can only calculate stress or strain in reference to another earlier point in the cardiac cycle. Both stress and strain are important in disease progression. Differences among healthy populations, however, have not been extensively explored, due in part to the difficulty of in vivo measurements. With the advancement of solid tissue imaging in MRI, it is possible to begin to characterize the tissue properties of the vascular wall in vivo.[50-53] This creates an opportunity to measure "normal" ranges for these parameters and to identify potential differences between groups of healthy subjects. For example, little work has been done to assess if these normal ranges differ among men and women. It is possible that the differences in risk for cardiovascular disease processes could be partially explained by differences in the underlying solid mechanics of the vessel between the sexes.

1.3 Wall Shear Stress on the Vascular Wall

1.3.1 Influence on Endothelial Cells

As described previously, WSS represents the force exerted on the vascular wall as viscous blood passes over it. Responses to this shearing stress are mediated through membrane-bound proteins known as mechanotransducers , ion channels and chemical

gradients in addition to the cell's cytoskeleton. The moving fluid induces conformational changes in protein structure of these mechanotransducers or increased flow of ions and substrates across the cell membrane. Among these proteins are integrins (activated upon immediate exposure to a shear stress), receptor tyrosine kinases, ion channels (which affect membrane permeability), and PECAM-1. The cell membrane itself has been shown to change its diffusion coefficient when exposed to normal physiological variations of WSS.[29, 30, 32, 33, 35, 54] Response by the cytoskeleton to shear stress is explored in the theory of tensegrity.[55] This theory describes how these extracellular forces change the shape of the cellular skeleton at an elemental level, similarly altering genetic expression and intracellular signaling pathways.

The cell responds to these forces through activation of intracellular signaling pathways so that changes in flow-responsive gene expression that regulate vascular health are induced. For example, Nitric Oxide Synthase-3 (NOS-3) is activated in response to arterial flow and induces vasodilation. This is important because a key marker of declining vascular health is endothelial dysfunction, the inability to dilate in response to changes in flow.[56-59] Genes involved in the thrombotic pathway, including thrombomodulin and tissue plasminogen activator, have also been demonstrated to be flow sensitive. In the event of low flow, these thrombotic genes are upregulated, which explains the development of deep vein thromboses (DVTs) in the lower extremities in the presence of homeostasis. Perhaps most importantly are the genetic targets which are recruited in inflammatory processes such as vascular cell adhesion molecule-1 (VCAM-1), intracellular adhesion molecule-1 (ICAM-1), transforming growth factor β (TGF-β), and macrophage chemotactic protein-1 (MCP-1).[60] All of these inflammatory genes are upregulated at sites of disturbed flow in which the WSS vector is oscillatory rather than steady and unidirectional. It is the influence of these genes that are most interesting when discussing the role of WSS in the development of cardiovascular disease. Indeed, sites of

high oscillatory shear stress coincide with sites of early and advance atherosclerotic disease such as the carotid artery, the coronary arteries, and the abdominal aorta.[61]

1.3.2 Relationship of WSS to the Development of Vascular Disease

While the endothelium is the site of the force reception and mechanotransduction, the other layers of the vessel wall are also responsive to the forces. As mentioned above, in sites of disturbed wall shear stress there is a higher expression of pro-inflammatory genes. A net result of this is an increase in the production of reactive oxygen species (ROS) which exceed the endogenous ability of the vascular wall to quench them.[62] These ROS are capable of acting as signaling molecules affecting changes in the expression of genes or levels of protein that regulate cellular health and function.[63] This oxidative environment leads to oxidized DNA, proteins, and lipids and cellular damage, thus recruiting more pro-inflammatory cell types. In the smooth muscle, the presence of low WSS has been shown to stimulate migration resulting in neo-intima formation, another hallmark of early vascular disease.[64] While the migration of smooth muscle can lead to an increase in the wall's volume, there is a concurrent upregulation of matrix metalloproteinases which result in extracellular matrix degradation.[65, 66] This produces a heterogeneous effect around the circumference of growth and remodeling. An increased deposit of oxidized lipid content as a result of the pro-inflammatory, high oxidative stress environment changes the diffusion constant of the cellular membranes which leads to more changes in the makeup of the vessel wall.[67] Depending upon the extent of each of these transformations, the region of blood vessel can go on to develop a number of different pathological morphologies including a stable plaque phenotype with increasing intraluminal remodeling and subsequent narrowing, a vulnerable plaque which is at risk for rupture or erosion and thrombosis, or (of particular interest to the project at hand) aneurysmal formation in which the heterogeneous remodeling of the site leads to an eventual dangerous dilation of the vessel with the potential for rupture.

1.4 Abdominal Aortic Aneurysms

1.4.1 Pathology and Pathogenesis

Like most other cardiovascular disease, the development of an abdominal aortic aneurysm (AAA) is multifactorial with contributions from genetics, anatomical variations, mechanics, biochemistry, and lifestyle choices.[68] Unlike other atherosclerotic-based diseases, however, AAA have uniquely specific risk factor profiles with smoking being very highly correlated and diabetes being protective against AAA.[69] In the end, an aneurysm develops most commonly in the infrarenal supra-iliac aorta rather than in the suprarenal aorta. Because we are concerned with the initiation of AAA in this study, a relevant difference between these two regions is the existence of a triphasic waveform in the abdominal aorta in which there is caudal (forward) flow in systole, cranial (reverse) flow in early diastole, and caudal flow again in late diastole and only biphasic flow in the suprarenal aorta.[70] This increase in flow reversal creates in an increase in oscillatory shear, which we expect to elevate vascular inflammation, in the abdominal aorta compared with the suprarenal aorta. To bolster this proposed relationship, observations in AAA murine models show that the aneurysm co-localizes with the highest sites of oscillatory flow in the suprarenal aorta rather than the infrarenal aorta as it is in humans.[71] Thus in two organisms, aortic aneurysms form preferentially at sites where WSS oscillation is high prior to disease onset.

As the disease progresses, the vessel becomes unable to maintain a physiologically normal diameter due to changes in its mechanical properties, mostly in the content of the wall's elastin, collagen and smooth muscle.[72-75] Hypertension has a correlation with the development of an aneurysm and it can be hypothesized that stresses resulting from the cyclically high blood pressure may induce further degradation of the vessel wall and pathological remodeling of the wall. A hallmark of the abdominal aortic aneurysm is the destruction the medial layer organizatoin eventually leading to medial

necrosis.[75-77]. It has been demonstrated that MMP activity is significantly elevated in the wall of aneurysms when compared with non-diseased aortas.[77] Combined with proteinase activity of matrix metalloproteinases (MMPs) acting to degrade both elastin and collagen, this process results in a weakening of the wall as these are the primary load bearing constituents. Ultimately, it is this focal weakening that leads to the pathological dilatation and potentially to the rupture of the abdominal aorta.

1.4.2 Epidemiology

As the development of AAA is slow and insidious, the primary affected populations are those in their 60s and 70s (or in the case of women, their 70s and 80s). The estimated prevalence of this disease is between 1.3 and 8.9% in men and 1.0 and 2.2% in women.[12, 78] As a whole, white men aged 55 and older with a history significant for smoking are at a higher risk than their female, younger, smoke-free counterparts.[79] As discussed previously in section 1.1, women seem to be protected from developing the disease and the majority are not diagnosed until approximately a decade later in life than men.[17] Overall, smoking is the strongest independent risk factor with 90% of aneurysmal patients having a history of cigarette use. In addition to age, a history of smoking, and sex, other notable risk factors include family history of aneurysm, and hyperlidemia (though hyperlidemia is much less associated with AAA than it is with other cardiovascular disease).[80-82] Because the disease is asymptomatic for many patients, often an aneurysm diagnosis is made incidentally on unrelated imaging studies. Screening for the disease is recommended for men aged 65 to 75 who have ever smoked and is recommended on a case by case basis (in evaluation of additional risk factors) for men aged 65 to 75 who have never smoked.[16, 18, 68] However, some studies suggest that screening based on aortic diameter is not the most effective method of identifying aneurysms at risk for rupture and requiring intervention.[83]

1.4.3 Treatment and Prognosis

While potential molecular targets have been identified to prevent the progression of the disease, there is no current recommended medical therapy to control AAA. This field is active, and many are looking at protease inhibitors such as doxycycline to slow the rate of growth. However recent negative results raise questions surrounding the utility of this drug therapeutically.[84, 85] Lifestyle modifications, particularly smoking cessation and hypertension control, are recommended to curb the growth of the aneurysm after diagnosis, while regular imaging is used to track the growth rate. The only available interventions are open surgical repair and endovascular stent placement. There have been numerous trials to assess the utility of open repair vs endovascular repair in either elective or recommended surgery groups stratified by aortic size. [86-89] The current recommendations for AAA endovascular intervention in the United States are when the aneurysm exceeds 5.5 cm or becomes painful and symptomatic. Surgical intervention has not been shown to be beneficial in men whose aneurysms measure less than 5.0 cm or in women with aneurysms less than 4.5 cm.

1.5 The Role of Innate Vascular Properties in Controlling Hemodynamics

There are many potential intrinsic vascular properties that contribute to differences in the WSS profile of a vessel. In this study, we limited out focus to three specific properties that we expected to: 1) exhibit significant influence in the abdominal aorta and 2) be different between men and women. Specifcally,we elected to look at vessel radius and curvature, peripheral flow profiles, and vessel displacement and strain.

1.5.1 Geometry

The primary sites of atherosclerosis development are regions of disturbed flow as described previously. These sites of disturbed flow often coincide with changes in the cross sectional area of the vessel or in the vessel trajectory, and sites of bifurcations.[90] This is particularly true in the peripheral vascular system at the site of the aortic bifurcation into the left and right common iliac arteries.[91, 92]

With respect to the influence of cross sectional area, the carotid artery bulb is a common site of atherosclerosis because of the change in cross sectional area between the common carotid artery and the internal carotid artery. This change induces vortical flow patterns and high shear stress oscillations on the outer wall of the carotid bulb.[39, 93, 94] This location coincides with early intimal-medial thickening that, in the face of progressive atherosclerosis, can eventually lead to occlusion and necessitate intervention.[95] Beyond just area changes, the radius of a vessel plays a significant role in the wall shear stress. In cases of equivalent flow conditions, the wall shear stress will be inversely proportional to the cube of the vessel radius.

In addition to vessel size, the changes in vessel trajectory, measured by both curvature and torsion, play a very important role in how the wall shear stress profile develops around the circumference. In the aortic arch, the primary site of early atherosclerotic disease is on the inner curvature on the vessel.[96] The curvature experiences a lower time averaged wall shear stress when compared with the outer curvature as well as more oscillations. Similarly in the abdominal aorta, computational studies have indicated that the highest levels of oscillatory shear occur on the posterior of the vessel. This coincides with the greatest degree of intimal medial thickness as well as the inner curvature of the vessel. [71, 97, 98]

1.5.2 Peripheral Resistance

Compared with the general population, patients with above the knee amputation carry a 9 fold increased risk of developing an abdominal aortic aneurysm even when analysis controls for all other primary risk factors.[99] The pathophysiological mechanism for this has not been well elucidated. However, studies in humans in which an amputation is simulated (via inflation of a blood pressure cuff to well above systolic blood pressure) show that there is a consequential increase in the extent of oscillatory flow, and thus oscillatory shear, upstream in the abdominal aorta.[100]

Additionally, patients who are diagnosed with peripheral arterial disease show a higher susceptibility to developing AAA relative to other cardiovascular disease.[101, 102] While this has not been shown mechanistically, it is possible that the increased impedance of the peripheral arterial system as a result of vascular disease might affect aortic hemodynamics in a similar manner as the amputee population. Similarly spinal cord injuries which are known to decrease distal aortic flow and promote low and oscillatory shear conditions in the aorta also are independently associated with AAA.[103, 104] Given the elevated risk of AAA in these conditions that are known to limit or decrease peripheral flow, it is important to evaluate the role of peripheral resistance in controlling aortic hemodynamics in men and women.

In considering the differences in peripheral resistance as they pertain to men and women, the pelvic anatomy represents the biggest divergence in structures between the sexes in the periphery. Interestingly, the uterine arteries (branches of the internal iliac arteries which supply pelvic blood flow) in women is the one of the only peripheral vessels that does not exhibit flow reversal under normal physiological conditions and also has a very high flow rate per gram of tissue.[105, 106] In this way, it is possible that differences in the resistance or impedance of this artery, as a result of pathological conditions or surgical interventions, may mediate changes in aortic hemodynamics profile in women.

1.5.3 Tissue Mechanics

The relationship between the mechanical properties of the vessel wall and the impact on hemodynamics has been widely acknowledged. Changes in the stiffness of the walls mark the age-related decline of vascular health, particularly in the abdominal aorta.[41, 107, 108] A stiffer aorta has lost the Windkessel effect of the peripheral arterial system which describes the expansion of the aorta (and other large elastic vessels) during systole and the retention of that blood as the systemic blood pressure reaches that of the

left ventricle.[109] Once systole has ended, the fibers in the vessel wall which have extended in response to the pressure loading recoil and dispel the blood to the periphery during diastole. In this way, the vessel acts as a capacitor. Stiffening (or a reduction in the compliance) of the vessel consequently reduces its.

If we consider the other anatomical structures surrounding the aorta (as well as many other vessels) we expect vessel displacement to differ as a function of circumferential and longitudinal position. These differences contribute to an asymmetric displacement around the vessel circumference. In this way, various regions of the vessel may be more predisposed to stretching of the aforementioned microstructural fibers in the wall and alter the extent to which the vessel is able to retain flow in a reservoir during systole. The heterogeneity of not only the surrounding anatomy but also of the tissue properties will relate to a difference in the imposed stresses and strains.

1.6 Cardiovascular Biomechanics Imaging

1.6.1 Fluid Imaging

Phase contrast MRI (PCMR) is an MR sequence used to visualize and quantify vascular flow.[110-113] PCMR uses the difference in phase shift between static and moving tissue created by an applied magnetic field gradient to measure velocity in a defined direction. In PCMR, two image sets are acquired in the sequence. If the tissue is static, these two images will cancel each other out and there will be zero phase shift. If the tissue moves, however, as in the case of blood flow then a phase shift directly proportional to the velocity in the direction of the gradient will be produced in the pixel. Varying the strength and the direction of this gradient allows us to assess velocity over a certain range (set by a defined velocity encoding value) and in a direction either through the plane of the image or in the plane of an image.[110]

There are numerous applications of phase contrast imaging in the cardiovascular system including peak velocity measurements, velocity profile measurement, and perhaps most widely used is flow measurement. [114] Using the velocity data from the phase images, one could segment a region of interest and the sum over the product of the image pixel area and the individual velocities to create a flow waveform. This is one of the most common applications of PCMR. PCMR has been shown to reliably quantify flow when verified through the use of flow pumps and realistic phantoms of human anatomy.[112] When resolution of the image, signal to noise ratio (SNR) and the segmentation algorithm are optimized for a specific vessel, the flow errors quantified are less than 5%. Because PCMR's high reproducibility in determining of flow waveforms we elected to use flow as a primary input method to quantify WSS in this study.

1.6.2 Tissue Imaging

Much of the focus in studying tissue mechanics in the cardiovascular system in MRI has been centered on cardiac mechanics. Applications in the vascular system are limited due to the potential MR resolution relative to the size of vessels. Much of what has been studied, particularly in the abdominal aorta, focuses on quantifying compliance and distensibility.[52, 115-118] Compliance measurements are often estimated through the use of pulse wave velocity (PWV, the amount of time it takes the systolic wave front to travel from one location of the vascular system to another).[50, 119, 120] This type of calculation relies heavily on assumptions including a presumed (homogeneous) wall thickness as well as an imprecise method of determining aortic length. Despite these shortcomings, PWV measurements have still been shown to be a reasonably predictive biomechanics biomarker in the general population for cardiovascular disease risk.[121] Distensibility measurements are most often made using in-plane cine MR image acquisitions in which high resolution black blood images are acquired at multiple time points throughout the cardiac cycle.[122] The lumen is segmented at each time point and

the area is calculated and tracked from one time point to the next. While this method does provide information about how the vessel lumen changes in diameter, it does not provide much information about the actual tissue mechanics properties.

A sequence commonly used in cardiac mechanics is Displacement Encoding with Stimulated Echoes (DENSE).[123] This sequence allows for the evaluation of the displacement of tissue inside each voxel. In the vascular setting, there is only one published report of using this sequence in the aorta.[124] In that study, displacement was measured at one time point in systole and another time in in diastole and a single displacement and strain value was computed around the vessel circumference using these two time points. In the studies involving cardiac mechanics, the sequence was used to capture displacement information at many times over the cardiac cycle. In this way it is possible to define displacement fields over the vessel as a function of time. Strain can then be calculated by a variety of methods[125-128]. Using this technique, it would be possible to make inferences about the heterogeneity of mechanics around the vessel. Application of this method in a cine fashion in the vessel represents a novel imaging technique for quantifying vascular mechanics.

1.7 Summary

The underlying pathophysiological differences in the development of cardiovascular disease between men and women remain poorly understood, particularly in the case of abdominal aortic aneurysms. While the prevalence is higher in men than women, the burden of mortality is much greater for women once they have developed the disease. For this reason, there is a need for a sex-based approach to studying this and other CVD processes as cardiovascular disease remains the most common cause of death among both men and women in the United States. The ability to screen for risk factors specific for this disease has the potential to improve management of the disease. However, the currently identified risk factors are limited to lifestyle choices and do not

include any underlying pre-dispositions that are of considerable importance. The research proposed in this study has the potential to identify those women who are at increased risk for the disease, allowing for early intervention and even prevention and thus reducing the burden of mortality and morbidity.

CHAPTER 2

Hypothesis and Specific Aims

Abdominal aortic aneurysms (AAA) are 4-5 times more prevalent in men than women and tend to occur earlier in life in men. Although the prevalence is greater for men, the risk of mortality within the AAA population is higher for women. This increase in mortality persists with optimal surgical intervention in aneurysms at risk for rupture. Despite this dichotomy between the two populations, little work has to been undertaken to evaluate what possible pathophysiological mechanisms drive the difference in disease development.

Both cardiovascular solid and fluid mechanics have been shown to be important in the development of inflammation-mediated vascular disease. However, their role in sex-dependent pathophysiology has been only minimally explored. Previous work has shown that biomechanics may explain rupture risk and mortality within the AAA population but the hypothesis that mechanics may explain why men are more likely to develop the disease than women has not yet been tested. The objective of this project is to evaluate if the biomechanics of the abdominal aorta are significantly different between healthy men and women. We evaluated the role of WSS and particularly oscillatory shear was chosen as a primary endpoint of interest because of the co-localization of oscillatory shear with the development of early vascular disease in the abdominal aorta. Further, the project seeks to assess which innate vascular properties could explain such a difference in hemodynamics. In addition to the fluid biomechanics, we evaluated the aortic wall tissue displacement and strain to study any potential differences in the tissue mechanics between the sexes. Beyond the physical properties explored in this project, there are many other important biological factors that could contribute to differences in the risk of disease development in progression.

While there are many potential differences that exist between men and women which could result in a difference in WSS patterns. We examined three vascular properties that we hypothesized to have a strong association to hemodynamics as a result of differences between the sexes: geometry, peripheral resistance and tissue displacement/strain.

Vessel curvature is known to play an important role in influencing the development of WSS profiles in other regions of the vascular system. For this study, we examined the geometry of the abdominal aorta in its role of hemodynamic differences between men and women because the female lumbar spine exhibits a higher degree of lordosis (anterior curvature) in order to allow for a greater pelvic opening. In addition to curvature, we elected to look at the aortic radius along the length of the vessel because it is known that in the population as a whole, men are larger than women. Mathematically, WSS should be inversely proportional to the cube of the radius if all other conditions are equivalent. Thus differences in the actual size of the vessel may contribute to any observed differences in WSS.

Peripheral resistance may differ between men and women because of the anatomical differences between the sexes in pelvic structures. The presence of a uterus creates a low resistance network that exists solely in the female peripheral arterial system with no anatomic male analog and may influence hemodynamics in the aorta. We expanded on this hypothesis and identified patient populations whom we expected to have altered uterine artery flow to assess the contribution to aortic hemodynamics. We included women with symptomatic fibroids which are large highly vascularized uterine tumors which can be treated by arterial embolization (to starve circulation and induce tumor necrosis) to provide us with a representation of reduced uterine artery resistance. We also recruited women with a medical history significant for hysterectomy. In the case of hysterectomy, we expect there would be an increase in the resistance of the uterine artery once the organ is removed. In this way we sought to evaluate the differences in

peripheral flow and aortic WSS at baseline between men and women as well as when peripheral conditions are modulated.

Finally, we proposed that tissue mechanics, specifically vessel wall displacement and strain, may be different between men and women, given the relationship between increased aortic stiffness and increased risk of cardiovascular disease. We elected to explore how such measurements might differ between the sexes using in vivo measurements because prior histological studies have suggested differences in the extracellular collagen content and orientation of the abdominal aortas of men and women. Differences in baseline tissue mechanics could predispose men to development of the disease or could explain why women are more likely to rupture once AAA develops.

2.1 Central Hypothesis

Our primary hypothesis for this work is that abdominal aortic hemodynamics are significantly different between men and women. More specifically, we hypothesize that men will exhibit more oscillatory shear than women which pre-disposes them to an increased risk of abdominal aortic aneurysm.

Stemming from this primary hypothesis we proposed 3 sub-hypotheses, namely that this difference would be mediated by aortic geometry, peripheral resistance in the lower body, and tissue displacement and strain.

2.2 Approach

To test our hypothesis we recruited healthy men and women, free of cardiovascular disease and its major risk factors, as well as patients with altered uterine artery blood flow. We acquired non-contrast angiograms of the aorta and peripheral vasculature, phase contrast magnetic resonance images of blood velocity in the abdominal aorta and peripheral vessels, and displacement encoding of the aortic wall with stimulated echoes (DENSE) image sets. We developed a novel method for quantifying WSS from two dimensional phase contrast images and applied it to all

volunteer groups. We then evaluated aortic geometry and peripheral flow profiles to assess their relationship with aortic WSS data independently.

2.3 Aim 1a: Differences in Wall Shear Stress Profiles of Men and Women

Assess circumferential and longitudinal differences in the abdominal aorta wall shear stress profiles of men and women by phase contrast MRI.

The purpose of this aim was to develop a novel method to measure WSS in the abdominal aorta using 2D PCMR so that we could answer the question: Are there differences between men and women's abdominal aortic wall shear stress profiles? Using this method, we quantified oscillatory shear index and time averaged WSS magnitude and compared how these parameters change between healthy men and women.

The hypothesis for this aim was: *Men exhibit a greater degree of oscillatory shear in the abdominal aorta than women*. This could explain, at least in part, the increased risk of developing aortic aneurysms for men when compared with women.

To test this hypothesis, we recruited healthy men and women aged 30-42 and performed multiple PCMR acquisitions along the length of the aorta. We then applied our method for quantifying WSS, and mapped WSS values for each volunteer to a normalized two dimensional map describing circumferential and longitudinal changes of these metrics. This methodology allows us to create average WSS parameter maps for both sexes that were spatially equivalent relative to each volunteer's own anatomy.

2.4 Aim 1b: Role of Geometry Differences in Wall Shear Stress Profiles

Determine how aortic curvature and radius differs between men and women and to determine if these geometric properties influence regional wall shear stress in a sex-dependent manner.

The second part of this aim proposes to answer two questions. First, is the curvature or radius of the abdominal aorta significantly different between men and women? In

women, the region of the spine to which the abdominal aorta is bounded is more lordotic (curved anteriorly) than in men due to the tilt of the pelvis. As a result it is reasonable to wonder if this difference in skeletal anatomy is associated with a difference in vascular geometry. Secondly, does a difference in curvature or size relate to any differences in hemodynamics? It is known that the shape and size of a vessel can dramatically influence the WSS profile and so it is reasonable to hypothesize that differences in geometry can explain differences in wall shear stress parameters such as oscillatory shear index.

The hypothesis for this aim is: *differences in aortic radius will be associated with differences in WSS profiles between men and women.* We will determine if these two geometric parameters will have an effect on the differences in WSS between the two populations.

To test this hypothesis, we acquired non-contrast angiograms of the abdominal aorta and peripheral vessels in addition to the PCMR images acquired as part of Aim 1a. We created three dimensional reconstructions of the vasculature and determined vessel centerlines and computed the curvature and radius of the vessel as a function of position along the length and compared these values between the sexes. We then evaluated if local geometry correlated with sex-dependent differences in wall shear stress between men and women.

2.5 Aim 2: Contribution of Peripheral Resistance to Wall Shear Stress

Ascertain the role of peripheral resistance as mediated by uterine artery blood flow on the aortic hemodynamics of women than men.

The purpose of this aim was to answer the question: does the presence of uterine artery blood flow correlate with differences in aortic hemodynamics? Peripheral resistance is known to play an important role in WSS profiles. Lower limb amputees have a significantly higher risk of developing AAA than do the rest of the population, and they also have an increase in their peripheral resistance as a result of the appendage loss.

Conversely, presence of the highly vascularized uterus could reduce the peripheral resistance thus lowering the amount of flow reversal in the abdominal aorta and decreasing the level of pro-inflammatory oscillatory shear. Further, population studies have shown that parous women who experience increased uterine artery flow as a result of the pregnancy are less likely to develop AAA when compared with non-parous women. For these reasons, we elected to look at patient populations for whom we expect to have altered uterine flow.

Our hypotheses for this work were three fold:

1. *Men will exhibit higher peripheral resistance than women as assessed by internal iliac and external iliac flow reversal as a proxy measure.*
2. *Women who have had hysterectomies will have higher peripheral resistance than women with intact uterine anatomy.*
3. *Women who have uterine fibroids requiring intervention will demonstrate lower peripheral resistance than women without fibroids.*

Because the uterine arteries are too small to measure its flow by MRI, and because men lack a uterine artery, we elected to quantify flow through the internal iliac arteries which supply blood to the pelvis and are the parent vessels of the uterine arteries. We also quantified flow in the external iliac arteries to control for any differences in lower body mass that may exist between our patient and control groups.

To test these hypotheses, we recruited separate populations of women aged 30-42 either prior to embolization to treat uterine fibroids or following a hysterectomy procedure. For all these women, phase contrast imaging was acquired in the abdominal aorta halfway between the renal artery origin and the aortic bifurcation to quantify WSS. PCMR images were also taken in the internal and external iliac arteries to measure the flow wave forms. These same image sets were acquired in our healthy volunteers from Aim 1 and comparisons of results were made amongst all four groups. We also evaluated the relationship between each of these peripheral flow conditions and aortic OSI.

2.6 Aim 3: Measuring Tissue Displacement and Strain in Men and Women

Determine whether aortic wall displacement over the cardiac cycle as measured by DENSE MRI differs between men and women and assess whether circumferential strain varies amongst these two populations.

The purpose of this aim was to assess if we could measure a difference in the displacement or circumferential strain of the abdominal aortas between men and women. DENSE MRI has previously been used in the myocardium to quantify displacement and to assess cardiac function using strain values. Until now, this sequence had not been utilized in the vascular system in a *cine* fashion and so its implementation provides a novel application of the technique.

The hypothesis for this aim was: *women will experience a higher degree of displacement in the aorta when compared with men*. Histological studies have shown that men and women have a different orientation in the microstructural elements (collagen and elastin) that contribute to the mechanical properties of the vessel wall. These alignments suggest a higher compliance in women although no one has shown this in vivo. Additionally, collagen and elastin production are under control of an estrogen response element (ERE) in the aorta increasing the likelihood of a dependence on sex.[129, 130] Thus it is possible that these biochemical configurations may contribute to a difference in the larger scale biomechanics of the abdominal aorta.

To answer these questions and test our hypotheses, we use time resolved displacement encoding MRI imaging techniques (known as DENSE) in the distal half of the abdominal aorta in the volunteers described in Section 2.3 above. This imaging technique allowed us to quantify displacements that were smaller than the resolution of the image itself which was an advantage over other tissue tracking imaging techniques. From these image acquisitions, we computed the displacement values around the circumference of the vessel and quantified circumferential strain. We then made regional comparisons between men and women as well as within each volunteer. Further we

assessed how these measurements may be related to the wall shear stress profiles discussed previously.

2.7 Significance and Innovation

There is a pressing need for sex-based research in cardiovascular disease, especially in those diseases where the risk and prognosis is very different between the sexes such as AAA. Progress has been made in assessing the sex-dependent risk of rupture of AAA when looking at biomechanical forces. Until now, however, little work has been done to assess what role those biomechanical forces may play in the risk of developing the disease. This work has the potential to identify which specific biomechanical variables of the male aorta make it more susceptible to developing the disease. It is acknowledged that screening for AAA in women is sub-optimal due to the low incidence in the population. Thus, additional information about biomechanics could improve selection of the sub-population of women at risk for the disease. In this work we hope to identify women with specific vascular properties that result in more pro-inflammatory wall shear stress profiles.

From a methodological standpoint, this work contributes two new techniques/methods to the cardiovascular research community to measure biomechanics *in vivo*. Our 2D PCMR WSS measurement method is less sensitive to noisy velocity measurements and detection of vessel wall location than previously reported methods which utilize the same imaging modality. This method can be employed rapidly with good repeatability and may serve as an additional cardiovascular biomarker by which risk for aortic disease can be tracked and assessed in a patient. Additionally, this work is the first to utilize cine DENSE imaging in the abdominal aortic wall and to assess sex-dependent differences in aortic wall motion. Until now, there have not been many proposed MRI measurements capable of evaluating strain in the vessel at multiple points around the circumference of the aorta.

Thus, the research presented herein has the potential to contribute a basis for how sex-dependent cardiovascular research is performed. The results can also inform future population studies to confirm that the proposed sub-groups of women we suspect are at higher risk for development of AAA. The two methods proposed here provide new clinical tools for quantifying and assessing cardiovascular disease risk.

CHATPER 3

QUANTITATION OF WALL SHEAR STRESS FROM 2D PHASE CONTRAST MRI

This chapter is adapted from a manuscript in preparation for submission to the Journal of Magnetic Resonance Imaging entitled "A Novel Method for Quantifying Wall Shear Stress from 2D Phase Contrast MRI Using a Modified Version of the Womersley Solution"

3.1 INTRODUCTION

As the body of literature on the importance of cardiovascular hemodynamics in vascular disease localization and progression grows, the need for rapid and accurate quantification of relevant mechanics parameters becomes increasingly important.[31, 35, 131-133] One such parameter is wall shear stress (WSS), the frictional force blood exerts as it passes over the arterial wall. If we approximate the vessel as a purely cylindrical geometry, we can quantify the magnitude of WSS as

$$WSS = \mu \left(\frac{\partial v(r)}{\partial r} \right)_{r=0} \tag{3.1}$$

Where μ is fluid viscosity, v is the velocity parallel to the wall and r is the radial distance from the wall towards the center of the lumen. Because this value is related to the flow and the cardiac cycle produces pulsatile flow, the magnitude and the direction of the vector changes throughout the cardiac cycle. Both direction and magnitude of WSS affect the function of endothelial cells and have been implicated in the localization and development of atherosclerosis and aneurysms. Low magnitude in and oscillatory direction of WSS are known to elicit the expression of pro-inflammatory genes, induce endothelial dysfunction, and promote medial-intimal thickening.[26, 32, 33]

Phase contrast magnetic resonance (PCMR) is an imaging sequence that encodes the velocity of the spins contained within a voxel in a direction, normal to or in the plane of an image.[113] Using the acquired velocity values and pixel size, it is possible to trace a vessel boundary and quantify *flow* by summing the product of area and velocity for each pixel included in a contour. Such calculations have been shown to be accurate, reliable, and reproducible in phantom and human studies. [111] The sequence has been used in numerous clinical applications including valve regurgitation assessment, vessel stenosis, and WSS quantification.[110]

Previously described methods have used PCMR to quantify WSS based on pixel-by-pixel *velocity* values rather than flow. [133-135] These methods rely directly on velocity measurements in individual voxels, which can be sensitive to noise, baseline drift, and susceptibility artifacts. Correct identification of the vessel wall boundary becomes increasingly difficult as the resolution of the images relative to the size of the vessel decreases and during the diastolic phase of the cardiac cycle when the velocity (and therefore MR signal) is much lower.[133, 136] Furthermore, these individual velocity based-methods are affected by partial volume effects at the wall. Voxels that encompass the area closest to the wall, which contain the most important velocity values for determining WSS (i.e., they define the velocity gradient) may also contain part of the vessel wall. Error in identifying the wall position obscures the true velocity near the wall and results in an under-prediction of WSS depending on how much of the static wall is contained within the pixel.[136] Thus, there is a need to develop a method which is independent of direct velocity measurement and can accurately quantify WSS from PCMR imaging data.

Herein, we describe a method for quantifying WSS around the circumference of the vessel that utilizes *flow* as a primary input rather than individual velocity values. We demonstrate the robustness of this method by sensitivity analyses, and the accuracy of the method by comparison to a computational fluid dynamics (CFD) simulation.

3.2 METHODS

3.2.1 Overview of the Methodology

The Womersley solution is an analytical solution to the Navier Stokes equation for time-varying, axisymmetric, fully developed, unidirectional flow in a circular, rigid, straight tube.[137] The primary inputs required for this solution are flow as a function of time, vessel radius, fluid viscosity, and fluid density. Direct application of this solution is a simplification in the case of the abdominal aorta. However, while flow near the renal arteries and iliac bifurcations is more complex and susceptible to the formation of secondary flow characteristics, the main trunk of the aorta in a healthy individual is expected to exhibit mostly unidirectional flow.[70] To obtain flow as a function of time, we used 2D PCMR imaging which reliably captures flow rate in an *in vivo* setting. Our application of the Womersley solution involved evaluating regional flow in overlapping sectors of the vessel around the circumference. Thus, with an approximation of vessel radius, local flow waveforms were used to determine WSS as a function of time and circumferential position.

3.2.2 MRI Acquisition & Lumen Segmentation

Slice position and orientation for phase contrast images were planned on initial scout images and rapid non-contrast angiograms. Slices were oriented perpendicular to the primary direction of the vessel in the head foot direction and were set in the abdominal aorta 1.5 cm below the renal arteries and ending at 1.5 cm above the aortic bifurcation. 2D PCMR images used the following parameters: repetition time (TR) 41.9 msec, echo time (TE) 3.53 msec, signal averages =5, flip angle= 30 degrees, voxel size= 1.33x1.33x5mm, venc =150 cm/s, and 30 phases over the cardiac cycle.

PCMR images were acquired at the inlet of the abdominal aorta and at three sites distal for WSS quantification, accuracy and sensitivity analysis. We also acquired a Quiescent Interval Single Shot (QISS) non-contrast angiogram of the aorta from the renal arteries to 3 cm below the iliac bifurcation with resolution 0.5x0.5x3.0 mm.[138] Scans were acquired on a Siemens 3T scanner (TRIO, Software VB17). The Institutional Review Board approved the study and informed consent was obtained.

Vessel segmentation was manually defined using the magnitude images at peak systole using Segment v1.9 R2626 (http://segment.heilberg.se) and then copied to the remainder of the frames and adjusted employing edge detection using a thresholding algorithm.[139] All boundaries were reviewed and adjusted if needed and imposed on the phase images as well. The segmented lumen contour was exported from Segment as x-y point locations in the coordinate system of the image for each time point.

3.2.3 Quantification of Regional Flow

Using the xy-point locations, eighty overlapping sectors were defined from the centroid of the vessel to the edge of the lumen with a central angle of 90 degrees to include approximately a quarter of the lumen in each sector (Figured 1B). A pixel was included in a defined sector if more than 50% of its area fell within the sector. Flow vs. time was quantified in each sector as defined by

$$Q_j(t) = \sum_{i=1}^{n} v_i(t)A \tag{3.2}$$

in which Q_j is the flow rate through the sector j at time t, v is the velocity in pixel i at time t, n the number of pixels contained within sector j, and A is the total pixel area. An independent flow waveform was determined for each sector (Figure 3.1C).

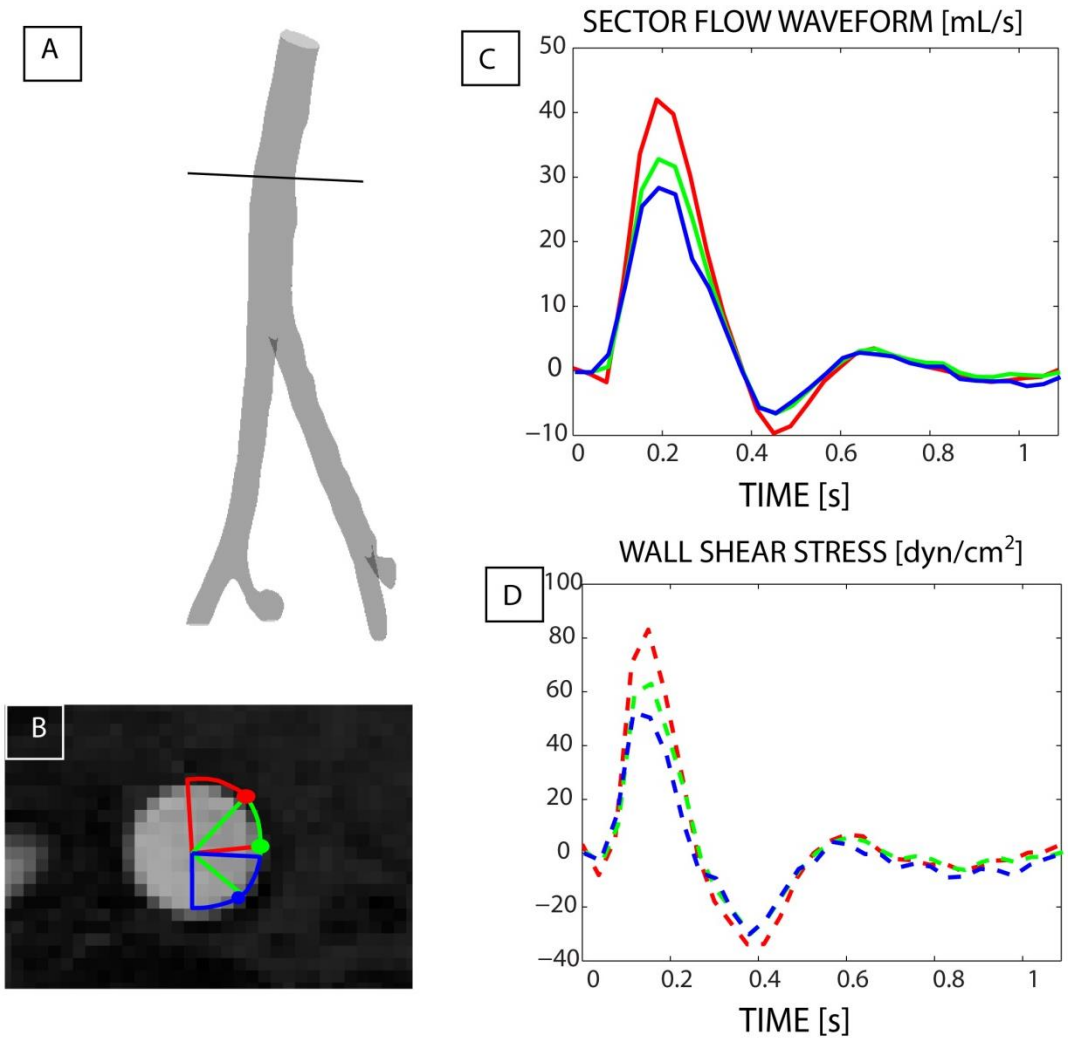

Figure 3.1. Explanation of Wall Shear Stress Calculation and Parameter Mapping. (A) Indicated line shows an example of a PCMR image location in the abdominal aorta. (B) Representative magnitude image from the PCMR data with three unique sectors in red, green and blue. Filled circles define location were WSS values are mapped to for regional analysis. (C) Flow waveforms as a function of time calculated from each of the three colored sectors defined in (B). (D) WSS waveforms from each of these sectors.

3.2.4 Application of Womersley Solution

The flow waveform calculated for each of the 80 sectors was divided sector's percentage of the full lumen area to estimate what flow would be over an entire vessel. Each of these

waveforms was converted to the frequency domain via Fourier transform. The first ten harmonics of this transform were used in the frequency domain expression of the Womersley solution because their sum was found to accurately recreate the flow waveform. In application of the solution, we use the first harmonic to define equations for the steady axial pressure gradient $\left(\frac{dp}{dz}\right)$ and wall shear stress (τ) for each sector *j*:

$$\left(\frac{dp}{dz}\right)_{j,0} = Q_{j,0}\frac{\pi R^4}{8\mu} \tag{3.3}$$

$$\tau_{j,0} = -\left(\frac{dp}{dz}\right)_{j,0}\frac{R}{2} \tag{3.4}$$

As well as equations for the remaining 9 harmonics (*n*=1,..9):

$$\left(\frac{dp}{dz}\right)_{j,n} = Q_{j,n}\left(\frac{\rho*\omega*i*n}{\pi R(t)^2}\right)\left(\frac{1}{1-\frac{2i^{1.5}\alpha J_1(i^{1.5}\alpha)}{i^3\alpha^2 J_0(i^{1.5}\alpha)}}\right) \tag{3.5}$$

$$\tau_{j,n} = \left(\frac{\mu i^{1.5}}{R(t)\rho\omega}\right)\left(\frac{\alpha}{n}\right)\left(\frac{dp}{dz}\right)_{j,n}\frac{J_1(i^{1.5}\alpha)}{J_0(i^{1.5}\alpha)} \tag{3.6}$$

Summing the 10 harmonics at each of the 30 time points, *t*, we generate shear stress profiles in sector *j*:

$$\tau_{j,t} = \sum_{n=1}^{10}\tau_{j,n}e^{-in\omega t} \tag{3.7}$$

for which ρ is the density of blood = 1.06g/cm^3, ω is the frequency of the cardiac cycle, μ is the viscosity = 3.5 CP, and α is the Womersley number defined as $\alpha = R\sqrt{\frac{\omega}{\nu}}$ (where

ν is the dynamic viscosity). *R(t)* is the radius of the vessel, calculated by fitting a circle to the vessel contour at each time point. Note that *R* is a function of time but the vessel is assumed rigid at each time point.

The calculated WSS value for each time point was placed at the central point on the arc of the sector (Figure 1B). Furthermore, oscillatory shear index (OSI) was calculated by

$$OSI = \frac{\int_0^T \tau^* dt}{\int_0^T \tau dt} \tag{3.8}$$

where τ is the WSS waveform, τ* is WSS in the opposite direction of the primary shear vector and T is the length of the cardiac cycle.[36] *Thus the circumferential heterogeneity of the WSS parameters can be evaluated which is not possible with a direct application of the Womersley solution.*

3.2.5 Sensitivity & Repeatability

To assess the sensitivity of our WSS calculation methodology to the radius as an input variable, we evaluated how 5% and 10% changes in the calculated area of the circle fitted to the vessel contour affects the WSS results. These changes were chosen because the pixel resolution is roughly 10% of the average radius in the abdominal aorta of a healthy individual. This corresponds to an error in the lumen contour of approximately one pixel.

Inclusion of a voxel's contribution in our calculation of flow is a Boolean process (it is either in or out) dependent upon whether or not more than 50% of a voxel's area is included within the boundaries of a sector's contour. To test the influence of partial volume effects, we calculated WSS waveforms when the inclusion of a pixel was no longer a binary decision, i.e. we included all pixels that fell within a sector in our flow

calculation. For those pixels whose area was less than 100% within a sector, we quantified the percent area of the pixel that was contained in the sector. The percentage was then multiplied by the flow through that pixel and added to the sector flow calculation. Figure 2 offers a visual explanation of the partial volume inclusion.

To assess how our WSS results would vary between two independent flow measurements, we repeated a PCMR acquisition in the same location at separate times during the course of a single study. The subject remained in the scanner between the two acquisitions and approximately 15 minutes separated each independent acquisition.

3.2.6 CFD Simulations

To assess the accuracy of our method against an accepted standard of measurement, we compared the results of our method against the results from a computational fluid dynamics (CFD) simulation, which provides higher spatial and temporal resolution of the velocity field but at a much greater computational cost. Non-contrast angiogram images were segmented using the general segmentation tool in Segment, visceral vessels were removed and the inlets and outlets were defined perpendicular to vessel centerlines. The inlet of the computational geometry was cut to correspond to the location of a PCMR image set, which was acquired approximately one diameter below the renal artery bifurcations. The resultant geometry was expressed as 3D point cloud and wrapped with a surface defined by non-uniform rational B-splines (Geomagic Studio 11, Geomagic, Inc., Research Triangle Park, NC). Flow extensions were added to the two iliac vessels at a length of 7 diameters to ensure fully developed flow (ICEM CFD, ANSYS 14, Ansys INC., Canonsburg, PA). The volume was discretized using an unstructured tetrahedral mesh (ICEM CFD) and included a boundary layer to resolve near wall flow patterns. Average velocity data from the PCMR images were interpolated to 300 equally spaced time points and applied in the simulation as a series of blunt (uniform) velocity profiles. Outlets were assumed to be pressure free and a

no-slip condition was applied to maintain a zero velocity at the wall. Blood was assumed to be incompressible, Newtonian fluid with a density of 1.06g/cm^3 and dynamic viscosity of 3.5 cP, identical to values used in the method proposed in this study. Convergence criteria were set to residual errors < 10^{-4}. Using the inlet velocity data and the geometry, the pressure-velocity equations defined by the Navier Stokes equations were solved by a SIMPLE solving scheme and second-order spatial discretization was used to solve the velocity field in Fluent (ANSYS 14). This method is consistent with one previously described in detail.[140] Three cardiac cycles were simulated and data from every 10th time-step of the third cardiac cycle were analyzed to match the 30 time points from the phase contrast images. Following solution convergence, resulting velocity fields were post-processed to calculate the WSS vectors at each surface node. WSS vectors were exported for each of the surface nodes that fell on a plane defined by the position vectors of the PCMR images.

3.2.7 Statistics

For both our radius and sensitivity analyses, we compared the results using time averaged wall shear stress magnitudes, average absolute differences in wall shear stress as well and the root mean square error. We computed Lin's concordance correlation coefficient to assess the similarity between the WSS values calculated from each acquisition in our repeatability studies.[141]

To compare the results of the CFD simulation to those derived from our method using the phase contrast data and the Womersley solution, all WSS data points from our method were matched to the closest point on an extracted CFD results plane. To quantify the differences between the WSS values our methods produced and those produced by the CFD simulation, we evaluated time-averaged WSS magnitude differences, average absolute difference between spatially and temporally equivalent shear stress values and performed a Bland Altman analysis to assess mean difference and correlation.

3.3 RESULTS

MR images were successfully acquired and evaluated according to methods described above.

5.3.1 Sensitivity & Repeatability Analysis

Comparisons between WSS results derived from our method's application to two independent PCMR acquisitions show strong agreement. Figure 2 summarizes the results of our repeatability study with a scatter plot of the WSS values comparing the results of the repeated phase contrast acquisitions. In comparing the repeatability of the methods, we calculated Lin's concordance correlation coefficient to be 0.96 which indicates a high reliability of our method to reproduce the same result from one phase contrast acquisition to the next. The average and standard deviation WSS from the first and second acquisitions are 14.2±2.28 dyn/cm^2 & 14.4±3.03 dyn/cm^2 respectively which was statistically non-significant. The average absolute difference of WSS(calculated as the absolute value difference for each of the 30 time points at all 80 locations around the circumference) between the first and second acquisition was 3.75±3.89 dyn/cm^2. 75% of the WSS measurements showed less than a 5.19 dyn/cm^2 difference between the two acquisitions.

Our sensitivity analysis evaluating potential errors in the lumen contour definition demonstrated our method's robustness to radius calculation. Figure 3 summarizes the results of our radius sensitivity analysis. For the original contour and each of the four imposed area error conditions (-5%, +5%, -10% and +10%) the average and standard deviation of wall shear stress magnitudes were 13.4 ±2.39 dyn/cm^2, 14.3±2.60 dyn/cm^2, 12.9±2.36 dyn/cm^2, 15.1±2.74 dyn/cm^2, 12.3±2.25 dyn/cm^2 respectively. Table 1 presents the average difference in WSS between the original lumen contour measured across all three slices for each of the prescribed error percentages.

Table 3.1: Summary of error values obtained from imposing errors on radius calculation

	Mean Absolute Difference (dyn/cm^2)	Root Mean Square Error
10% More	1.15±1.49	1.88
5% More	0.68±1.06	1.26
5% Less	0.80±1.33	1.55
10% Less	1.49±2.04	2.53

The contribution of adding partial volume of a pixel resulted in a small difference in the flow wave forms at each time point. Including results from all three slices we found the average absolute difference in flow between measurements to be 0.32±0.48mL/s and a root mean square error (RMSE) of 1.76 mL/s. This small difference in flow resulted in a small difference in WSS with an average difference over the whole cardiac cycle at each of the 80 points around the circumference of 0.93±1.27 dyn/cm^2 with 90% of the measurements showing less than 2.11 dyn/cm^2 difference and a RMSE of 1.58 dyn/cm^2. The average and standard deviation WSS magnitude for our method was 13.4±2.39 dyn/cm^2. The average and standard deviation for the inclusion of partial volume flows was 13.4±2.38 dyn/cm^2.

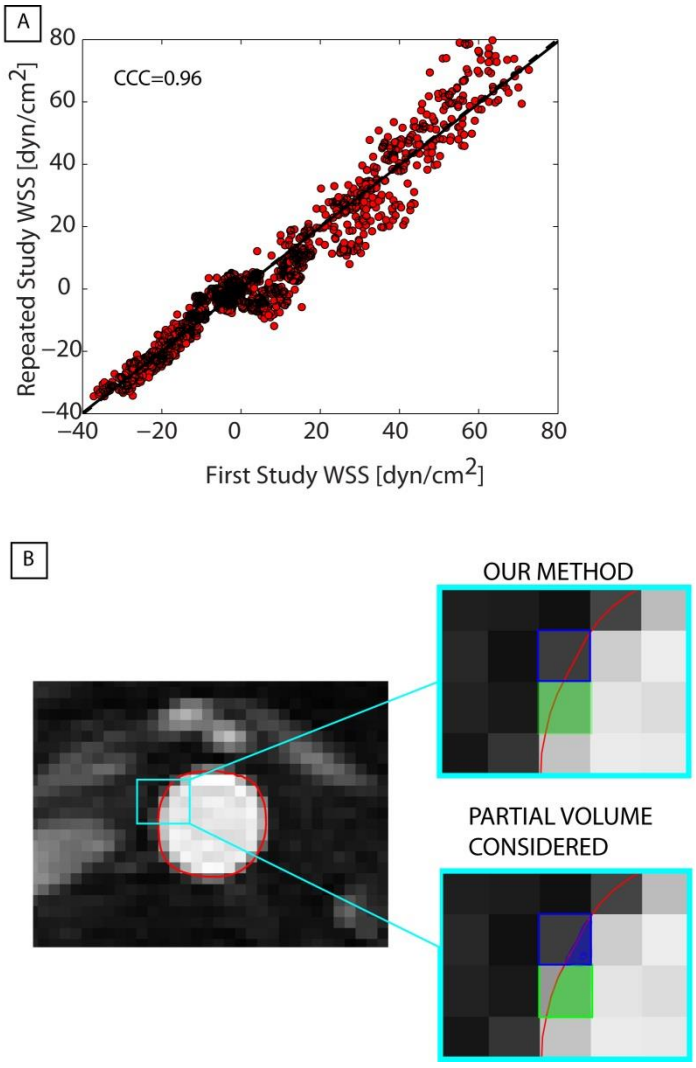

Figure 3.2 Repeatability Results and Partial Volume Explanation (A) Repeatability Results. Results of our repeatability study are represented in which the first study's wall shear stress values on the x-axis and the temporally and spatially matched values from the repeated study on the y-axis. (B) Explanation of Partial Volume Calculation. The red contour identifies the vessel boundary at this time point. In our method, the green highlighted pixel has more than 50% of its area inside the contour and thus would be included in the flow calculation while the blue pixel would not. In the lower right image, we highlight the partial area of the pixel included in the sector to be used for flow quantification.

Figure 3.3 summarizes the results of our radius sensitivity analysis. We found that changes in radius corresponding to the size of one pixel do not contribute significant

differences in the resultant WSS values. Table 1 presents the average difference in WSS measured across all three slices for each of the prescribed error percentages.

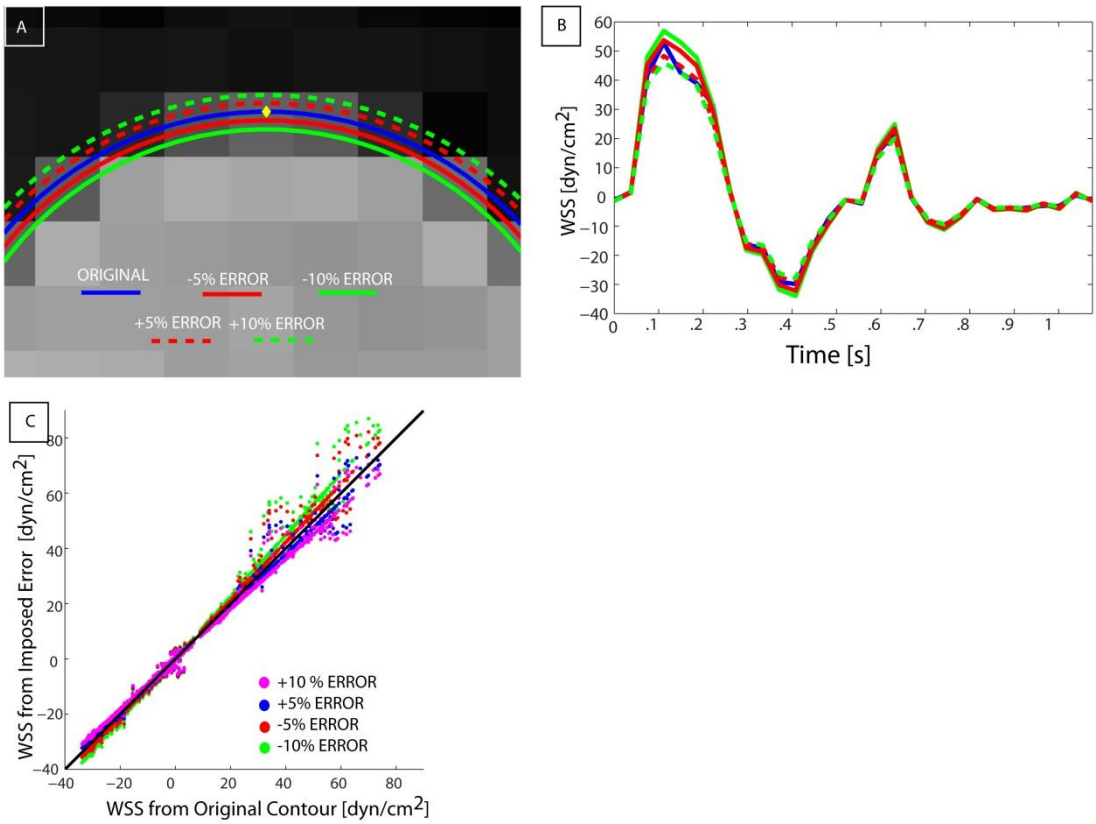

Figure 3.3 Radius Sensitivity. (A) For a given image from our PCMR acquisitions, we show the original contour in blue calculated from Segment. The red and green solid lines show the contours created by imposing a decrease of the contour area by five and ten percent respectively. The red and green dashed lines show the contours created by imposing a five and ten percent increase respectively. (B) For the yellow diamond in (A), we show the WSS waves calculated for each of the conditions with the same color scheme as in (A). (C) A comparison of the values obtained from the original contour (x-axis) with those calculated from each of the imposed areas (y).

3.3.2 Comparison to CFD

To compare the results obtained from the computational fluid dynamics simulation to our WSS measurements we performed a Bland Altman analysis using the temporally and spatially matched WSS values. The average and standard deviation WSS

magnitude from our method was 13.4±2.39 dyn/cm^2 compared to the CFD averages and standard deviations 15.0±1.91 dyn/cm^2. Figure 3.4 shows the correlation and the Bland-Altman plots for our results comparing all measured shear stress values. This analysis produced a Pearson coefficient of r=0.89 with an average difference across all points of 3.4 dyn/cm^2 and RMSE of 9.73 dyn/cm^2. 50% of the measured values had differences less than 6.66 dyn/cm^2.

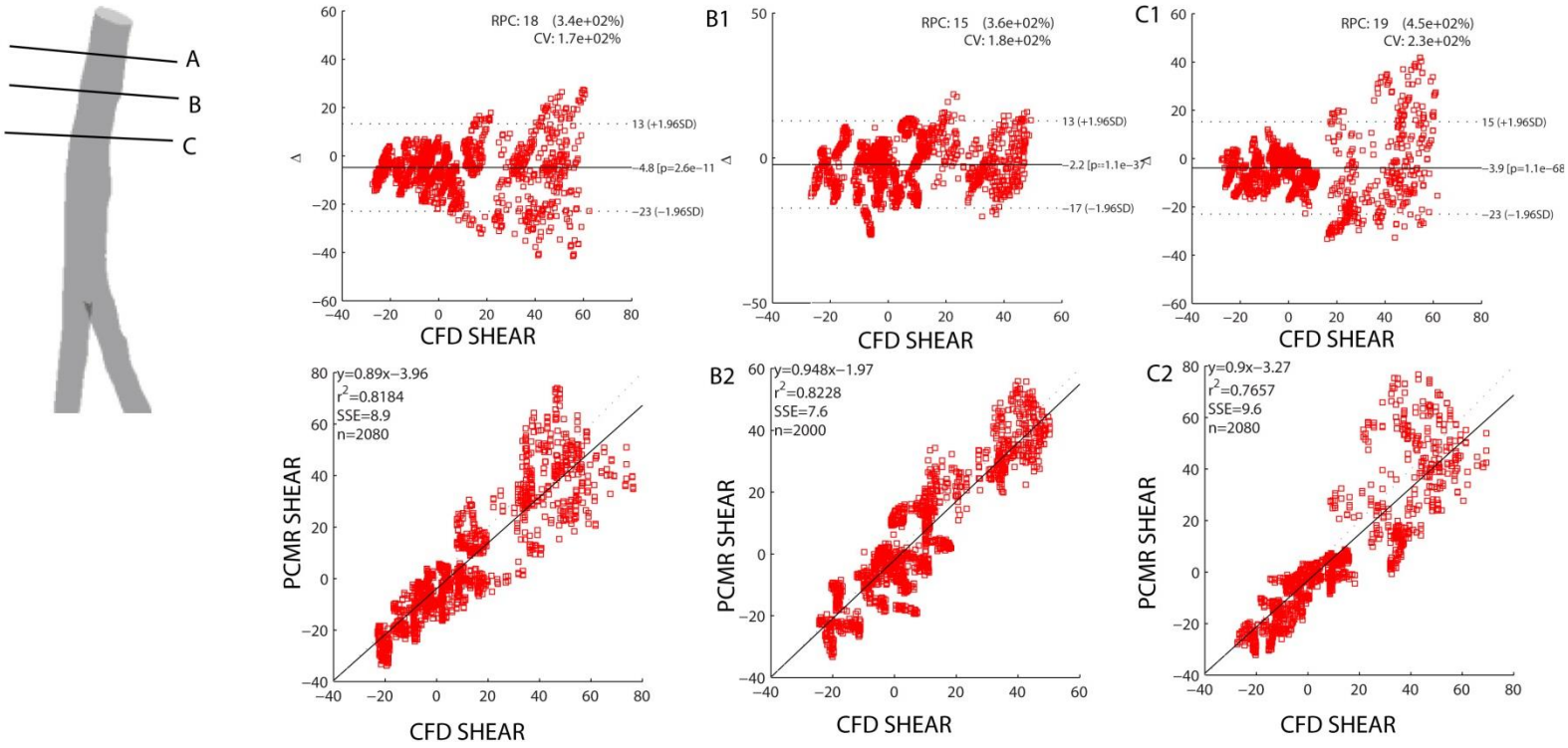

Figure 3.4 Comparison with CFD Simulations. We compared the results obtained from a volunteer-specific CFD simulation to those from our methods at equivalent temporal and spatial locations for each of the three PCMR image slice locations, A, B, and C shown as lines on the volunteer geometry. We performed and present the correlation plots and Bland Altman analyses for each of the slices independently.

3.4 DISCUSSION

We described a new method for quantifying unidirectional WSS from two dimensional PCMR. The method employs a previously described analytical solution to the Navier Stokes equation for unsteady, viscous, unidirectional, fully developed flow in a straight, rigid tube with modifications to account for the circumferential heterogeneity of the velocity profile in the aorta. The method is robust and insensitive to the primary input variables of radius and flow. The robustness of this method stems from its dependence on flow rather than exact pixel by pixel velocity values. Repeatability analysis confirms that our method produces nearly identical results in vivo from repeated MR acquisitions taken from the same location in a volunteer. Comparison with a CFD simulation utilizing patient derived boundary conditions demonstrates a strong accuracy of our method to those obtained from CFD.

While other methods exist to quantify WSS in the abdominal aorta using 2D phase contrast, these methods are dependent on knowing velocity values very close to the wall with high accuracy.[135, 142] Given the partial volume effects of voxels that include both the vessel wall as well as the lumen, correctly identifying the exact location of the wall is complex. These methods become increasingly less reliable as the resolution of the image decreases.

Recent advancements in 4D PCMR imaging have allowed for quantitation of WSS over the entire volume of the aorta.[143] These methods require significantly longer scan times and extensive post processing. Similar to the 2D phase contrast methods described above, which use the velocity field to derive WSS, correct identification of the vessel wall is very important when using 4D PCMR to obtain an accurate measurement. Our method could be applied to the 4D acquisitions from which a cross sectional flow profile can be derived. The use of this method in 4D flow imaging to quantify WSS is an important application of our future work.

With the growing body of evidence linking low and oscillatory WSS profiles to early atherosclerotic disease, WSS has emerged as a potential future biomarker for indicating cardiovascular disease risk. [30, 31, 36, 38, 98, 144] In light of this, there is a need for accurate quantification of WSS to confirm the established relationships between low and oscillatory wall shear stress and the development of vascular disease in longitudinal studies in humans.[40] In addition to the method proposed here and those described above, there are many methods that currently exist to quantify WSS. However, methods such as CFD can be computationally expensive.[145] Given these limitations, a rapid method to quantify WSS could have profound impact on monitoring the risk of individuals before clinically evident disease develops. The design of our method allows for little user independence and is dependent almost exclusively upon the established reliability of phase contrast MRI to quantify flow.[111] Thus, we believe our method could have significant clinical impact in preventative cardiovascular medicine as a result of its low imaging and computational costs.

While this method reduces the need for high SNR and resolution other 2D PCMR methods require, it is limited in its scope of application. Because of the assumptions in the solution for Womersley flow, this method may not be sufficient in areas of expected secondary flow conditions such as the carotid bulb or in an aneurysm.[94, 104] Additionally, the level of WSS distribution is linked to the level of flow heterogeneity that is detected around the circumference of the vessel. Consequently, although this method is much faster than CFD simulations, it does not detect the same level of spatial resolution of which CFD is capable. Additionally, the non-isotropic resolution of our images results in WSS values that are spatially averaged over an MR slice thickness. WSS values are expected to change over areas smaller than the thickness (5mm) used for this study. However, given that the target population for this method's application is to track the WSS parameters over time as an indicator of cardiovascular risk, such highly resolved resolution most likely is not necessary. The level of temporal resolution is also

inferior to what is possible with CFD, however, both spatial and temporal resolution can be increased for PCMR at the cost of increased imaging time. [110]

In conclusion, we developed a novel method of quantifying wall shear stress from two dimensional phase contrast MRI which is repeatable, robust, and accurate when compared to results obtained from computational fluids dynamics simulations. Numerical results are consistent with what has been previously reported. This method of determining patient specific WSS could be an important methodological contribution through its potential to be used to identify early indicators of abdominal aortic disease.

CHAPTER 4

DIFFERENCES IN WALL SHEAR STRESS BETWEEN MEN AND WOMEN AND THE RELATIONSHIP OF WALL OF SHEAR STRESS TO AORTIC GEOMETRY

4.1 Introduction

Given the relationship of many cardiovascular diseases to the biomechanics of the vascular environment, it is probable that differences in biomechanics among populations can help explain differences in disease propensity or outcome.[48, 146, 147] Of particular relevance to vascular pathologies is the wall shear stress, the stress exerted on the endothelial cells by the force of viscous blood moving across the surface.[132, 140] Multiple locations in the cardiovascular system demonstrate the development of pathological dilation in response to oscillatory wall shear stress patterns with low average magnitude including the ascending aorta in the presence of a stenotic valve as well as the aorta immediately distal to a coarctation. In abdominal aortic aneurysms, the underlying biomechanics are not well delineated in the most at risk group for developing the disease. It is possible that members of this population are exposed to pro-inflammatory wall shear stress profiles that promote the development of the disease. Specifically, since men are significantly more likely to develop the disease than women we elected to evaluate whether differences in biomechanics exist between the sexes. While there are many biomechanical properties that are related to cardiovascular disease, we elected to explore wall shear stress as it relates strongly to early vascular disease in the aorta.[37, 98, 148] In these studies it was shown that sites of the abdominal aorta that experienced the highest degree of oscillatory shear index (OSI) quantified by

$$OSI = \frac{\int_0^T \tau^* dt}{\int_0^T \tau dt} \quad (4.1)$$

(in which τ is the wall shear stress as a function of time and τ* is the wall shear stress vector in the opposite direction of the average vector) also had the greatest degree of intima-medial thickening. Thus we explored whether differences in this parameter exist between men and women.

There are many vascular properties which could contribute to the development of wall shear stress profiles. One property is the shape or geometry of the vessel. Many sites in the body that are prone to atherosclerosis are known to be so due to their vessel morphology. The carotid artery has a rapid expansion from the common carotid artery moving into the bulb of the internal carotid. This bulb is known to exhibit high atherosclerotic potential due to the secondary flow conditions here that result in significant oscillations of the wall shear stress vector.[149] Additionally, the dilation of the aortic root after a stenotic valve produces significant second flow profiles that are posited to promote progression of vascular disease.[150] Thus the radius of the vessel and how the radius changes along the course of a vessel play an important role in the development of the wall shear stress profile and how the vessel will remodel. Previously, population studies have shown that men have larger diameter aortas on average when compared with women.[122] What has not been assessed is whether these differences in size are correlated with differences in hemodynamics between the sexes. We elected to explore if these factors are related and specifically if these changes in radius could explain differences in the aortic OSI values.

In addition to radius, the vessel curvature can impact wall shear stress variations around the circumference. Specifically, blood vessel curvature has been shown to have a strong influence on how the burden of oscillatory shear is distributed. In the aortic arch for example, the OSI is increased on the inner curvature of the arch and studies have shown localization of early atherosclerotic plaques to this same region.[96] In the

abdominal aorta, the posterior vessel wall aligns with the vessel's inner curvature and computational studies in human subjects have shown that the posterior of the vessel experiences the highest degree of oscillatory shear and shows the greatest degree of intimal medial thickening.[37, 148] We suspect that there may be a difference in aortic curvature as a result of the difference in skeletal structure between men and women in this region. The lumbar spine in women is more lordotic than in men and the female pelvis is tilted more posteriorly. Because the aorta is anchored to the spine in this region, it is possible that the vessel trajectory will follow the same differences in curvature that the skeletal anatomy does.

In this study, we enrolled healthy men and women to assess how WSS differs between the two populations, specifically looking for differences in oscillatory shear and in magnitude. We also quantified aortic curvature and radius to evaluate differences in geometry properties of the vessel that could contribute to differences in WSS. Finally we evaluated what influence each of these geometry properties might have on the observed hemodynamics and if there was a significant association between the two. We hypothesized that men would have a higher degree of OSI than women as this would contribute to an increased risk for AAA. We proposed that women would have a greater aortic curvature (with a smaller radius) than men and that this curvature would create a difference between men and women in the circumferential distribution of OSI.

4.2 Study Population

We recruited healthy (nominally cardiovascular disease-free) volunteers age 30-42. Volunteers were screened for MRI safety as per normal clinical protocols (no medical implants, no foreign objects in the eye, no claustrophobia, etc.). We acquired data for this aim from 15 women and 12 men (32±2.9 years old vs 31±1.9 years old, $p>0.05$). Enrollment of these study subjects was approved under the Emory Institutional Review Board.

4.3 Imaging Protocols

4.3.1 Non-Contrast Angiogram

Initial survey images were first acquired and a volume covering the aorta and peripheral vessels was defined for the angiogram. We used a quiescent interval single shot angiogram (QISS) originally designed to be used as a peripheral vascular runoff scan to identify sites of lower limb claudication.[146, 151] This scan was chosen because of its efficacy in the peripheral arterial system, its short imaging time, and its ability to image vessels without contrast administration. The scan protocol was adapted such that it covered the vascular anatomy from the inferior thoracic aorta (directly above the renal arteries) to a region below the iliac bifurcations through a series of transverse slices. The scan allowed for resolution of 0.5x0.5x3.0 mm^3 and a field of view (FOV) of 800x520 mm^2 which was adequate for our reconstruction purposes. Figure 4.1 shows representative images from this angiogram acquisition in one of our volunteers.

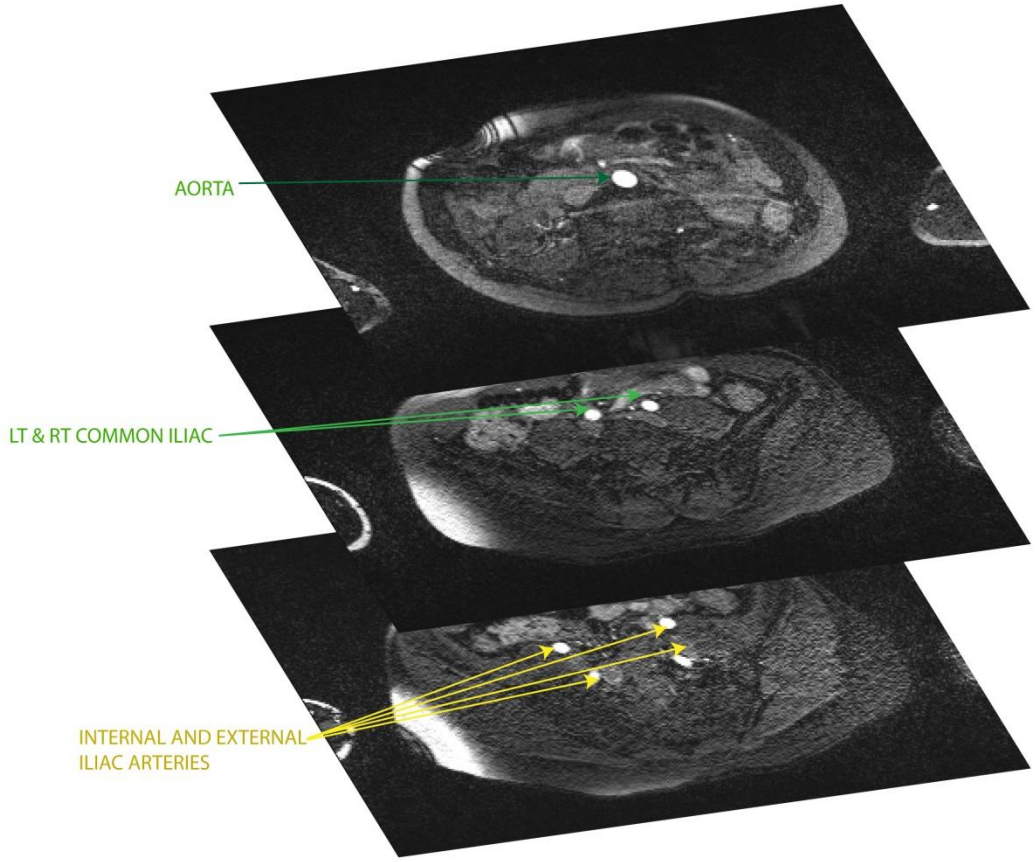

Figure 4.1 Non-Contrast Angiogram of Peripheral Arterial System. Representative images from the non-contrast angiogram of one of our volunteers showing points on interest in the peripheral vasculature.

4.3.2 Phase Contrast MRI

PCMR allows us to measure the velocity of blood in the vessel at multiple points throughout the cardiac cycle. We can match these velocity measurements to the geometry information from the angiogram. We acquired this sequence at multiple locations along the length of the abdominal aorta, acquiring 8-10 images series for each patient. This allowed us to obtain cross sectional through-plane velocity information for the entire aorta. Parameters for the EKG-gated phase contrast images were as follows: TR of 39.85s, TE of 3.39s, Flip Angle of 30°, FOV of 255x340 mm^2, resolution of 1.33x1.33x5

mm^3, velocity encoding value (Venc) of 150cm/s, yielding 30 time step images across the cardiac cycle.

4.4 Methods

For each volunteer we completed the following steps described in detail below:

1. Vessel segmentation from the non-contrast angiogram
2. Determination of centerlines for aorta
3. Fitting of centerlines in each dimension as a function of position along the aorta
4. Continuous radius and curvature calculation along the length of the aorta
5. Creation of normalized WSS map from PCMR data

4.4.1 Vessel Segmentation

The acquired angiograms were reconstructed using commercially available software (Segment, Medvisio), utilizing a level set segmentation (segmentation begins from a set of seed points and grows until it discovers regions of low intensity i.e. vessel boundaries). Following initial segmentation, the volumes were manually adjusted to exclude/include any gross misconstructions. The segmentation volume is loaded into VMTK and smoothed using a low pass filter. An example of the original and smoothed segmentations is shown in the left and center panel of Figure 4.2.

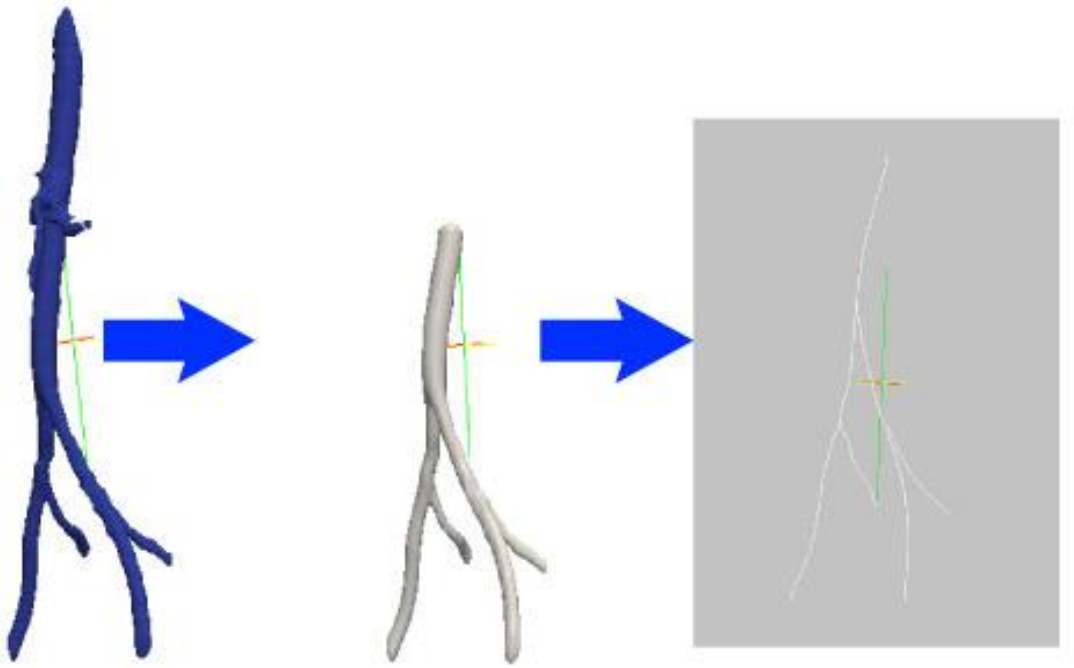

Figure 4.2 Aortic Segmentation and Centerline Definition.The leftmost panel of this figure shows our raw segmentation of the aorta and peripheral vessels including the visceral vessels. The central image is the vessel architecture after we removed the visceral vessels and smoothed the segmentation. The right image shows the centerlines for each of the vessels in the periphery created using a maximum inscribed sphere radius array.

4.4.2 Curvature & Radius Calculation

Centerline Calculation and Fitting

After segmentation smoothing, the centerlines were calculated in VMTK. This centerline protocol is based on maximum inscribed spheres within the boundaries of the surface and is designed to ignore small perturbations on the surface of the segmentation. The output from VTMK allows for identification of individual vessels based on branch point identification and the aortic vessel centerline was identified and (minimally) smoothed using a weighted linear least squares regression filter and a 2^{nd} degree polynomial model in Matlab (Mathworks, Natick, MA).

For each point *i* in a volunteer's centerline, we assigned an arc length value, *s*, based on the following equation in which x_n, y_n, and z_n are the coordinates of the centerline point *n* and $s(1)=0$.

$$s(i) = \sum_{n=2}^{i} \begin{array}{l} \sqrt{(x_n - x_1)^2 + (y_n - y_1)^2 + (z_n - z_1)^2} + \\ \sqrt{(x_n - x_2)^2 + (y_n - y_2)^2 + (z_n - z_2)^2} + \\ \ldots \sqrt{(x_n - x_{n-1})^2 + (y_n - y_{n-1})^2 + (z_n - z_{n-1})^2} \end{array} \quad (4.2)$$

Using the (*s*, *x*), (*s*, *y*) and (*s*, *z*) pairs for each point that defines the centerline and the respective arc length value, three separate 5th order B-Spline functions were created *X*(*s*), *Y*(*s*), and *Z*(*s*). In order to avoid "over-smoothing" a tolerance equivalent of the original angiogram voxel resolution was used in the spline fitting. This yielded an array as shown in Equation (4.1) which was used for curvature calculations

$$r(s') = [X(s'), Y(s'), Z(s')] \quad (4.3)$$

where *s'* a is new arc length array from 0 to the length of the vessel in 0.2 mm increments. Each of the three splines was evaluated for this new array. Figure 4.3 shows an example of how each of the coordinates were fit to the arc length and a comparison of the original data points with the new smoothed centerlines.

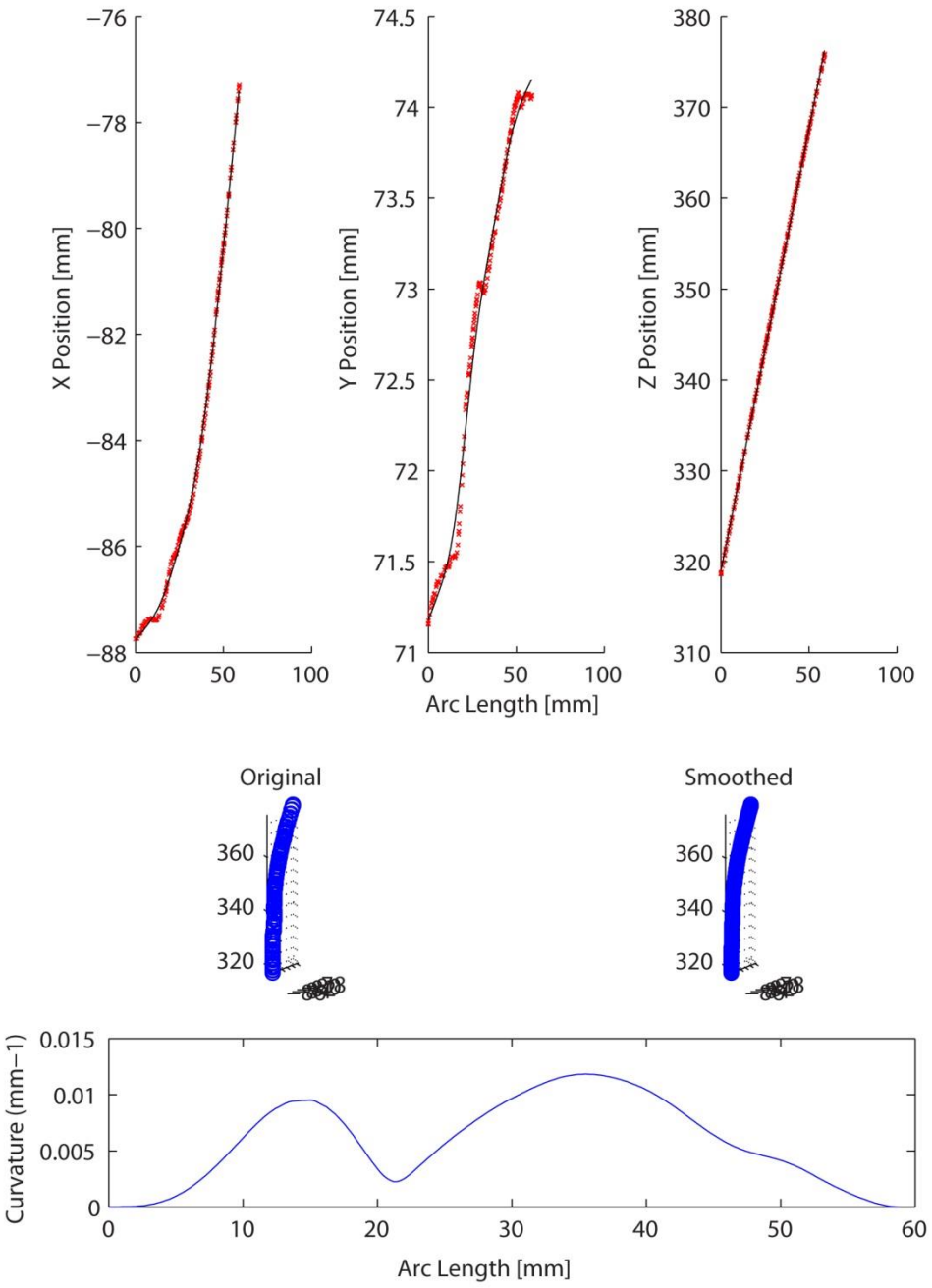

Figure 4.3 Centerline Spline Fitting and Curvature Calculation.The three plots at the top of the image show the original *x*, *y*, and *z* coordinates plotted in red as a function of their arc length. The black lines show the f 5th order B-Spline for each dimension evaluated at the equally incremented arc length array. The central panel shows the original vessel centerline (left) compared to the fitted and smoothed centerline (right) indicating a minimal loss of data integrity while reducing the noise. The plot at the bottom of the figure shows the curvature (method described below) calculated at each of the points in the smoothed centerline using Equation 4.3.

Curvature Calculation

Given the functions described above, we computed the curvature using the Frenet Serret theorem :

$$\kappa = \frac{|r\prime(s\prime)\times r\prime\prime(s\prime)|}{[r\prime(s\prime)]^3} \tag{4.4}$$

Where $r'(s')$ and $r''(s')$ are the first and second derivatives respectively of the fits X, Y, and Z described above and s' is the new arc length array evenly distributed by 0.2mm.

Radius Calculation

We first subdivided the segmentation surface into approximately 80,000 points. Then, using the centerline fits described above, a cross sectional plane was defined according to the equation for each centerline point has:

$$X(s) * \frac{dX}{ds} + Y(s) * \frac{dY}{ds} + Z(s) * \frac{dZ}{ds} + (X(s'), Y(s'), Z(s')) \cdot \left(\frac{dX}{ds}, \frac{dY}{ds}, \frac{dZ}{ds}\right) = 0 \tag{4.5}$$

where $(X(s'), Y(s'), Z(s'))$ are the coordinates of the point on the centerline & $\left(\frac{dX}{ds}, \frac{dY}{ds}, \frac{dZ}{ds}\right)$ correspond to the values of the centerline's tangent vector at this same point. This tangent vector is determined by the first derivate of the spline functions for each dimension. We then found points on the segmented surface that were within 0.25mm (a half the width of the segmentation voxel). Any points that fit fell within this margin were considered to be a part of the cross section at the centerline point used to define the plane. We then calculated the average radius for each cross section. In this way we were able calculate a continuous measurement of the radius along the length of the vessel.

Comparison Between Men and Women

The arc length of the entire vessel, starting from the renal bifurcation and ending at the start of the iliac bifurcation, was used to discretize each individual volunteer's aorta into 10 equally spaced bins. In this way, we could compare equivalent positions from one volunteer to the next. For example, the second bin in volunteer A would be the same relative position along the vessel as the second bin in volunteer B and would cover the 10^{th}-20^{th} percent of the aorta's total length. This allowed us to compare the average vessel radius and curvature at various positions along the length of the aorta to help discern the longitudinal differences in these parameters between the sexes while also reducing the influence of any noise in the data by averaging. We performed statistical comparisons in each of the ten bins for both curvature and radius, controlling for the repeated values from an individual volunteer by assessing the number of effective measures as described previously.[152] We then evaluated the relationship between average aortic radius and height and weight for each volunteer.

4.4.3 Wall Shear Stress Calculation

For each of the volunteer's acquired PCMR image sets we quantified the wall shear stress as a function of time in the cardiac cycle around the vessel's circumference using the methodology described in the previous chapter. We then computed the time averaged WSS (TAWSS) for each of the 80 time versus WSS graphs and the time averaged WSS magnitude as defined by

$$TAWSS = \frac{1}{T}\int_0^T |\tau| dt \tag{4.6}$$

where T is the length of the cardiac cycle and τ is the wall shear stress waveform.

To account for a range of both size and length of the abdominal aortas of the volunteers in our group, we mapped the sector flow and WSS data from each of the volunteers to a normalized matrix so that equivalent positions from each volunteer were being appropriately compared.

The location of each PCMR image set was determined in reference to the angiogram data described above. Using the Slice Location field in the DICOM header of the image set, the top axial position of the aorta (identified as the first angiographic image inferior to the renal artery bifurcation) and the bottom axial position (defined as the beginning of the iliac bifurcation), the axial location of the PCMR image set was quantified as a percentage of the total aortic axial length. This percentage was then identified as being in one of 10 equally spaced bins that represent subsequent segment lengths of the abdominal aorta divided into 10% increments. In this way we created a 10x80 matrix in which each of the ten rows corresponded to normalized percentage lengths along the abdominal aorta and each of the eighty columns was a normalized circumferential position indexed from the left most part of the vessel and moving towards the posterior.

This matrix was determined for each volunteer using all acquired slices for a volunteer. In some volunteers, we were not able to acquire a unique PCMR slice for each of the ten bins. When this was the case we filled in missing slice information using a two-dimensional interpolation method. In this method, each node in the matrix missing shear stress data was assumed to be related each of its neighbors. The missing data was then extrapolated from these relationships so that it would be consistent with its neighboring nodes. We confirmed that this method resulted in a less than 5% difference from calculated WSS values in volunteers for whom we had PCMR data for all 10 bins.

Because flow is a primary input for our method, we examined the relationship between flow and WSS in a sex-dependent manner. We used the flow wave forms for the quadrants used to calculate the WSS, and quantified net forward and reverse flow volumes. We applied the same methodology for both forward and reverse flow volumes to make direct comparisons between forward or reversal flow and resultant OSI or time averaged WSS magnitude to assess the influence of reverse flow on each of these WSS paramaters.

4.4.4 Comparison of WSS with Geometry

To assess the relationship between the differences we observed in the radius measurements between men and women and the differences in OSI, we plotted average radius along the length of the aorta and the average OSI over the entire aorta wall for each volunteer. For each volunteer, we also compared the average radius for each PCMR slice location against the average OSI at this level. These two analyses allow us to compare the OSI to the radius on both a global and local level.

Because curvature affects how oscillatory shear is distributed around the circumference, we quantified the relative difference of oscillatory shear between the site of peak OSI and minimum OSI around the circumference. For each volunteer we smoothed the OSI map around the circumference of the vessel by averaging over each circumferentially adjacent $1/10^{th}$ of the vessel. We then calculated the relative percent difference as the difference between the peak and minimum OSI averaged values normalized to the peak OSI value for each of the 10 bins along the length of the vessel. We calculated this for each of the OSI maps derived from PCMR images and plotted these values against the curvature at the same longitudinal location.

4.5 Results

4.5.1 Differences in Aortic Geometry

Figure 4.4 shows the aortic curvature and radius comparison between our male and female volunteers in each of these normalized bins. We also showed that the height of our volunteers weakly correlated with the average radius of the aorta with an $r^2=0.62$, however, we did not find any relationship between aortic radius and volunteer weight ($r^2=0.014$).

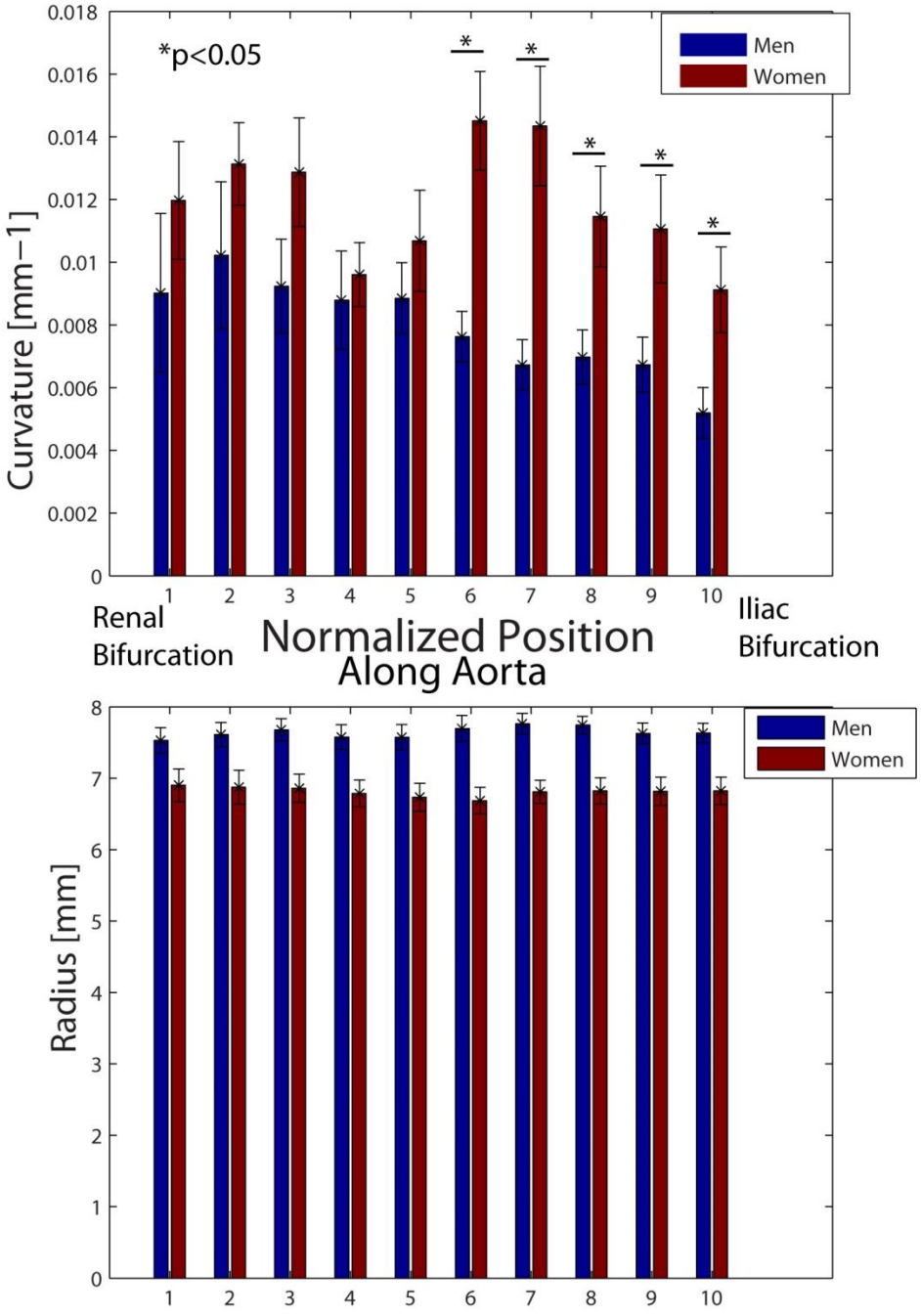

Figure 4.4 Differences in Aortic Radius and Curvature Between Men and Women. The top bar graph shows the average and standard errors for the curvatures in each of the bins. Our results indicate significant differences between the aortic curvature in the distal half of the vessel only with women having a larger curvature in the vessel We also found significant differences in every bin when comparing the aortic radius with men having a larger aorta. The size of the vessel appeared to remain constant along the length of the vessel, however.

4.5.2 Differences in Hemodynamics

In comparing aortic flow profiles between men and women we found a significant reduction in flow reversal in women when compared with men at each point in our normalized matrix. Figure 4.5 summarizes these results.

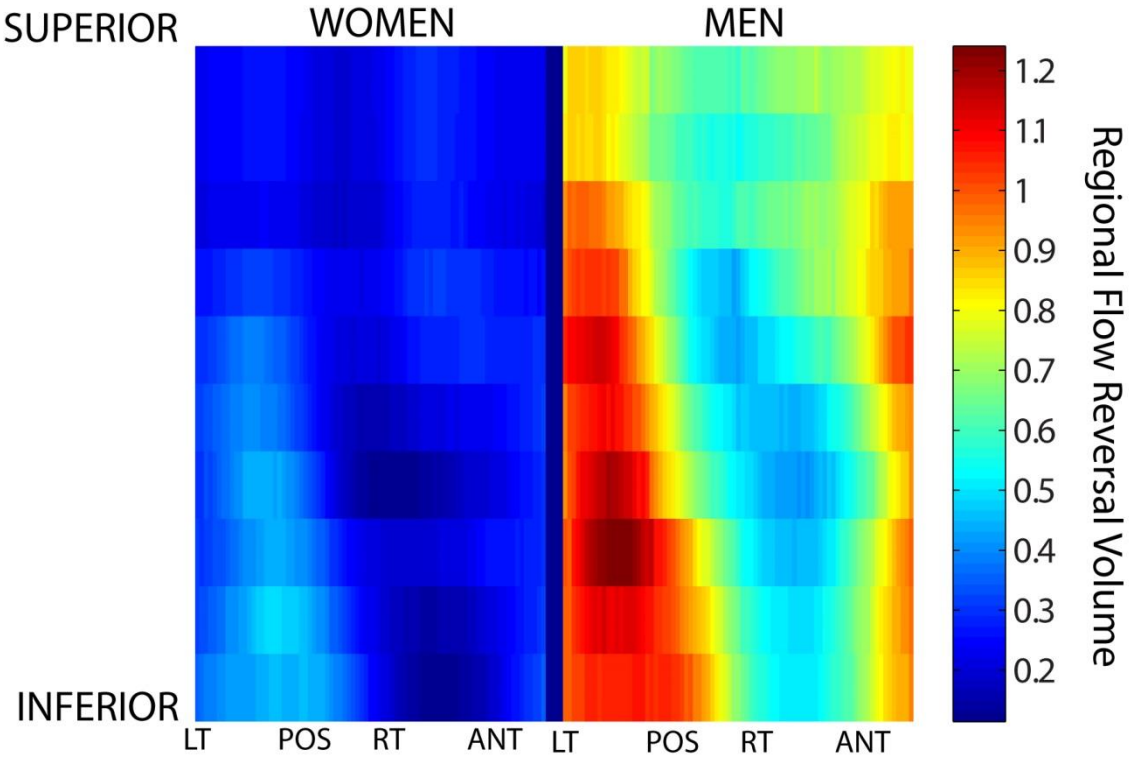

Figure 4.5 Regional Flow Reversal Differences Between Men and Women. Flow reversal is significantly reduced at all points in the female abdominal aorta compared with men as quantified by overlapping sectors around the circumference. Both men and women have the same spatial pattern of flow reversal changes, however, with the inferior and posterior of the vessel exhibiting the highest degree of reversal.

Figure 4.6 shows the average of for our male and female volunteers' calculated OSI on this normalized matrix. We performed a t-test for each parameter first globally (controlling for number of repeated measures), as well as on a point by point basis. In total the average OSI in men was significantly higher in men than women. On a point by point basis, this difference in OSI was also true at every point in the aorta.

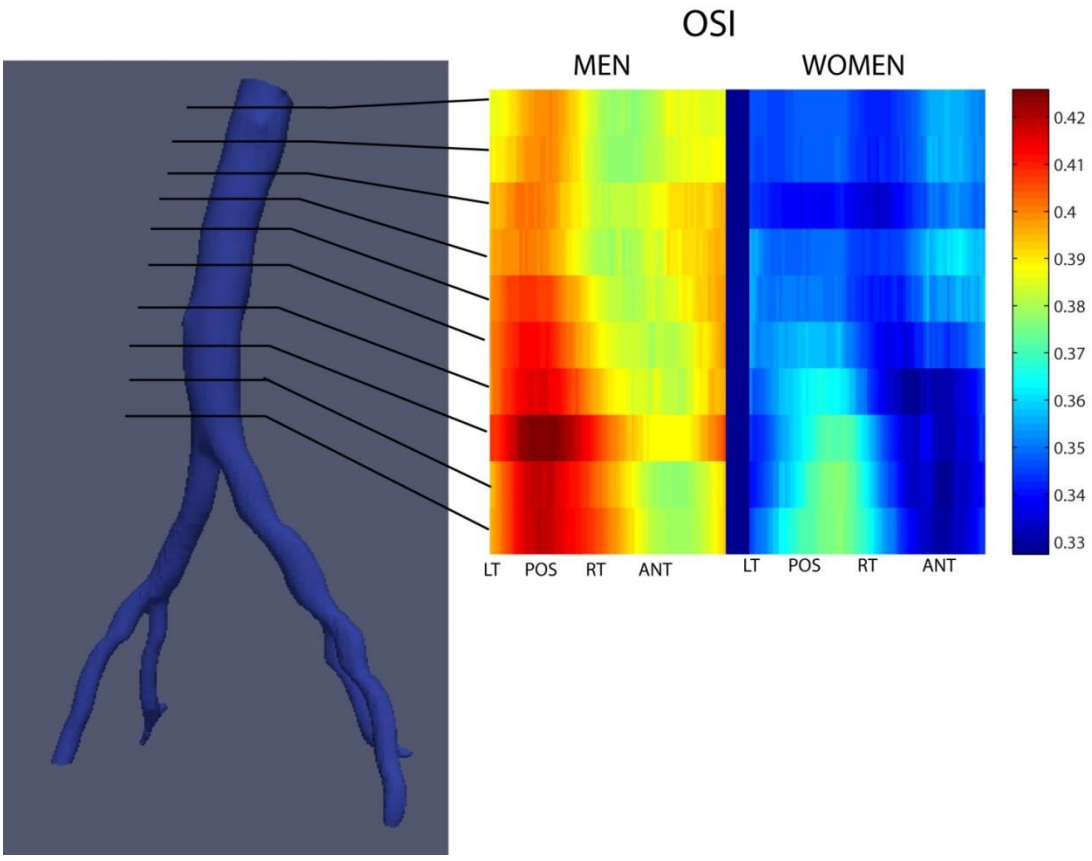

Figure 4.6 Differences in Aortic OSI Between Men and Women. The comparison shows the significant reduction in OSI in women when compared with men along the length of the aorta as well as around the circumference. This difference was significant on both a global and individual element basis.

We also showed that there were no significant differences in the time averaged WSS magnitude between men and women, however there were positional differences. Average WSS magnitude was highest in the superior anterior region of the vessel. These results are summarized in Figure 4.7.

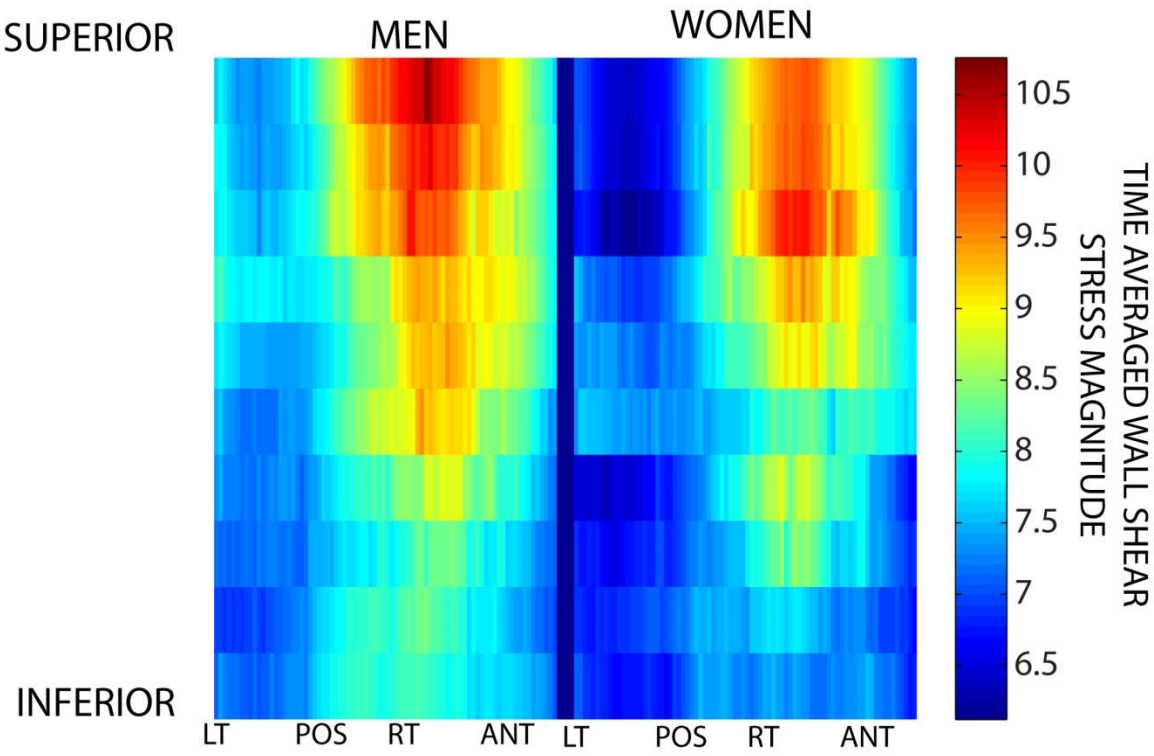

Figure 4.7 Similarities in Time Averaged Wall Shear Stress Between Men and Women. This figure summarizes our results showing no significant differences in the time averaged WSS magnitude between men and women.

Because flow is a primary input for our wall shear stress method and we noted significant difference in the extent of flow reversal, we looked to see what relationship would exist between our OSI measurements. Further we wanted to determine if the differences we observed in WSS were due only to differences in flow magnitude. For each of the OSI values calculated above, there is a corresponding flow waveform created from the PCMR data. We quantified the net forward volume and reverse volume for each volunteer using these flow waves and then plotted these values against the resultant OSI measurement. These results are summarized in Figure 4.8.

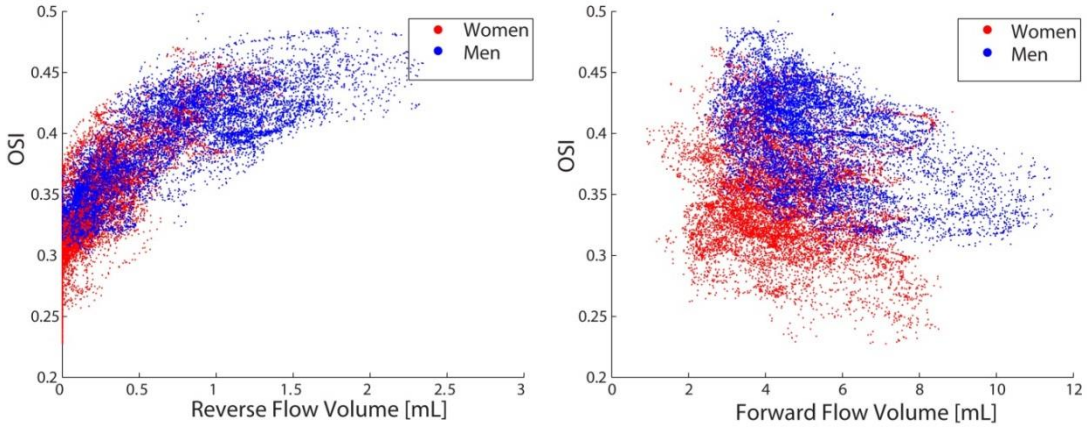

Figure 4.8 Relationship of Flow Volumes with Aortic OSI. For each volunteer, we quantified the reverse and forward flow volumes from the flow waves of each of the 80 sectors used to create the wall shear stress map. This figure is a plot, stratified by men and women, of each of these volumes compared to the OSI value calculated for that sector. We noted that on average, women tended to have a lower forward volume, and lower reverse volume than men. However, the OSI is much more dependent on reverse flow volume than on forward volume for both men and women.

4.5.3 Relationship of Geometry to Wall Shear Stress

Figure 4.9 shows the relationship between global OSI average and average radius for each volunteer divided by sex as well as a plot of the local calculated radius against the average OSI for each acquired PCMR slice. In both cases we observe an increase in the OSI with an increase in radius with weak correlation coefficients.

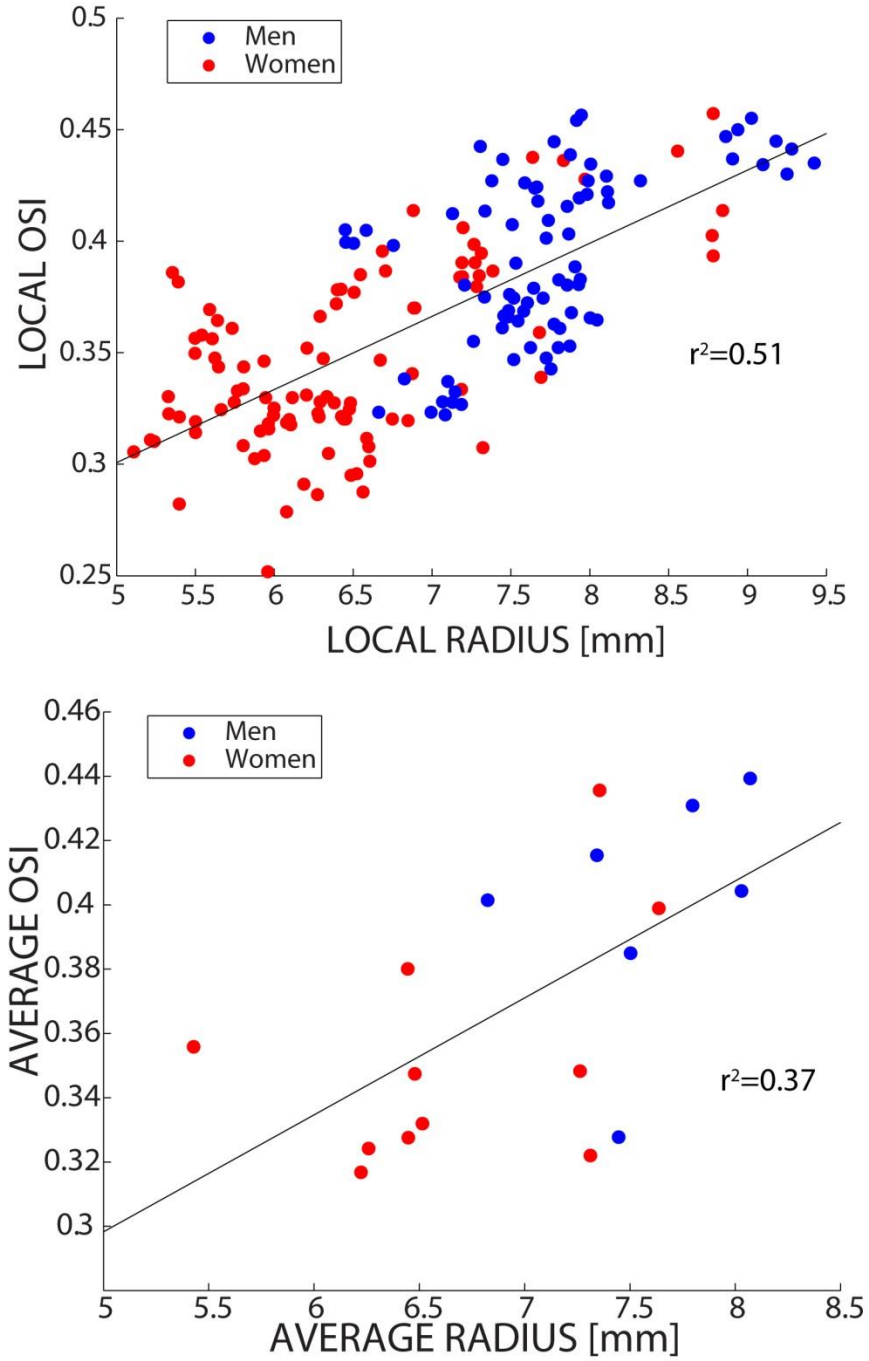

Figure 4.9 Relationship of Radius with Aortic OSI. The bottom panel of this image shows the moderate positive correlation between an increase in average aortic radius and average OSI over the entire aorta. The top panel breaks down this global average into local radius values plotted against the average OSI for the equivalent 10th percentile bin. The local comparisons seem to confirm the positive correlation between these two parameters.

The relationship between curvature and OSI is more complex, however, and we do not expect there to be a direct relationship between the curvature of a vessel and the average OSI as the curvature influences the distribution of the vessel increasing the OSI on the inner curvature relative to the outer curvature. We plotted the relative difference of OSI as described in the methods against the local curvature. Our results are summarized in Figure 4.10. We then plotted only the results from the distal half of the vessel in the second half of Figure 4.8 as this is where we saw differences in the curvature of the vessel.

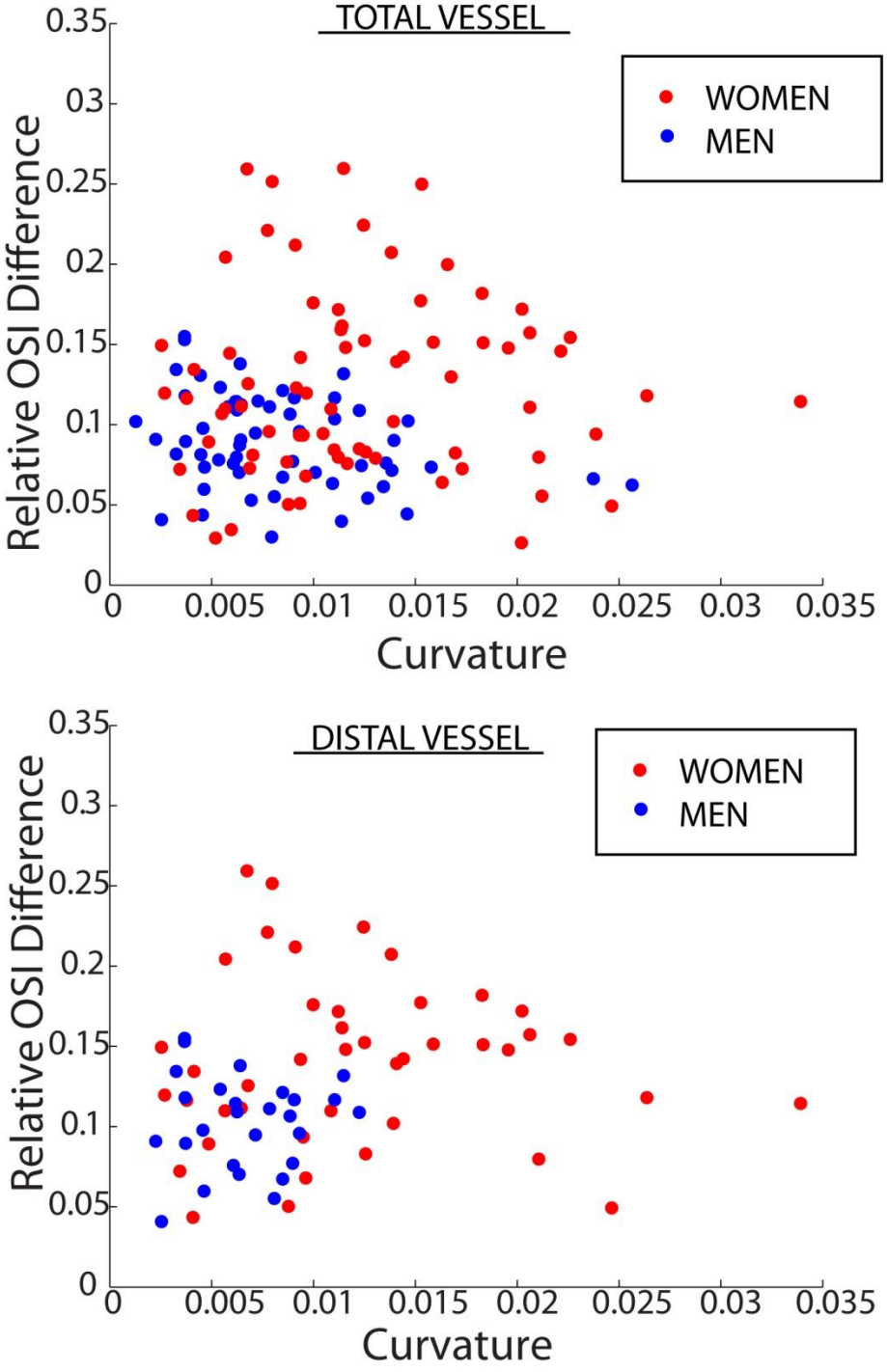

Figure 4.10 Influence of Aortic Curvature on OSI. This figure summarizes our results comparing the relative OSI difference between max and minimum OSI in a 10th percentile bin to the local curvature in that same bin. While there did not appear to be an obvious relationship between the two parameters, we did note that women appeared to have a higher relative OSI difference than men. In parsing out just the distal values, we noted that this seemed to be specific to the distal portion of the aorta.

Because there appeared to be a higher relative OSI difference in women than in men, we looked at this average difference in the proximal aorta and distal aorta and, using a two tailed t-test, found that the greatest relative OSI difference was in the distal female aorta. Our results are summarized in Figure 4.11.

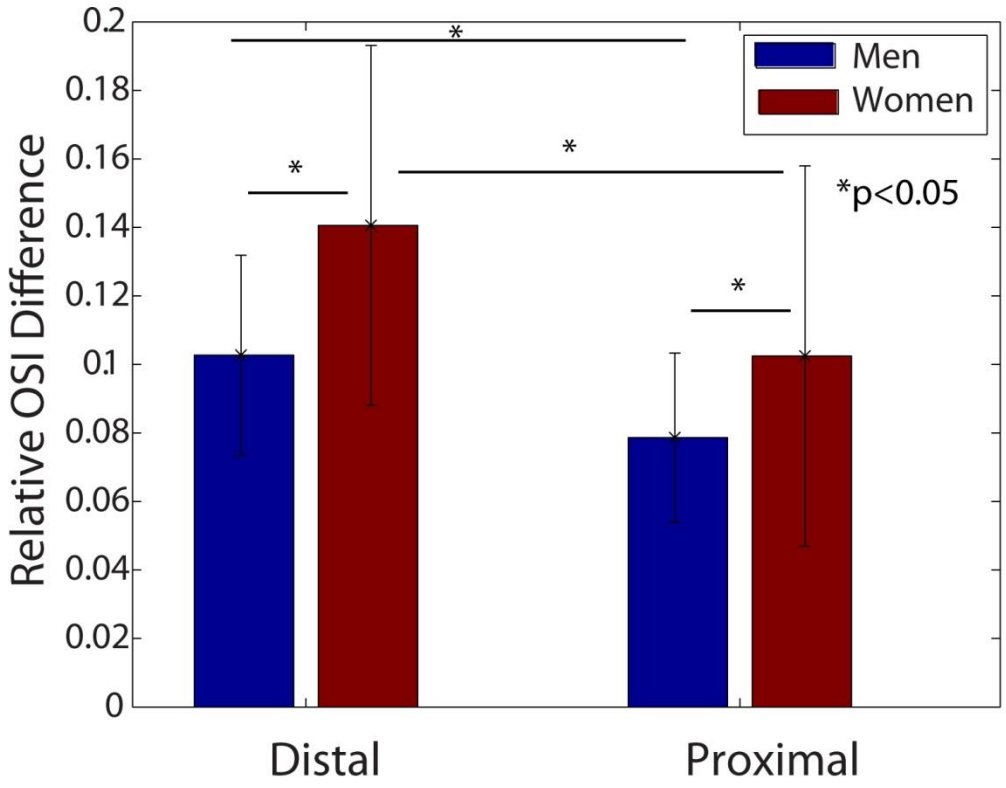

Figure 4.11 Increases in Relative OSI in the Distal Aorta. Women have a higher Relative OSI difference than men in both the distal and proximal regions of the vessel. For both sexes, there is an increase in relative difference in the distal compared to the proximal.

4.6 Discussion

In this study we showed a significant increase in the curvature of the distal abdominal aorta in men when compared with women and a significantly larger radius in men. We also showed that men have a higher estimated OSI than women, a result which correlates with the increase in flow reversal in men compared with women. Despite this

difference in OSI, we did not observe any difference in time averaged WSS magnitude between the sexes.

4.6.1 Differences between Men and Women in Radius and Curvature of the Abdominal Aorta

In our evaluation of aortic geometry, we compared both radii and curvature between men and women and noted significant differences in each of these measurements. Our results show that men on average have a larger aortic radiys when than women along the length of the aorta. This result confirms previous studies using MRI which evaluated the radius of the aorta for a single axial position in these populations.[153] This result is important because it reaffirms that the use of abdominal aortic size in assessing and diagnosing AAA may not be appropriate in women.[15, 18, 68] Specifically, if women have a smaller aortic radius at baseline before disease develops, than a diameter of 4cm in the aorta of a woman is a larger relative dilation than a diameter of 4 cm in a man. If possible, an important study would be to monitor the size of the abdominal aorta in women who are at risk for developing AAA (smokers, those with a family history, and some of the factors identified in this work) to evaluate how the diameter changes with time. This would allow for a determination based on percent increase in diameter to assess the development of AAA.

The curvature of a vessel can significantly influence the distribution of oscillatory shear, elevating the OSI on the inner curvature. In the abdominal aorta, previous work has shown an increase in OSI on the posterior of the vessel which corresponds to the inner curvature.[37, 148] We proposed that the curvature in the abdominal aorta may be different between men and women as a result of the differences in lumbar spine and pelvic anatomy. In comparing curvature, we noted significant differences only in the distal half of the abdominal aorta. Values obtained for our curvature measurements in this age group are similar to the range reported in a previous study where results were not

analyzed by sex[154]In addition to a potential impact on the hemodynamics, this difference in curvature may be important in how women are treated surgically. It is known that women have worse outcomes from endovascular aneurysm repair (EVAR) than men. [17] Because many of the trials assessing the efficacy of endovascular repair are performed in men, it is possible that these procedures are optimized for male aortic geometry which, as we've shown, is different than women.[155] No work has been reported on how differences in curvature may influence the risk of rupture or procedure outcome, however, it presents an interesting expansion of our results.

4.6.2 Differences in Aortic WSS Profiles and the Relationship to Flow

In this study we successfully implemented the 2D PCMR WSS methodology we developed in 27 volunteers. We showed that we can resolve differences in WSS around the circumference and along the length of the aorta between the two populations with this method. Our results indicate that men experience higher oscillatory shear at all locations in the aorta when compared with women. This finding supports our hypothesis that, prior to disease development, men are exposed to biomechanical forces that increase their risk for abdominal aortic aneurysms. Our observation could help to explain the results of a post mortem analysis which showed an increase in pre-atherosclerotic lesions of the aorta in men compared with women in a similar age group.[156] To our knowledge, no previous work has shown that the aortic WSS differs between men and women in a healthy population. It remains unclear if this difference underlies the observed difference in risk of disease development. To confirm this connection, more work into the early biomechanical risk factors for AAA should be performed. Currently, much of the biomechanics studies in this disease are focused on risk of rupture while initiating pathophysiological factors remain unexplored.[157-159]

With our method to quantify WSS, flow is a primary input and in our assessment of the relationship between reverse flow volume with OSI and forward flow volume with

OSI, we found a strong relationship between the extent of flow reversal and the resultant OSI. We found no identifiable relationship between forward flow volume and OSI however. When stratified by sex, we observed that women had a lower degree of flow reversal at all locations in the abdominal aorta. Although we observed a reduction in the average forward flow volume for women when compared with men, this difference did not appear to correlate with our observations in OSI differences.

4.6.3 Relationship of Geometry Findings to Observed Differences in OSI

We assessed the influence of the observed differences in curvature and radius on the measured OSI. Our first evaluation of the average radius along the length of the aorta and its relationship to the average OSI around the entire circumference showed a positive correlation wherein a larger vessel radius correlated with a greater OSI. While most of the higher radius measurements came from our male volunteers, it is important to note that there were some female volunteers who had larger aortas as well and their OSI values were also higher. This is interesting because a larger radius does not necessarily imply a larger degree of flow oscillation. We would expect this larger radius to be more closely related to differences in the peak shear stress which we did not include in our analysis as it is not expected to contribute AAA risk.

With the greater curvature of the aorta in women over men, we expected to find that women would also have a larger difference in the anterior-posterior OSI values. On average there was an increase in difference between the maximum and minimum OSI values relative to the maximum OSI value in the distal aorta for women over men. This implies that there is a larger heterogeneity in the OSI around the circumference in women than in men, which is expected if the curvature is greater. It is possible that for women, this could translate into a greater propensity for developing early aortic disease in the posterior vessel relative to the anterior when compared with men however the overall reduction in OSI in women still decreases their risk relative to men. Previous studies showing that the early increases in intimal medial thickening happen in the posterior

vessel preferentially did not include a sex-based analysis.[98, 148] Such an analysis may be warranted to further the understanding of early pathophysiological differences in aortic aneurysms between men and women.

4.6.4 Summary

This chapter presents novel observations about the differences in aortic shear and geometry between men and women. The greater oscillatory shear in men vs. women would increase the risk for early vascular disease that is proposed to underlie the early stages of AAA development. This greater oscillatory shear correlated strongly with the extent of flow reversal in the vessel and the women in our study demonstrated a lower volume of flow reversal when compared with men. For both men and women, larger aortic radius correlated with a greater oscillatory shear. If this relationship were truly causal and size of the vessel were best predictive of aneurysmal development and disease, we might expect that no women under a certain threshold would experience AAA. However, given that women who develop aneurysms often develop smaller dilations than men and are at a higher risk for mortality, size cannot be the only determining factor. Finally women have a larger curvature in the distal aorta which may create differences in the shear distribution that affect how early disease forms preferentially. Additionally, such differences in geometry could be important surgical considerations for those women who go on to develop the disease as most of the vascular treatments are based on trials done almost exclusively with men. We believe that these findings may help further the understanding of how this disease pathophysiology differs between men and women.

CHAPTER 5

MODULATION OF UTERINE BLOOD FLOW INFLUENCES AORTIC HEMODYNAMICS IN WOMEN

5.1 Introduction

Among the many factors controlling the hemodynamic patterns in a vessel with pulsatile flow, distal resistance is one of the most important. For example, high systemic peripheral resistance leads to an elevated systolic pressure against which the left ventricle must pump. The increase in pressure leads to pathological remodeling of the heart.[160] Similarly, in the setting of pulmonary hypertension, the right ventricle will remodel as a result of high resistance in the lung arteries. [161]

In the abdominal aorta, however, there are multiple outlets and networks into which blood can flow. The renal arteries supply blood to the kidneys which, in a healthy state, exhibit a low resistance network to promote perfusion throughout the cardiac cycle. A second outflow for the abdominal aorta is the inferior mesenteric artery which supplies part of the bowel with blood. This second outlet receives considerably less flow than the two primary outlets: the renal and the common iliac arteries. The common iliac arteries provide flow to the pelvis and lower limbs after bifurcation into the internal and external iliac arteries respectively. Outside the physiological condition of exercise, the resistance of the iliac arteries is generally higher than the renal arteries. It is the result of this disparity in resistance networks at the superior and inferior regions of the abdominal aorta that generates the oscillatory flow normally observed between these outlets.

Conditions that affect these arterial networks and the organs they supplycan impact the abdominal aorta. For example, previous work has shown that inflating a blood pressure cuff above the knee to pressures above normal systolic values will significantly impact abdominal aortic hemodynamics. [100] Specifically, there is an increase the

extent of oscillatory shear, a known inflammatory biomechanical mechanism. This is of particular interest because patients with above the knee amputations are known to be at significantly elevated risks for developing an abdominal aortic aneurysm.[99, 162] It is reasonable therefore to posit that the elevation in peripheral resistance may be what promotes an increase in exposure to pro-inflammatory biomechanical conditions and therefore increase risk of disease. Such a hypothesis can be bolstered by evidence showing the high co-incidence of abdominal aortic aneurysms with peripheral arterial disease (PAD), in which lower limb arteries are significantly atherosclerotic and present a fairly high resistance network.[101, 102] It is possible, however, that this second association is a result of the relationship between smoking and the risk of these two diseases. A patient cohort known to have an increase in risk for AAA are patients with spinal cord injury (SCI).[163] With these patients there is decreased blood flow to the lower limbs as a result of decreased innervation and muscular activity further supporting the hypothesis that increases in peripheral resistance affect the abdominal aorta in a way that promotes AAA formation.

While each of these conditions is associated with changes in the external iliac artery, little has been done to evaluate what influence, if any, the resistance of the internal iliac artery may play on aortic hemodynamics and disease. When comparing the aortic WSS profiles of men and women this question is of particular importance because the anatomy supplied by the internal iliac artery is significantly different between the sexes. The presence of the uterus in a woman changes the resistance profile of the internal iliac arteries dramatically as the uterine artery is one of the only arteries in the periphery to exhibit no flow reversal, except in the case of pre-eclampsia in which there is elevated spiral artery impedance.[164] Interestingly, population studies have shown that a women's reproductive history has a relationship with the risk of developing an AAA. Non-parous women are more likely than those women who have been pregnant and given birth to develop an aneurysm. [22]While it's possible that hormonal status may play a

role in this observation, it is also known that pregnancy can increase uterine artery flow by a factor of 50.[165] Given this observation and the fact it has also been shown that hormone replacement therapy (HRT) has no significant effect on reducing the development or progression of AAA in women([19]), we propose that this protective effect of previous pregnancy may be due to the changes in hemodynamics in the pregnant women with a reduction in uterine artery resistance as the placenta develops.

In this aim, we elected to explore how changes in peripheral flow as measured by PCMR, particularly in uterine artery & pelvic flow may mediate aortic hemodynamics. We identified two patient populations whose conditions we would expect to either increase or decrease uterine artery flow. First, we looked at women with uterine leiomyomas, commonly called fibroids, which are non-malignant tumors in the uterine wall which are known to be highly vascularized and very low resistance due to the leaky nature of the tumor's blood vessels. The treatment for this condition is highly dependent on its very low resistance. Second, we studied women who had undergone hysterectomies (often with fibroids as the indication for surgery) but retained normal ovarian function. This second group would present an increase in the internal iliac artery resistance as the low resistance vessel network in the uterus would no longer receive blood flow. With these two populations and our healthy controls we sought to identify a correlation between changes in peripheral flow, specifically changes in the uterine artery, and aortic WSS profiles. We hypothesized that a reduction in internal iliac artery oscillatory flow would correlate to a decrease in aortic OSI.

5.2 Methods

5.2.1 Study Population

To accomplish this aim we used the volunteers described in Chapter 4 for our control population. Of this group, there were 7 men and 5 women for whom we had both aortic and peripheral flow data. We recruited 12 women with symptomatic fibroids

requiring intervention and 4 women who underwent a hysterectomy within 6 months prior to their enrollment in our study.

5.2.2 Phase Contrast MRI

PCMR images were acquired at approximately the midpoint of the abdominal aorta between the renal artery bifurcation and the iliac bifurcation in our volunteers. Additional phase contrast images were acquired for each of the common iliac daughter vessels, i.e. the left/right internal and external iliac arteries. When possible, all four arteries were acquired in a single phase image set, however, many volunteers required more than one acquisition to reliably identify the lumen of each vessel through the cardiac cycle. Parameters for the phase contrast images were as follows: TR of 39.85s, TE of 3.39s, Flip Angle of 30°, FOV of 255x340 mm^2, resolution of 1.3281x1.3281x5 mm^3, venc of 150cm/s, yielding 30 time step images across the cardiac cycle.

5.2.3 Wall Shear Stress Calculations.

Using the method described in Chapter 2, we quantified OSI around the circumference of the aorta using the PCMR image series obtained from the midpoint of the vessel.

5.2.4 Peripheral Flow Calculations

For each of the four iliac branches, we used Segment (MEDVISIO) to define the contour of the lumen at peak systole and used the tracking feature to copy and track the contour to each of the remaining 29 frames. Each frame was reviewed and if necessary, manual adjustments were made to correct the lumen definition. Flow waveforms (flow vs time) were created using the velocity values for each pixel. The net forward and reverse volume for each wave was calculated as the area under the curve above and below the x-axis respectively as seen in Figure 1 below. The Oscillatory Flow Ratio (OFR) was then calculated as the ratio of the net reverse volume to the net forward volume.

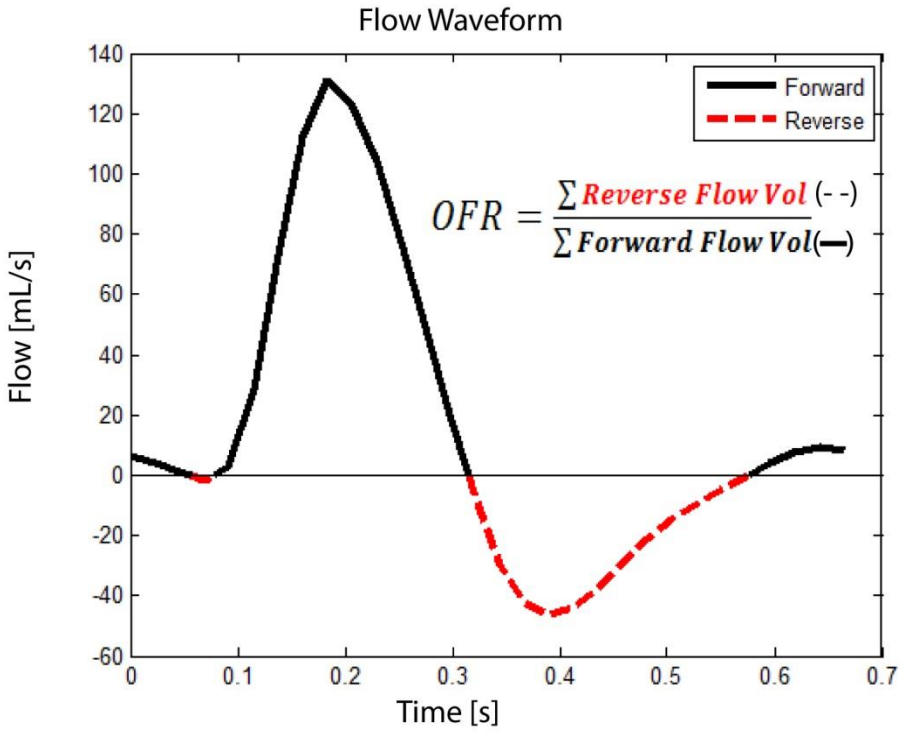

Figure 5.1 Calculation of Oscillatory Flow Ratio. We quantified the Oscillatory Flow Ratio (OFR) as described in the figure as a proxy for the resistance in our peripheral arteries. The positive and negative contributions of the integration of the flow curve for each vessel indicated the forward and reverse volumes through that vessel respectively. We then summed each of these volumes for both the left and right internal or external iliac arteries to assess the OFR for either the internal or external iliac artery. We also evaluate the total peripheral OFR by summing the reverse and forward of all four iliac bifurcations and quantifying the ratio.

We chose to evaluate flow and OFR in the periphery rather than WSS for two reasons. First, the method we described previously to quantify WSS from PCMR would not be reliable in these peripheral vessels because the diameter of these vessels is only 2-4 times greater than the image resolution. Second, we were interested in the WSS in the abdominal aorta because we believe it to be related to early vascular inflammatory processes increasing risk for AAA. By comparison, we were not interested in disease risk of the internal or external iliac arteries in this study (although the role of WSS in PAD pathology is important). For this study, we are only interested in how changes in the flow

profiles (as a proxy measure for resistance) of these peripheral vessels may affect the upstream hemodynamics.

5.2.5 Analysis and Comparisons

We first compared the OSI values around the circumference at the midpoint of the abdominal aorta amongst all volunteers. Because each volunteer will have measurement at the same relative 80 points around the vessel we could average the results of circumferentially equivalent places within each of our four groups. Here, we reported the mean and standard error of each of the four groups at each of the normalized positions.

Next we evaluated the peripheral flow profiles amongst all groups. We quantified forward and reverse flow by direct integration of the area above and below the flow vs time curve respectively in the left and right internal and external iliac arteries for each volunteer. We then evaluated the OFR as the sum of reverse flow in both the left and right internal or external iliac artery divided by the sum of forward flow for the same arteries. In doing so we ignored any differences in vessel flow between the right and left peripheral arterial systems. Comparison of the left and right vessels in each volunteer indicated that there were no appreciable differences in the flow volume or rates between the two sides. For each group we averaged the internal and external iliac OFR values of all patients and made statistical comparisons between each group using a two-tailed t-test. We performed similar comparisons to evaluate how each of the forward and reverse flow volumes in the internal and external iliac arteries differed. This comparison allowed us to assess whether differences in forward or reverse flow were responsible for dissimilarities in the calculated OFR.

Finally, we evaluated how changes in iliac OFR were related to differences in aortic OSI. For each volunteer, we averaged the OSI around the circumference of the aorta and plotted it separately against the internal iliac OFR, external iliac OFR, and the total iliac OFR (quantified as the net reverse volume of all four iliac vessel normalized to

the net forward volume) to look for any relationship. In these evaluations we made purely qualitative assessments of the relationships, though an increase in numbers for all four groups would improve the potential for statistical comparison.

5.3 Results

The wall shear stress profiles around the circumference of the vessel were determined for each of the volunteers of the study populations described above and the OSI was quantified. Figure 5.2 shows the average and stand error of the mean plotted at each normalized circumferential position for each of our populations.

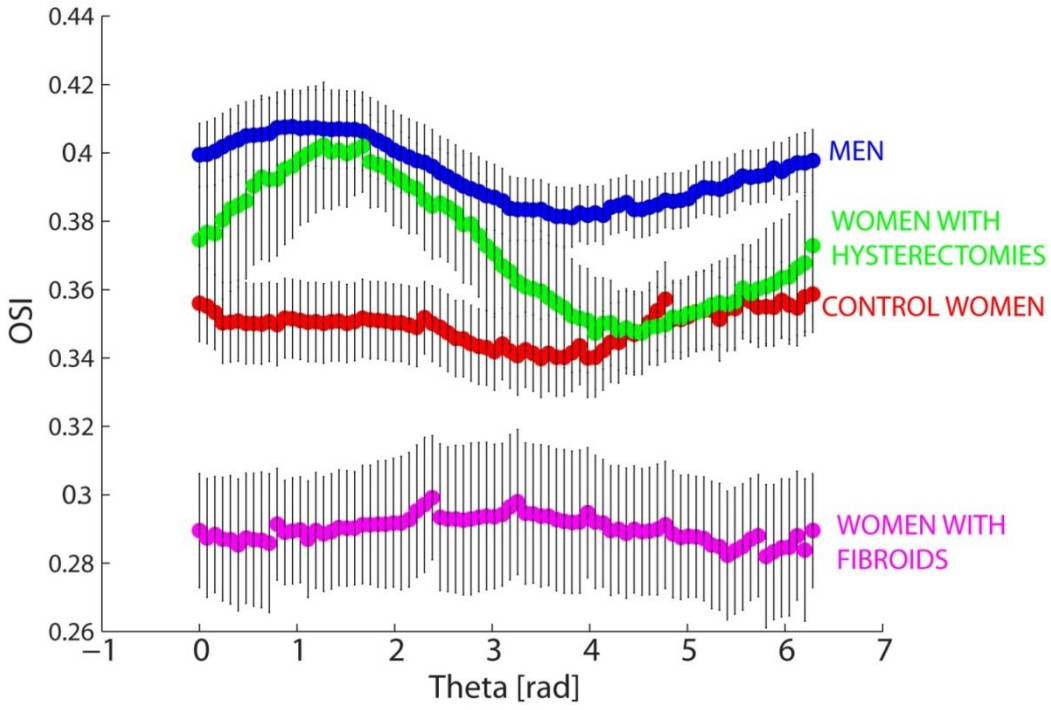

Figure 5.2 Circumferential Differences in OSI Between Healthy Men and Women, Women with Fibroids and Women with Hysterectomy. This figure is a summary of the average OSI values taken around the circumference of the aorta beginning on the left side (theta=0), moving towards the posterior and ending at the left side again (theta=2π) for each of the four groups studied in this aim. The average and standard error of the mean are plotted at each normalized circumferential position for the midpoint of the abdominal aorta. As expected from our results showing differences in aortic WSS between healthy men and women, men exhibited significantly higher OSI than women at all points around the circumference. Our population of women with symptomatic uterine fibroids showed a

reduction in OSI compared to all groups and a much more homogeneous circumferential distribution. Our hysterectomy group appeared to be only significantly different than our patient group with fibroids and while the OSI on the posterior of the vessel is higher than healthy women, the anterior of the vessel is much more similar.

For all the volunteers in each of these four groups, we quantified the OFR for the internal and external iliac arteries. Figure 5.3 summarizes our results showing the average and standard error of the mean for each group. Using a two tailed t test between each population, we found significant differences in the internal iliac OFR of men compared with both control women and with women with fibroids $p<0.05$ and between control women and women with fibroids, as well as a significant difference in the external iliac OFR of men with women with fibroids $p<0.05$.

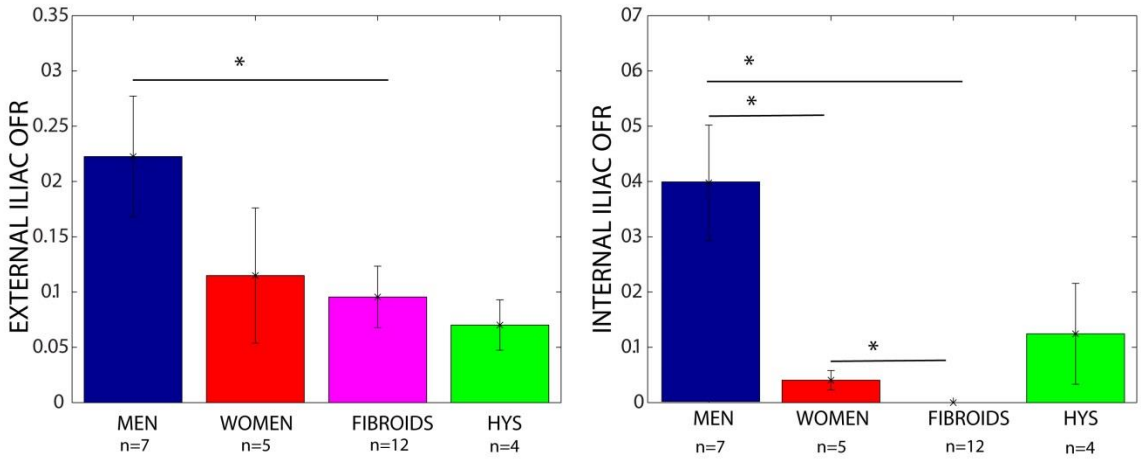

Figure 5.3 Internal and External Iliac OFR Comparisons. We found significant differences between healthy men and women with fibroids in the external iliac arteries. We also found differences between men and healthy women, men and women with fibroids, and healthy women and women fibroids in the internal iliac OFR. While the OFR in the internal iliac artery of our patient group with hysterectomy was greater than in our healthy women group, the difference did not reach significance.

Given the differences we observed in the each of the arteries' OFR values among the populations, we assessed whether differences in the forward or reverse volumes were driving these differences. Figure 5.4 shows our results for the average and standard error of them mean of the forward and reverse volumes of each of the four groups.

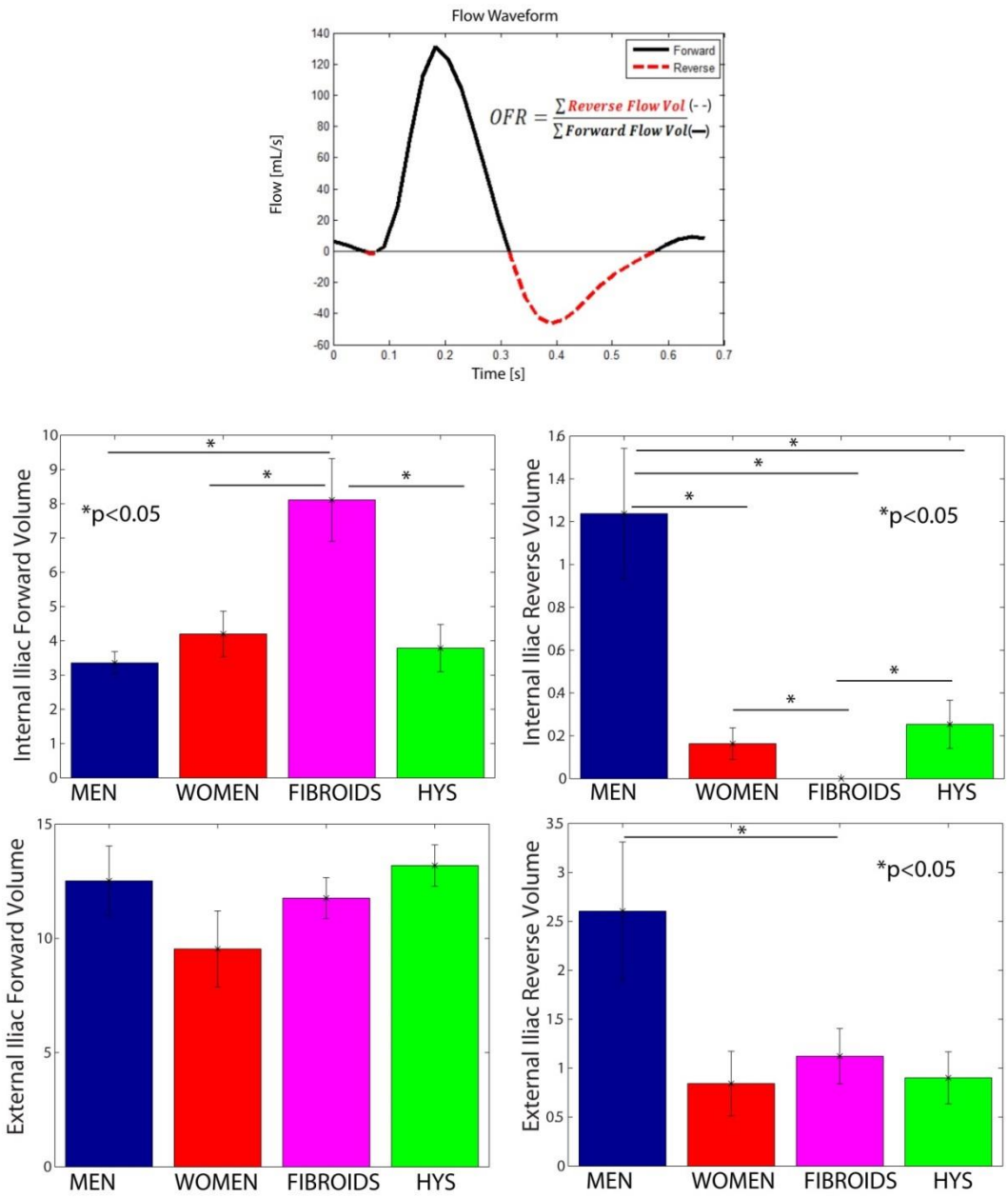

Figure 5.4 Comparison of Iliac Forward and Reverse Flow Volumes. To assess whether changes in the forward or reverse flow could explain differences observed in the OFRs, we evaluated each of these volumes in both arteries amongst all groups. Our subjects with fibroids showed a higher internal iliac forward flow volume and lower reverse flow volume than all other groups. Internal iliac reverse flow volume was different among all group comparisons except for our healthy women compared with women with hysterectomies. There were no differences in the extent of forward flow volume in the external iliac artery however there was a significant reduction in external iliac reverse volume in healthy men compared to women with fibroids.

Finally, we assessed how these differences in peripheral flow oscillations might relate to the average OSI calculated at the midpoint of the abdominal aorta. Figure 5.5 shows the relationship of the internal iliac artery and OSI on the left and external iliac artery OFR and OSI on the right for each volunteer.

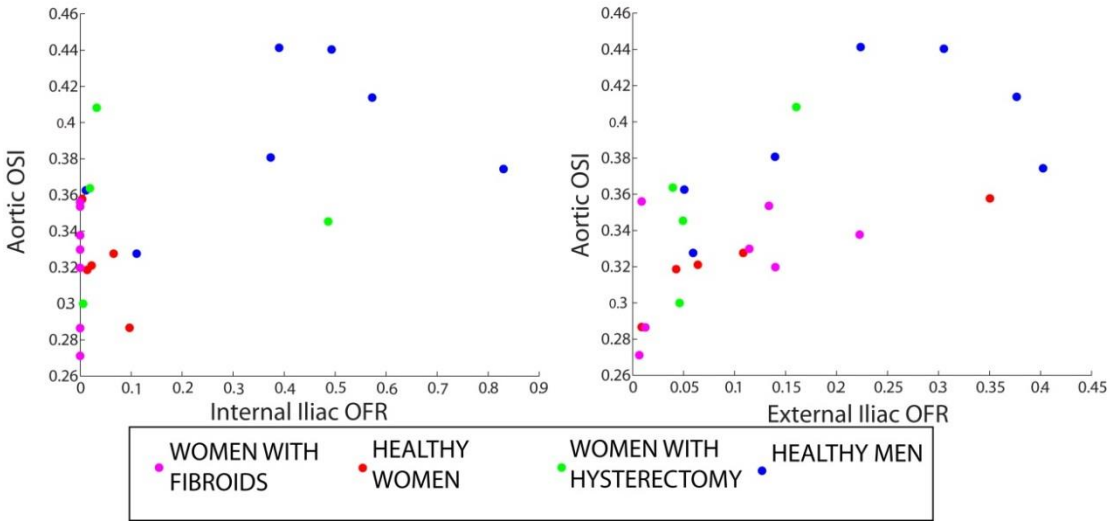

Figure 5.5 Relationship of Internal and External Iliac OFR with Aortic OSI. Our evaluation of Internal Iliac OFR with average aortic OSI around the circumference at the midpoint of the abdominal aorta showed a very weak, almost non-existent positive relationship. There was a slightly stronger positive relationship between the external iliac OFR and average aortic OSI. This is not unexpected given that there is roughly 2-3 times the flow volume through the external iliac artery compared to the internal iliac artery and so it would contribute a larger effect to the upstream hemodynamics.

We then created a combined OFR for both the internal and external artery using the sum of the forward and reverse volumes for all four vessels of each volunteer. We then plotted these values to assess what relationship might exist. We assessed multiple forms of functional fits to this data to assess the best description of the relationship. We found the a two term power function yielded a better goodness of fit (r^2= 0.5830) than a linear fit (r^2=0.4898).

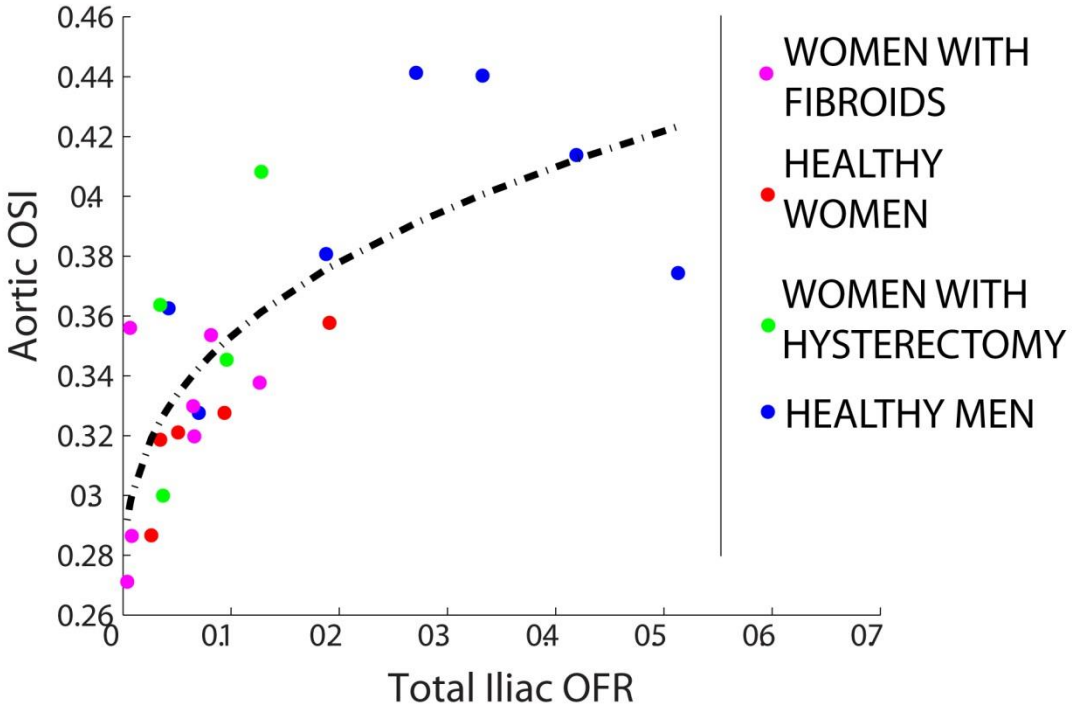

Figure 5.6 Relationship of Total Iliac OFR with Aortic OSI. Creating a combined peripheral OFR that sums both internal and external iliac artery forward and reverse flow volumes, we find the strongest relationship to aortic OSI. The relationship appears to be more linear at lower peripheral resistance and somewhat asymptotic as the peripheral OFR increases. This division also appears to be along sex lines, with the female groups demonstrating a greater change in OSI with smaller changes in peripheral OFR.

5.4 Discussion

The purpose of this aim was to evaluate how peripheral flow might differ between men and women, and to assess if these differences would be related to the observed differences in aortic hemodynamics. The major findings of this aim were that women with uterine fibroids have a decreased average aortic OSI relative to women without fibroids and men, women who have had a hysterectomy show a (statistically non-significant) increase in OSI compared with women with intact uterine architecture, and the aortic OSI in women appears to be more sensitive to changes in peripheral flow oscillations as measured by PCMR compared with men.

5.4.1 Differences in Aortic OSI

In comparing the aortic hemodynamics among these four groups we first found a significant reduction of the OSI at every point around the circumference in our fibroids groups compared with the other three populations. As expected from our work described in the previous chapter, our control women had a reduced OSI compared with our control men. Finally, the hysterectomy group showed no significant differences between either the healthy male or female controls however the observed values were more similar to men in the posterior of the vessel and more similar to women in the anterior. This hysterectomy group also showed the highest degree of heterogeneity in OSI around the circumference compared to the other 3 groups. Given the low number of women with hysterectomies enrolled in the study and the high intra-population variability we observed, it is still possible that this group does exhibit significantly different WSS profiles than healthy women and further study is necessary.

These patient groups were chosen because we expected that the affected peripheral arterial systems would alter aortic hemodynamics that might influence risk for AAA. This phenomenon is observed in patients with spinal cord injuries (SCI) who are at an increased risk for developing AAA.[163] A previous study showed that in these patients there is a reduction in mean aortic flow rates coupled with a decrease in iliac flow rates as well. [103] Patients with PAD are similarly at increased risk for developing AAA.[101] One study showed there are reduced flow rates in many of the peripheral vessels included the common femoral which is the primary daughter branch of the external iliac artery evaluated here.[166] It remains unanswered, however, if this induces an increase in aortic OSI prior to AAA onset.

5.4.2 Differences in Peripheral Flow

Our results indicate, first, that there is a significant difference in the peripheral flow resistance using OFR as a proxy measure. This difference is limited to a reduction in OFR in the internal iliac artery of women when compared with men. When we evaluated

how this parameter changed in the setting of low resistance uterine fibroids, we found a further reduction in the OFR of this group of subjects. When we compare these groups against those women who have undergone a hysterectomy we find that the reduction in comparison to men no longer holds. The increase in OFR in the post hysterectomy group is not significantly different from healthy control women. Collectively, these data indicate that modulation of the uterine artery affects the internal iliac flow profile significantly. It is worth noting that the internal iliac OFR of the post-hysterectomy cohort were not significantly lower than the healthy male group as they were with both other female groups. This reinforces our hypothesis that changes in the uterine artery profile will have an important impact on flow in the internal iliac artery. It is known that with menopause, there are decreases in uterine artery flow which are partly controlled by estrogen status.[167] A previous case control study showed that women with AAA who reach menopause earlier in life have a larger aneurysm. [168] These studies support the trends in our data showing that women with hysterectomy have an increase in flow reversal compared with healthy women in the internal iliac artery.

Because OFR is (as the name suggests) a ratio, we explored if forward flow, reverse flow, or both are driving the differences we observed above. As Figure 4 shows, we found significant differences in some of these volume measurements related to the identified differences in Figure 3. Most notably our patient population with symptomatic fibroids exhibited nearly zero flow reversal in the internal iliac artery. This was significantly lower than all three other groups and was physiologically expected given the very low resistance of the fibroid tumors. Additionally, the reduction in internal iliac OFR in healthy women when compared with men appeared to be driven by a reduction in flow reversal rather than any differences in forward flow. The lack of significant differences in external iliac artery flow volumes was an interesting outcome given that we may have expected differences in flow volumes due to the differences in lower limb muscle and size between the sexes. However a previous study looking at sex and age

dependencies on lower limb blood flow showed that in this age group, men and women had similar hyperemic responses to exercise.[169] This study also showed that older women (60-80 years old) had better preservation of hyperemia than men of a similar age. This observation suggests that changes in external iliac (and consequently femoral artery) flow with age may be another important consideration when evaluating women for increased risk of AAA.

5.4.3 Relationship of OSI to Peripheral Flow Oscillations

Finally, the most significant component of this study was to evaluate how any of these changes in peripheral flow may translate upstream to differences in abdominal aortic hemodynamics. While we hypothesized that the changes in internal iliac artery would mediate differences in aortic shear, there did not seem to be a direct relationship between the internal iliac resistance and the average aortic OSI. We noted a weak relationship with the external iliac artery oscillatory flow but the strongest relationship seemed to arise from a combination of the internal and external iliac artery flow waves. This last comparison is probably the most appropriate given that both arteries are contributing simultaneously to the aortic hemodynamics. Further it appears that this relationship is dependent upon the extent of peripheral flow reversal as a power function best described the relationship between total peripheral OFR and aortic OSI. Our female volunteers (regardless of condition status) all had lower total peripheral OFR than our male group. This suggests that the aortic OSI in women is more sensitive to differences in peripheral flow than it is men. Thus our overall hypothesis that women who experience changes in uterine artery flow either by normal physiologic (pregnancy or early menopause), pathophysiology (tumors) or interventional (hysterectomy) pathways could have an altered risk of aortic disease requires further investigation

5.4.4 Limitations and Future Work

A primary limitation of this study is the relatively low numbers of volunteers in each group of interest when compared to the spread of values we obtained from both patients and volunteers. This is, in part, due to the difficulty of capturing the internal iliac arteries in a cross sectional plane especially in women, for the internal iliac artery must curve posteriorly around the uterus. Further, we did not measure uterine artery blood flow directly, only internal iliac arterial flow. There are other branches of the internal iliac artery supplying the pelvic musculature which may contribute differences between men and women; however, this would not explain the differences we observed with the specific patient populations we chose.

An ideal next step for this work would be an intra-volunteer comparison of women with fibroids after each patient has had her embolization procedure as well as a comparison of women prior to and after their hysterectomy. This experiment would allow us to assess the changes in peripheral flow when only uterine blood flow has been altered. Additionally, this would allow us to further delineate the role of pelvic flow and its influence on arterial flow. Another follow up study would be the evaluation of conditions such as early hysterectomy, both with and without ovarian function retention, and the relationship with AAA development. A literature search reveals no such population analysis, however, the low incidence of AAA in women and the declining use of hysterectomy in young women may make such an evaluation difficult. A final worthwhile study would be to look at how uterine flow changes at the peri-menopausal and post-menopausal time may affect aortic hemodynamics as we expect changes in peripheral vasculature at this time in a women's life to correlate with the increase in risk for AAA.

CHAPTER 6

AORTIC WALL DISPLACMENT AND STRAIN AS MEASURED BY DENSE MRI

6.1 INTRODUCTION

In the setting of vascular health, changes in the tissue mechanics of the vessel wall can have considerable effects on the long term prognosis of vascular disease.[108, 170] It has been observed that aortic compliance (the ability to expand in response to a pressure load) decreases with aging. Consequently, this alters the systemic resistance and increases the required work output of the heart increasing risk of myocardial disease.[41, 107, 116, 171] In the setting of progressive aortic disease, changes in the wall's material properties can have considerable impact on the risk of disease specific sequela. For example, changes in the microstructural property of the aorta early on could pre-dispose the vessel to remodel in a pathophysiological deleterious manner.[172-174] AAA results from the pathophysiological expansion of the vessel with progressive stages of destructive remodeling by way of MMPs and cathepsins followed by stages in which new extracellular matrix is laid down.[175, 176] This persistent remodeling results in a heterogeneous makeup of the vessel wall structure and components. Localized sites of adverse remodeling can be expected to be associated with high risk of rupture in the disease as well.[21, 157, 158] Given the importance of the solid biomechanics in the late stages of AAA, having an understanding of baseline properties could highlight the particular profiles of patients at risk for development and progression of the disease. Given the strong familial history and the associated genetic loci related to biomechanics, utilizing a method to quantify tissue mechanics properties and track over time can lead to a better assessment of risk of disease development.

It has been demonstrated that aortic stiffness is an independent predictor of cardiovascular morbidity and all-cause mortality.[121] Stiffness has been shown to

increase with age, and when comparing men and women this rate of increase is significantly different with age.[177] Most notably, women appear to have a much slower increase in stiffness through their life until they reach menopause at which point there is a sharp increase in aortic stiffness and they approach the same level of stiffness as men. This increase in stiffness correlates strongly with the onset of many cardiovascular diseases and it precedes AAA in women by approximately 20 years. In vivo estimations of collagen and elastin show that there is larger age related increase in the stiffness of isotropic elastin and anisotropic collagen in men than in women who. [171]

The optimal method for quantifying solid mechanics and tissue properties of a blood vessel involve generation of pressure diameter curves, use of bi-axial testing, and histological staining for microstructural quantitation.[24, 25] However, if the need is to measure mechanics in vivo, these tests are not possible. Thus, imaging techniques coupled with computational methods can play a vital role in the quantification of mechanical properties in the vessel. This project proposes the application of Displacement Encoding with Stimulated Echo (DENSE) MRI in the vessel wall of the abdominal aorta of healthy men and women to assess the differences between the sexes in both displacement and strain. In this technique, the phase of the MR signal is used to acquire the in-plane displacement for each voxel in both primary image directions.[178] Unlike other displacement measuring techniques that utilize the image magnitude and implement speckle or tissue tracking, DENSE is able to resolve displacements that are smaller than the resolution of the image itself. Previously, DENSE imaging in the aortic wall has only been reported in one study. In that work, the displacement was measured in the ascending aorta at mid diastole and peak systole to assess asymmetric stretch profiles around the circumference. [124] The technique has been used much more extensively to evaluate cardiac mechanics. The obvious advantages of this technique in the myocardium stem from the greater thickness of the heart wall. While technically difficult, the application of this method in the abdominal aorta to assess the asymmetry of both

displacement and strain around the circumference can provide insight to the variability of the mechanics of this vessel both at baseline and in the setting of diseases such as abdominal aortic aneurysm.

In this study we proposed to measure the displacement around the circumference of the abdominal aortic wall at 20 points during systole and early diastole. We also applied a two-dimensional strain interpolation function to quantify strain around the vessel. We then compared our results between healthy and men and women and assessed what influence this displacement measurement may have on the aortic WSS profile.

6.2 METHODS

6.2.1 Volunteer Enrollment

The same healthy volunteer population described for our WSS and peripheral resistance calculations were used for this study. While DENSE images were successfully acquired for 11 female and 10 male volunteers, noise and poor signal prevented the inclusion of two female and two male volunteers. Therefore, 8 male and 9 female volunteers were included in the analysis.

6.2.2DENSE Imaging Protocol

For each volunteer enrolled, we performed a single DENSE acquisition. The MR image plane was positioned perpendicular to the direction of the vessel in the distal third of the abdominal aorta in order to minimize the amount of longitudinal motion of the vessel through the plane of the image as shown in Figure 6.1.

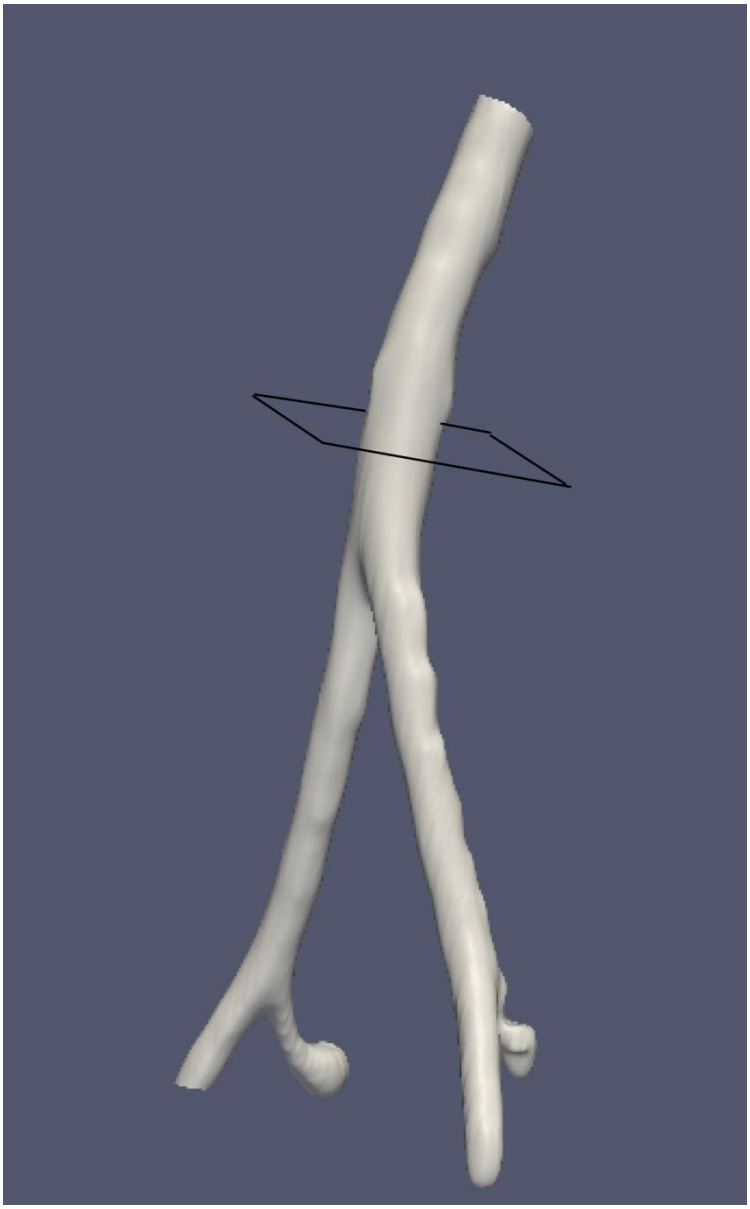

Figure 6.1 DENSE Image Acquisition. Placement of the DENSE image acquisition location was in the distal half of the abdominal aorta where we confirmed there to be less respiratory and longitudinal motion due of anatomical restrictions.

Heart rate and breathing were both monitored in volunteers to ensure correct temporal acquisition. Twenty times points were acquired over approximately the first third of the cardiac cycle following R-wave triggering with a temporal resolution of 0.015 ms. Storage of images at these time points were only kept if the diaphragm was in a pre-defined location window to minimize the effects of any respiratory motion on the

displacement measurements. Phase images were acquired using a displacement encoding value of 0.25 cycles/mm to allow for conversion from phase values to displacement in millimeters. The sequence performed segmented spiral k-space sampling acquisition with the following parameters: TE of 1.25, TR of 16, 8 spiral interleaves per image, 1 spiral interleave per heartbeat, slice thickness of 8 mm, and reconstructed pixel size of 1.77mmx1.77mm. The resultant acquisition includes a magnitude, x-encoded phase, and y-encoded phase image for each of the time points.[126]

6.2.3 Displacement Calculations

For each of the magnitude images the inner and outer contours of the vessel were manually defined at each time point. All points inside in the inner contour and outside the outer contour were masked and no longer used in calculations. In this way, only voxels that were inside the vessel wall were included. Individual phase values in each of the image's principal directions were unwrapped and then converted to displacements using the displacement encoding value as described previously.[123] The result of this processing was a set of images for which the pixel values were the displacement of the voxel contents in the x and y directions. Any pixel outside the defined contours did not contain a displacement value.

Positions of each pixel inside the masked image were tracked from the initial time point and displacement maps were created for each pixel as a function of time in both directions. For each enrolled volunteer, we identified the peak displacement for each voxel (independent of direction or time point) to assess how this value changes with circumferential position.

Displacement values in the principal image directions (anatomically anterior-posterior and left-right) were then converted to a polar coordinate system centered at the centroid of the vessel and the circumferential and radial displacements were calculated according to the following equations:

$$\left|\vec{\boldsymbol{C}}_{\boldsymbol{i,t}}\right| = \left|\vec{\boldsymbol{D}}_{\boldsymbol{i,t}}\right| \sin \boldsymbol{\theta}_{\boldsymbol{i,t}} \tag{6.1}$$

$$\left|\vec{\boldsymbol{R}}_{\boldsymbol{i,t}}\right| = \left|\vec{\boldsymbol{D}}_{\boldsymbol{i,t}}\right| \cos \boldsymbol{\theta}_{\boldsymbol{i,t}} \tag{6.2}$$

$$\boldsymbol{\theta}_{\boldsymbol{i,t}} = \cos^{-1}\left(\frac{\vec{\boldsymbol{V}}_{\boldsymbol{i,t}} \cdot \vec{\boldsymbol{D}}_{\boldsymbol{i,t}}}{\left|\vec{\boldsymbol{V}}_{\boldsymbol{i,t}}\right|\left|\vec{\boldsymbol{D}}_{\boldsymbol{i,t}}\right|}\right) \tag{6.3}$$

Where $C_{i,t}$ is the circumferential displacement, $R_{i,t}$ is the radial displacement, $D_{i,t}$ is the displacement in the x and y direction, and $V_{i,t}$ is the vector drawn from the centroid at time t for the i^{th} pixel. Figure 6.2 shows a summary of this method

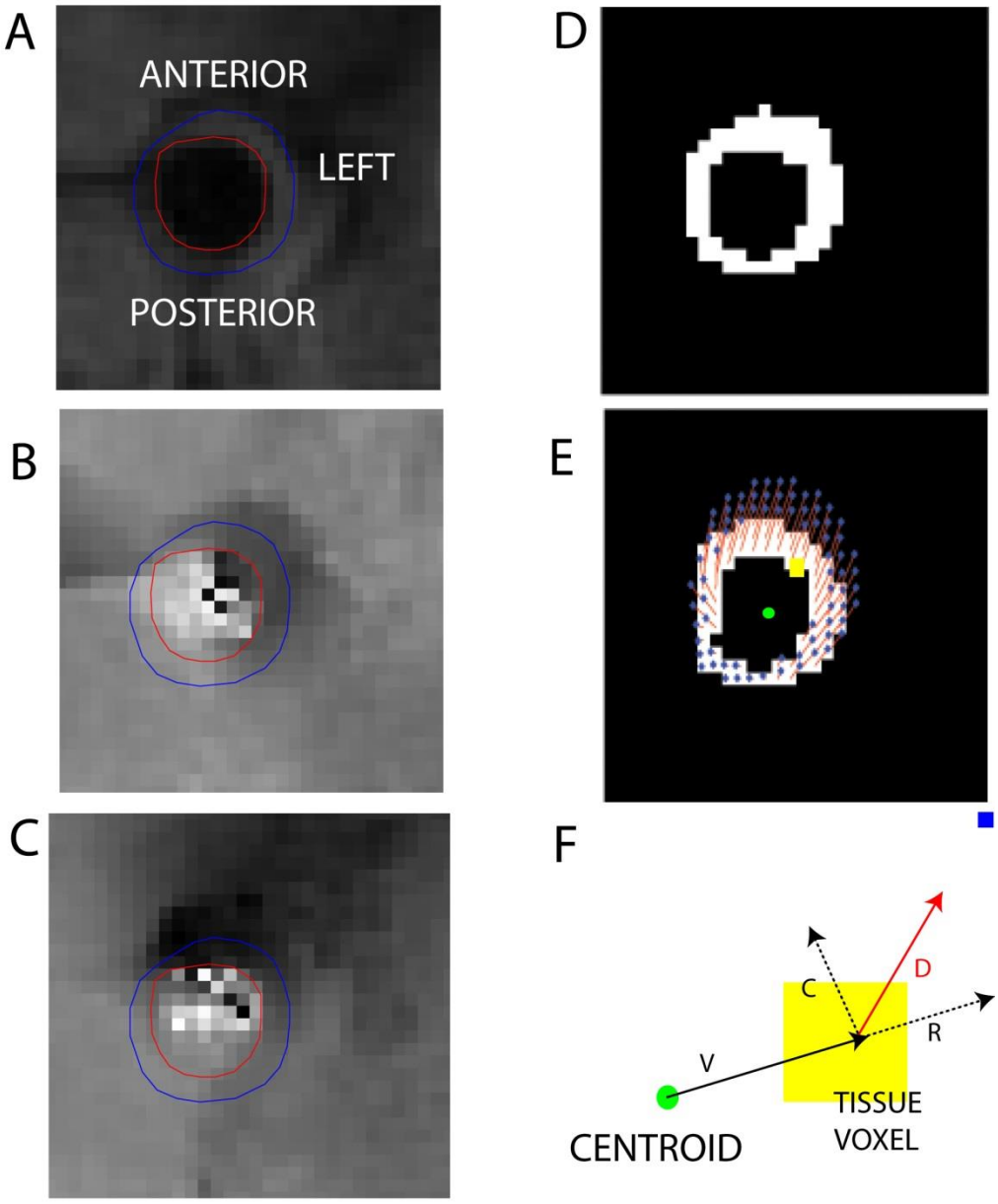

Figure 6.2 Summary of DENSE Image Processing and Circumferential and Radial Displacement**.** (A) Representative magnitude image at the time point of peak displacement for the volunteer. (B) Representative X-Encoded Phase image of time point of peak displacement. (C) Representative Y-Encoded Phase image of time point of peak displacement. (D) Masked image excluding all points outside the vessel wall. (E) Displacement vectors at peak displacement. Blue circles indicate current position of vessel at this time point connected by a red line to their original position. (F) **V** is the vector from the centroid to the voxel location in the reference image and **D** is the displacement vector at some time point in the primary x-y bases of the image. Using the angle between the **V** and **D** as defined by Equation 6.3, we can calculate the contributions of the circumferential and radial displacements, **C** and **R** respectively. The directions of these two displacement vectors are then dependent on the position of the voxel around the tissue wall.

For each enrolled volunteer, we identified the peak radial and circumferential displacement for each voxel to assess how these values change with circumferential position, whether these values varied between men and women, and if there was a relationship between the direction or magnitude of displacement and the WSS profile.

6.2.4 Strain Calculations

To calculate the strain, we employed a previously described based on the in-plane biaxial deformations of four tracked points that defined a quadrilateral in the reference configuration.[179] For our purposes, the reference configuration was defined as the first time point captured in the cine DENSE image set. To create the quadrilaterals used for this method, we began with the masked images described in the previous section. From the center of the vessel we created 60 overlapping sectors around the circumference defined by an opening angle of $\pi/6$ (the rationale for this number of sectors and opening angle are described later). For each sector, the innermost and outermost voxels on the vessel wall which the sectors' edges passed through were identified. In this way a quadrilateral could be created as shown in Figure 6.3

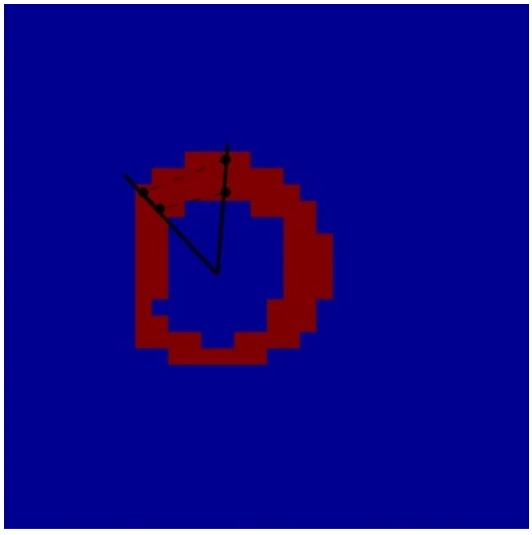

Figure 6.3 Quadrilateral Definition. For a given sector shown above we defined the quadrilateral by the inner and outermost pixels through which each leg of the sector passes. For each sector, quadrilaterals were only included in the analysis if there were

four unique point and four unique sides. If three points fell on the same line, the sector was not used.

The locations for each of these four points were then mapped to a normalized coordinate system using a transformation function so that the four corners of the quadrilateral were represented not in x-y space but in a normalized ζ_1-ζ_2 space using the following equations:

$$\boldsymbol{X_A\left(\zeta_1,\zeta_2\right) = \sum_{n=1}^{4} f^n\left(\zeta_1,\zeta_2\right) X_A^n}\ A=1,2 \qquad \textbf{(6.4)}$$

$$\boldsymbol{f^n\left(\zeta_1,\zeta_2\right) = \frac{1}{4}(1+\zeta_1\zeta_1^n)(1+\zeta_2\zeta_2^n)} \qquad \textbf{(6.5)}$$

Where X_A describes the vector positions of any point inside the quadrilateral, $\boldsymbol{\zeta_1, \zeta_2}$ describe the normalized positions and f^n is the interpolation function. The four vertices of the quadrilaterals was assigned $(\boldsymbol{\zeta_1^n, \zeta_2^n})$ values of (1,1), (1,-1), (-1,-1), and (-1,1) to create a normalized quadrilateral whose vertex connectivity matched the order of the four points in x-y space. To determine the normalized position $(\boldsymbol{\zeta_1, \zeta_2})$ for each of the pixels $(\boldsymbol{X_A^1, X_A^2})$ inside the defined quadrilateral, the system of equations created by the summation function 6.4 and the interpolation function 6.5 was solved using the known $\boldsymbol{X_A^n}$ position vectors in x-y space and the normalized positions $(\boldsymbol{\zeta_1^n, \zeta_2^n})$ indicated above . With this function, any point inside the quadrilateral can then be defined in the normalized coordinate system.

The 4 vertices of each quadrilateral in the reference configuration were tracked to each of the remaining time points in image and a displacement vector $\boldsymbol{u}_{i,t}$ for the ith tracked point at time *t* was created. This displacement vector was a function of the quadrilateral vertices in the ζ space according to the following equation:

$$\boldsymbol{u_A\left(\zeta_1,\zeta_2\right) = \sum_{n=1}^{4} f^n\left(\zeta_1,\zeta_2\right) u_A^n\, A = 1,2} \qquad \textbf{(6.6)}$$

To calculate the strain using these displacement vectors, we created a deformation tensor, **F**, using the equation

$$\boldsymbol{F = I + H} \qquad \textbf{(6.7)}$$

Where **I** is the identity matrix, and $\boldsymbol{H} = \frac{\partial \boldsymbol{u}}{\partial \boldsymbol{X}}$ (the referential displacement gradient) where **X** is the position vector in image space. Because we defined **u** in terms of the normalized $\boldsymbol{\zeta}$ we use the chain rule to calculate the gradient:

$$\boldsymbol{H} = \begin{Bmatrix} \frac{\partial u}{\partial X_1} \\ \frac{\partial u}{\partial X_2} \end{Bmatrix} = \frac{1}{J}\begin{bmatrix} \frac{\partial X_2}{\partial \zeta_2} & -\frac{\partial X_2}{\partial \zeta_1} \\ -\frac{\partial X_1}{\partial \zeta_2} & \frac{\partial X_1}{\partial \zeta_1} \end{bmatrix}\begin{Bmatrix} \frac{\partial u}{\partial \zeta_1} \\ \frac{\partial u}{\partial \zeta_2} \end{Bmatrix} = \frac{1}{J}\begin{bmatrix} \frac{\partial X_2}{\partial \zeta_2} & -\frac{\partial X_2}{\partial \zeta_1} \\ -\frac{\partial X_1}{\partial \zeta_2} & \frac{\partial X_1}{\partial \zeta_1} \end{bmatrix}\begin{bmatrix} \frac{\partial u_1}{\partial \zeta_1} & \frac{\partial u_2}{\partial \zeta_1} \\ \frac{\partial u_1}{\partial \zeta_2} & \frac{\partial u_2}{\partial \zeta_2} \end{bmatrix} \quad \textbf{(6.8)}$$

$$J = \frac{\partial X_2}{\partial \zeta_2}\frac{\partial X_1}{\partial \zeta_1} - \frac{\partial X_1}{\partial \zeta_2}\frac{\partial X_2}{\partial \zeta_1} \quad \textbf{(6.9)}$$

$$\frac{\partial X_1}{\zeta_1} = \sum_{n=1}^{4}\frac{\partial f^n}{\partial \zeta_1}X_1^n = \sum_{n=1}^{4}\zeta_1^n(1 + \zeta_2\zeta_2^n)X_1^n \quad \textbf{(6.10)}$$

Using the Green strain equation

$$\boldsymbol{E} = \frac{1}{2}(\boldsymbol{F}^T \cdot \boldsymbol{F} - \boldsymbol{I}) \quad \textbf{(6.11)}$$

coupled with the appropriate derivatives of the displacement function we can define the first and second principal strains (E_{11} and E_{22}, respectively) at each tracked position as follows:

$$E_{11} = \frac{\partial u_1}{\partial X_1} + \frac{1}{2}\left(\left(\frac{\partial u_1}{\partial X_1}\right)^2 + \left(\frac{\partial u_2}{\partial X_1}\right)^2\right) \quad \textbf{(6.12)}$$

$$E_{22} = \frac{\partial u_2}{\partial X_2} + \frac{1}{2}\left(\left(\frac{\partial u_1}{\partial X_2}\right)^2 + \left(\frac{\partial u_2}{\partial X_2}\right)^2\right) \quad \textbf{(6.13)}$$

Using the first and second principal strains we compute the radial and circumferential strain using a rotation matrix that depends on the circumferential position of the voxel of interest:

$$\begin{bmatrix} E_{rr} & E_{rc} \\ E_{cr} & E_{cc} \end{bmatrix} = \begin{bmatrix} cos(\theta) & sin(\theta) \\ -sin(\theta) & cos(\theta) \end{bmatrix} \cdot \begin{bmatrix} E_{11} & E_{12} \\ E_{21} & E_{22} \end{bmatrix} \cdot \begin{bmatrix} cos(\theta) & sin(\theta) \\ -sin(\theta) & cos(\theta) \end{bmatrix} \quad \textbf{(6.14)}$$

The circumferential position of the initial positions of the wall's tissue was assessed using the centroid of the vessel and for each voxel this value θ was used to create the rotation matrix. Figure 6.4 shows a colorimetric representation of the circumferential position for each vessel inside the wall.

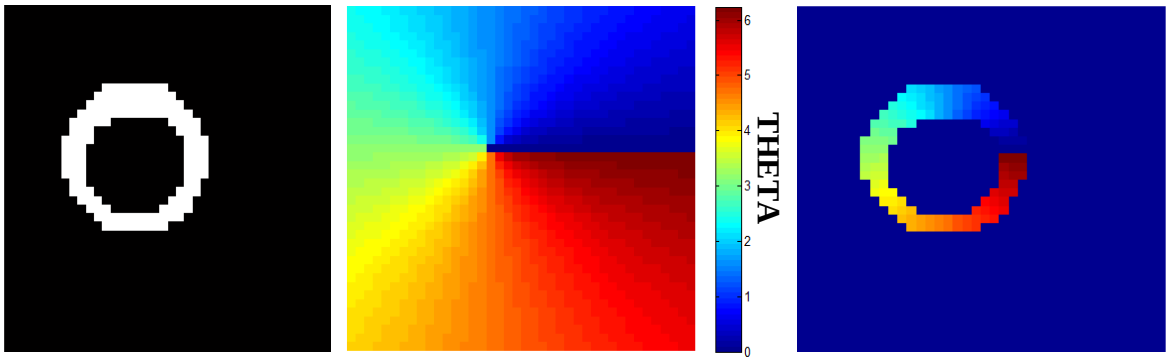

Figure 6.4 Circumferential Position Definition. From left to right, this figure shows how we mapped the circumferential position around the circumference to create the rotation matrix in Equation 6.14. The leftmost image is the same mask in Figure 6.1. This image is for the first time step and thus the reference configuration. The central panel is a colorimetric map showing the value of theta used for each of the points inside our frame based on the location of the centroid of the vessel. The final image shows the circumferential position for each of the pixels inside the vessel wall.

Given this set of equations we quantified strain at all points inside the vessel wall. For each of the 60 quadrilaterals defined, we assessed the strain at each of the voxels contained within the quadrilateral using the interpolation system described above. Because the sectors which created the quadrilaterals overlapped with one another, more than one strain value would be calculated for each of the wall's voxels. To assign a final strain value each voxel, we averaged the values obtained every time said voxel was included in a quadrilateral. We used the variance of these multiple strain values for a given voxel to decide how many sectors and the degree of opening angle to employ. We tested 60 & 80 sectors with an opening angle of $\pi/3$, $\pi/4$, $\pi/6$, $\pi/8$, & $\pi/10$ and calculated the combined variance for all voxels. We chose an opening angle of $\pi/6$ for 60 sectors because this minimized the total calculated variance. In this way we chose the conditions that gave us the most consistent results for each voxel.

For each enrolled volunteer, we identified the peak circumferential strain for each voxel to assess how this value changed as a function of circumferential position, whether

this value differed between men and women, and if there was a relationship between the circumferential strain and the WSS profile.

6.2.5 Regional Analysis

We divided each volunteer's map into 8 equally spaced sectors around the circumference and averaged displacement values within each sector across all volunteers. Figure 6.5 shows how sectors were defined and numbered throughout the remainder of the results. On average, a sector for each volunteer included between six and eight voxels.

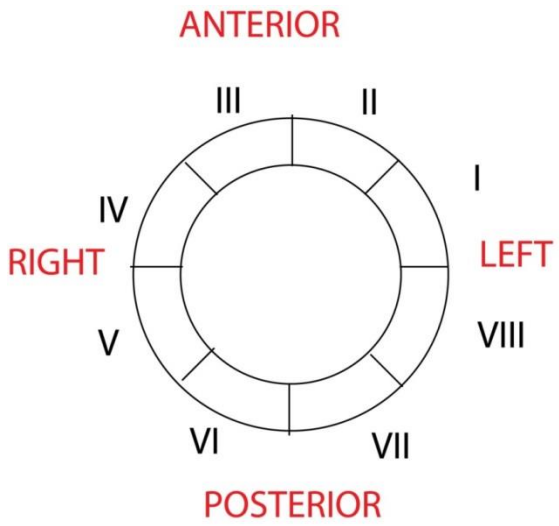

Figure 6.5 Vessel Wall Sector Definition. The vessel was divided into 8 equivalent sectors and the corresponding anatomical positions for each of the sector numbers are defined.

6.2.6 Analysis and Comparisons Between Men and Women

We performed an ANOVA test to compare the circumferential and radial displacement averages in each of the sectors to assess whether these values differed around the vessel. We performed the same analysis for the circumferential strain values.

To compare the displacement and strain values between men and women we began by comparing each of the quartile values and the overall spread of the data. After

dividing the data by sex, we compared circumferential and radial displacement as well as circumferential strain between men and women in each of the sectors using a two tailed t-test.

Finally we assessed how the tissue mechanics properties are related to the WSS profiles using the results described here and those obtained and described in Chapter 4. Using a similar sector analysis we calculated the average OSI in each of the sectors and paired it with the average displacement and strain values. We reported these as both individual volunteer plots and divided by sex to evaluate what relationship exists.

6.3 RESULTS

Both strain and displacement calculations were made for each of the 9 female and 8 male volunteers for whom usable DENSE images were acquired. Of those 17 volunteers, we also had hemodynamic data from PCMR for 6 women and 7 men to evaluate the influence of strain and displacement on WSS and flow profiles.

6.3.1 Circumferential Variation in Displacement

We first examined how net displacement magnitude would change as a function of circumferential position. For each volunteer, we identified the peak displacement at each pixel within the vessel wall and plotted this displacement as a function of the voxel's circumferential position. We divided the circumference into 30 sectors and averaged the results across all volunteers to make a global assessment of displacement in the population. Figure 6.6 shows our observation that the largest displacements occur on the anterior vessel wall.

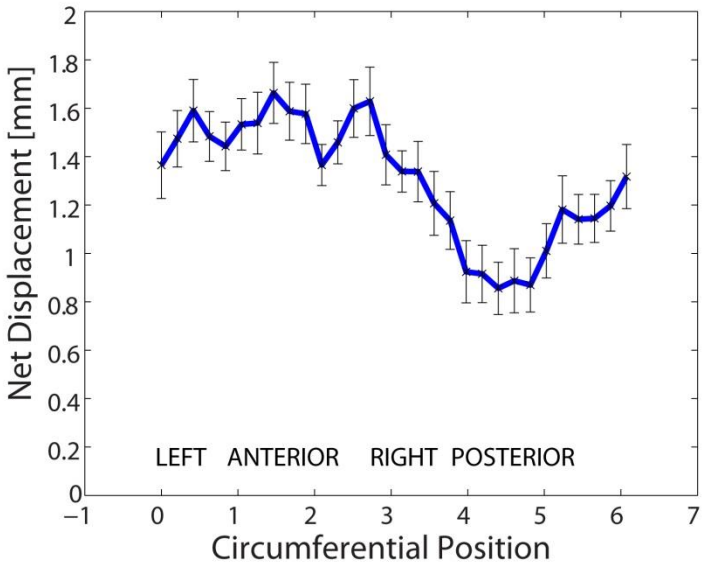

Figure 6.6 Average Net Displacement in the Aorta as a Function of Circumferential Position showing the average net circumferential displacement across all 17 volunteers for 30 equally spaced bins. We noted the net displacement seems to be highest on the anterior and antero-lateral walls of the vessel and lowest on the posterior. This result is expected given the posterior of the vessel is limited in motion by the presence of the spine.

To examine the directionality of the displacement vector, we resolved the displacement value into the radial and circumferential components as described in the Methods section. Plotting the data in the same manner as Figure 6.6, Figure 6.7 shows the differences in radial displacement as a function of position around the circumference of the vessel while Figure 6.8 shows the differences in circumferential displacement.

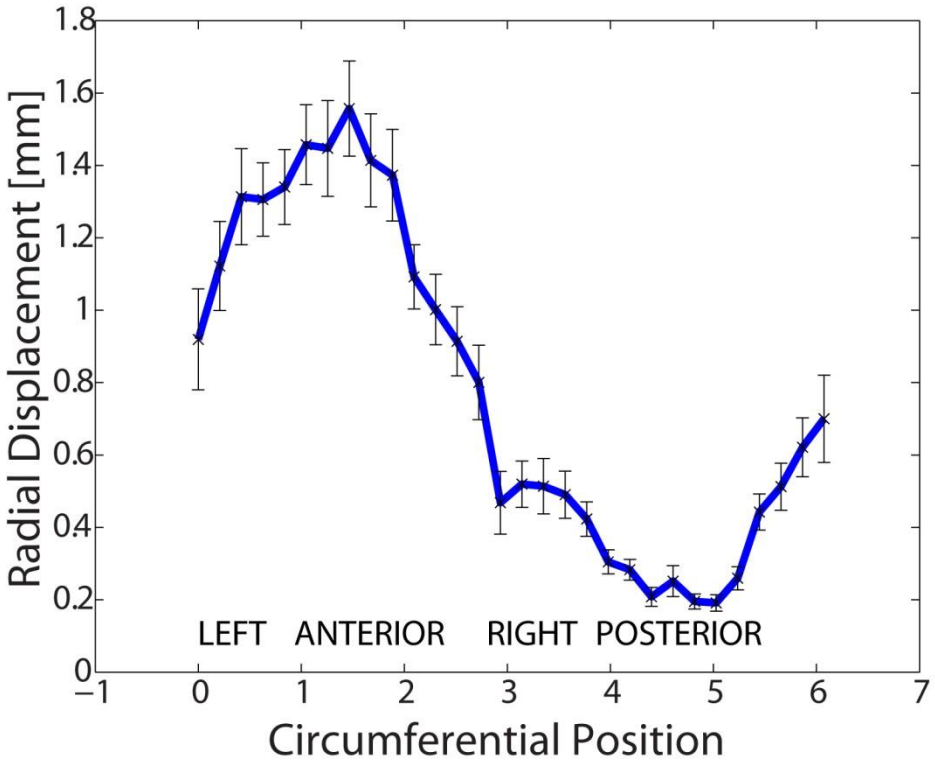

Figure 6.7 Average Radial Displacement in the Aorta as a Function of Circumferential Position. Similar to Figure 6.5, this figure shows the average radial displacement across all volunteers around the circumference of the vessel. We noted, again, the highest displacement to be on the anterior of the vessel, however displacement in the radial direction on the lateral walls is lower than on the anterior.

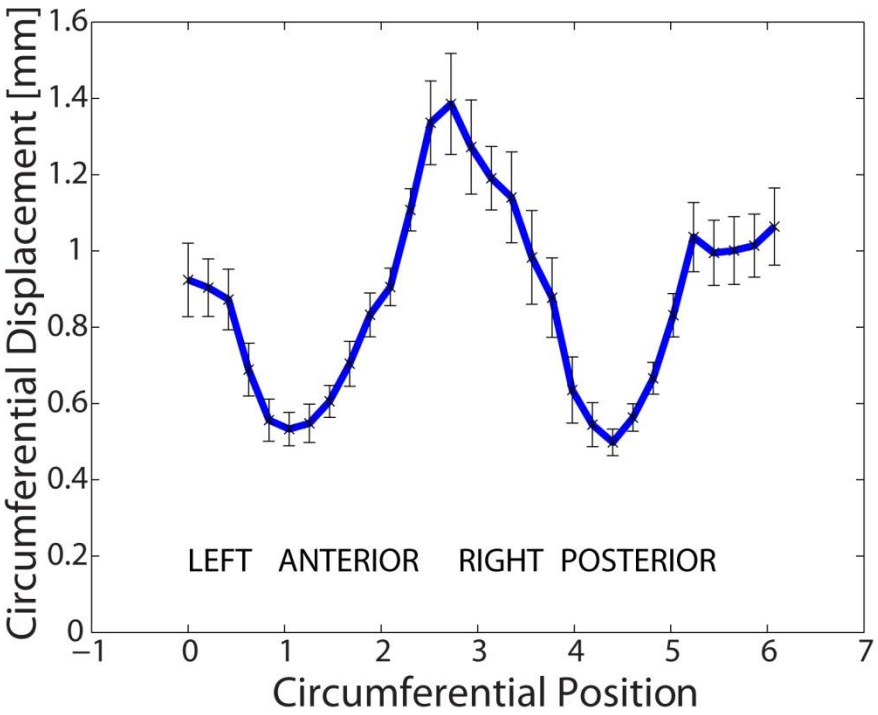

Figure 6.8 Average Circumferential Displacement in the Aorta as a Function of Circumferential Position. This is the average circumferential displacement curve across all volunteers at 30 equally spaced sectors points around the circumference. In comparison to the radial displacement curve seen above we noted that the circumferential displacement is highest on the lateral portions of the vessel.

Figure 6.9 shows the results for the net, radial and circumferential displacement measurements averaged in each of the 8 sectors. In using a one way ANOVA test for each of the measurements to compare across sectors, we found significant differences for all three displacement measurements around the circumference ($p>0.0001$). In a Newman-Keuls post-hoc analysis, radial displacement was significantly different in all but 3 pairwise comparisons (Sector 7 vs 6, Sector 5 vs 8, and Sector 3 v 2). Using the same procedure, circumferential displacement was significantly different in all but 5 pairwise comparisons (Sector 2 vs 6, Sector 3 vs 1, Sector 7 vs 1, Sector 3 vs 7 and Sector 8 vs 5). Net displacement was significantly different in 17 of the 38 pairwise comparisons. In comparing the average circumferential and radial displacements in each of the sectors we found significant differences around the entire circumference

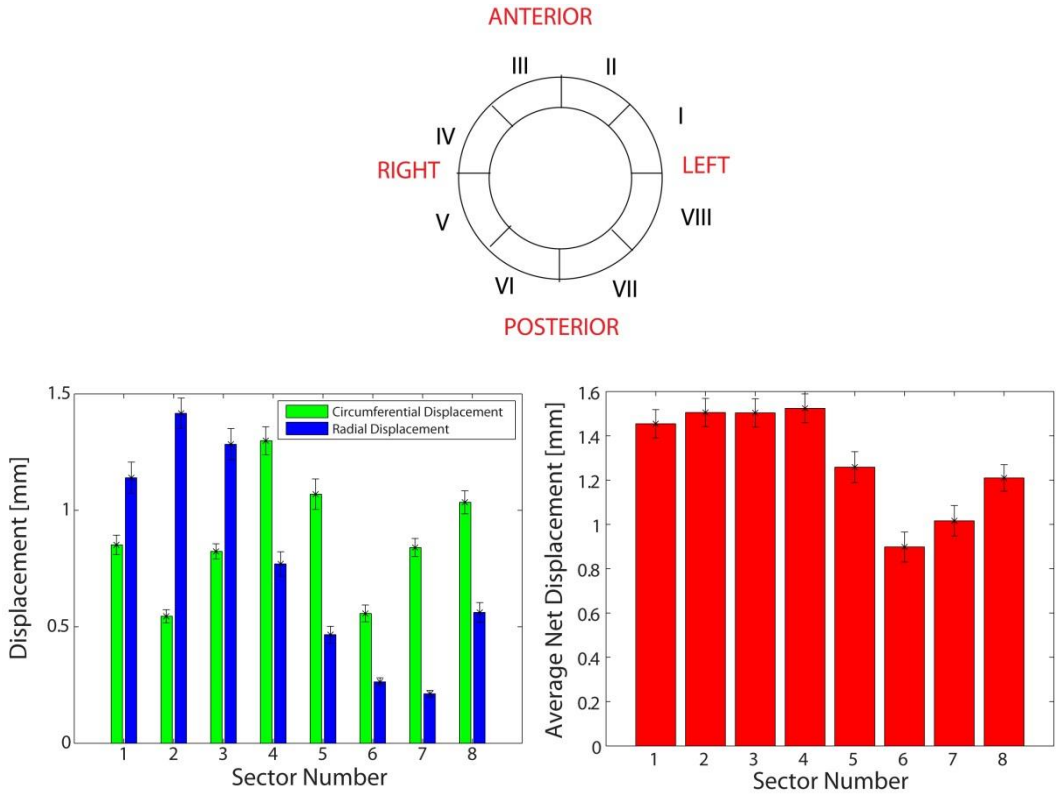

Figure 6.9 Differences in Displacement Magnitude and Direction around the Aortic Circumference. The left panel shows the average radial and circumferential displacements among all volunteers for each sector. The right panel shows the average net displacement. Overall displacement is lowest on the posterior of the vessel. The contributions of displacement in the circumferential and radial directions change with position around the vessel, where radial displacement is highest in the anterior sectors of the vessel and circumferential displacement is higher on the lateral walls.

6.3.2 Circumferential Variation in Circumferential Strain

Similar to our analysis of the displacement measurements, we assessed the maximum circumferential strain for each voxel. Figure 6.10 shows the peak strain as a function of circumferential position for each volunteer as well as the normalized curves for each volunteer.

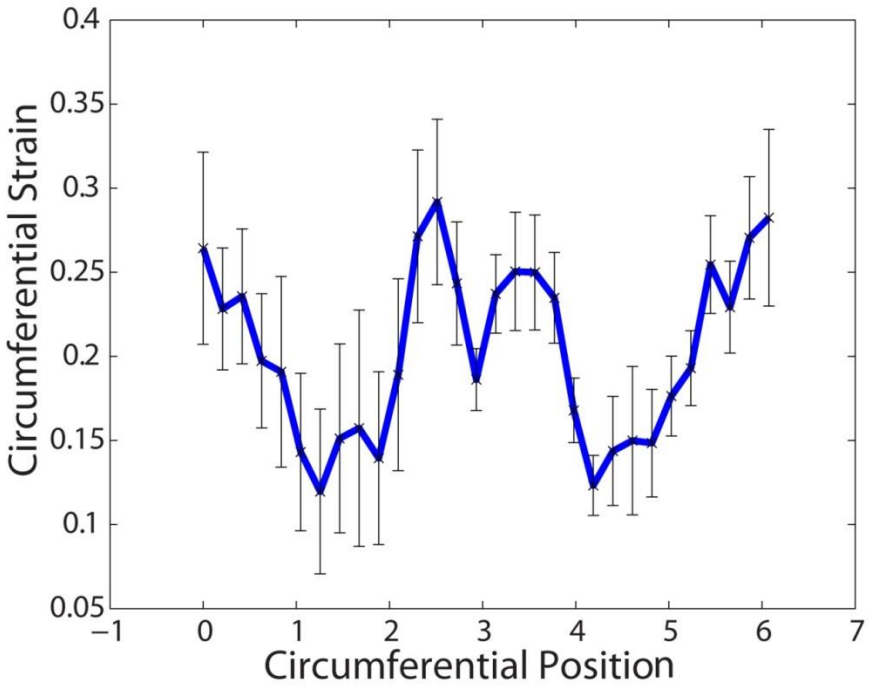

Figure 6.10 Average Circumferential Strain in the Aorta as a Function of the Circumferential Position. The circumferential strain was averaged across all volunteers at 30 equally spaced points around the circumference. Our results indicate a high level of circumferential strain on the lateral wall of the vessel.

We took the average of all the peak strains in each of the eight evenly spaced sectors around the circumference as shown in Figure 6.8. Performing a one-way ANOVA comparing the strain across all the sectors, we found a significant difference with $p<0.0001$. A post hoc analysis confirmed a significant differences between the lateral walls and the anterior/posterior of the vessel but no differences between the left and right sides.

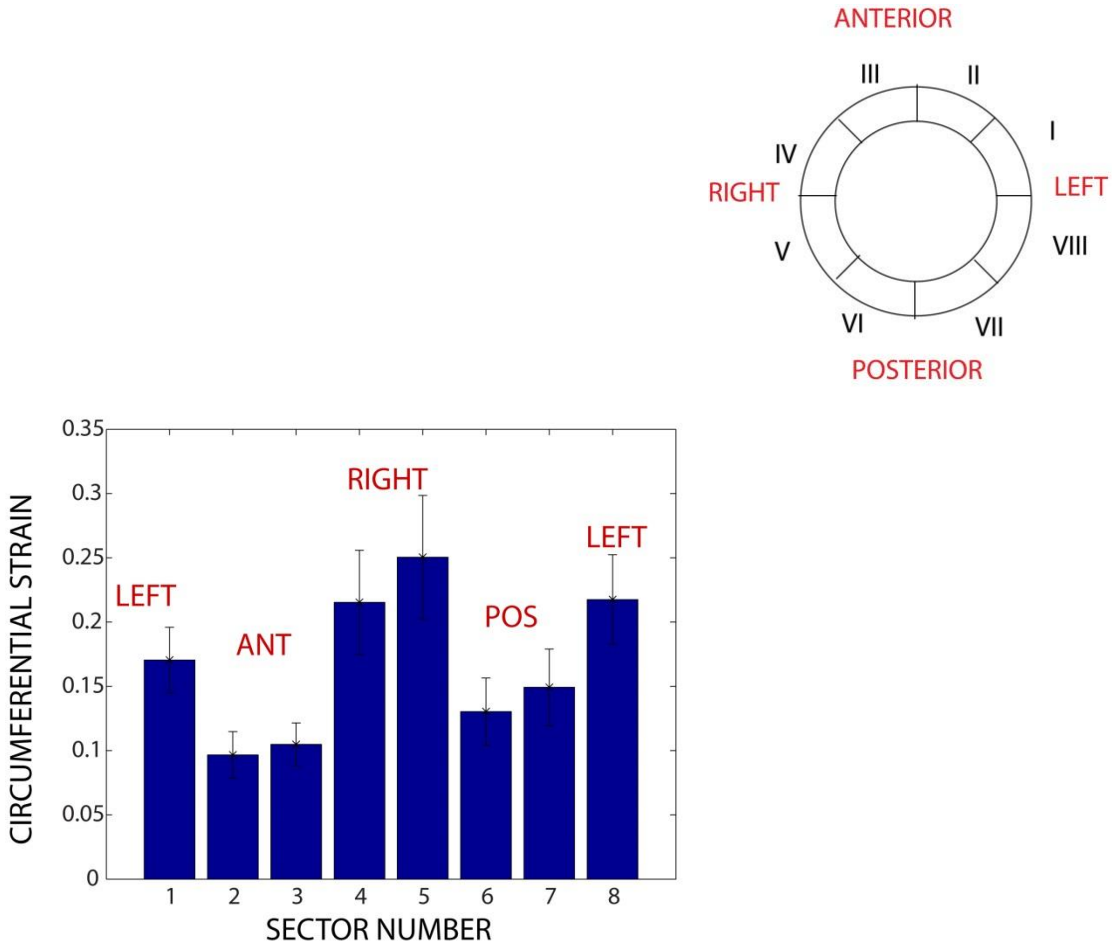

Figure 6.11 Peak Circumferential Strain in the Lateral Wall of the Aorta. The average peak circumferential strain in each of the sectors for all our volunteers are shown in the bar graph. The sectors with the lowest strain correspond to the right and right posterior of the vessel while the highest strain occur at the transition regions between the lateral walls and the anterior of the vessel.

6.3.3 Potential Differences in Displacement and Strain Between Men and Women

In addition to evaluating circumferential variation in both displacement and strain, we quantified differences between men and women. To compare displacement values calculated for each of the sexes, we also created box plots for each of the displacement directions. We found the ranges of circumferential and radial displacement for both men and women to not be significantly different. The box plots also allowed us to see that while there are a few measurements that qualify as outliers amongst our group, there is a fairly

close spread of measured displacement with median values and quartile values of 0.17 mm, 0.47 mm and 1.05 mm for women and 0.29 mm, 0.68 mm, and 1.17 mm for men.

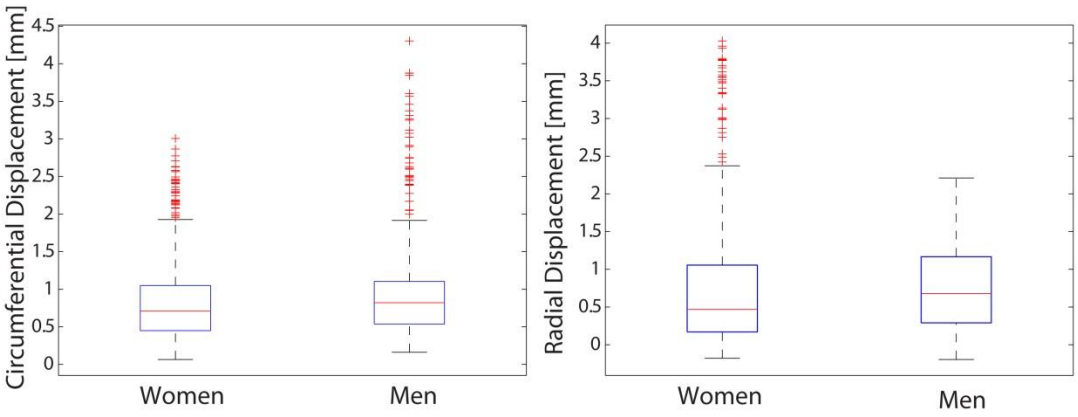

Figure 6.12 Spread of Displacement Data in Men and Women. Boxplots of the circumferential displacement values for all women and men (left) show similar median, first, and third quartile values. The men appear to have a few values that exceed those of the women on the upper end, but this is the result of high displacement measurements in one of the volunteers. The right image shows the same boxplots but for radial displacement. Again we note very a similar spread of values, however we have one outlier female with displacements exceeding all the male volunteers in our group.

Within each sector described in Figure 6.8 we compared the average displacement values between men and women. For the circumferential displacements, we found significant differences in sectors 2 through 6. For the radial displacements, we found significant differences only in sectors 6 & 7 with $p<0.05$. For most of these sectors, the average displacement value was higher for men than it was for women.

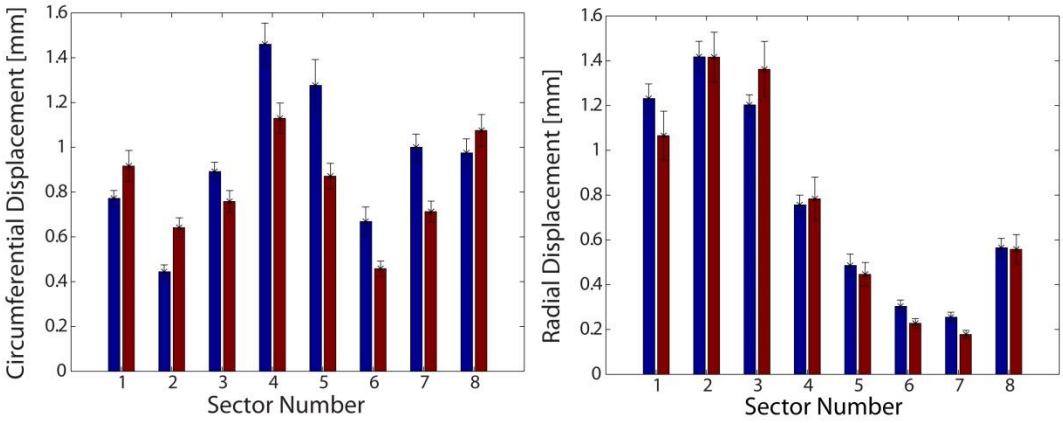

Figure 6.13 Comparison of Aortic Displacement Between Men and Women. Overall, both the men and the women follow the same trends in circumferential and radial displacement. We noted some significant differences within certain sectors, most often with men demonstrating a higher displacement value.

As with our results summarized in Figure 6.13, we created box plots for the circumferential strain values of men and women and a similar result was obtained. The quartile values for men were 0.057, 0.13, and 0.20 while the quartile values for women were 0.062, 0.13, and 0.22. These results are summarized in Figure 6.14

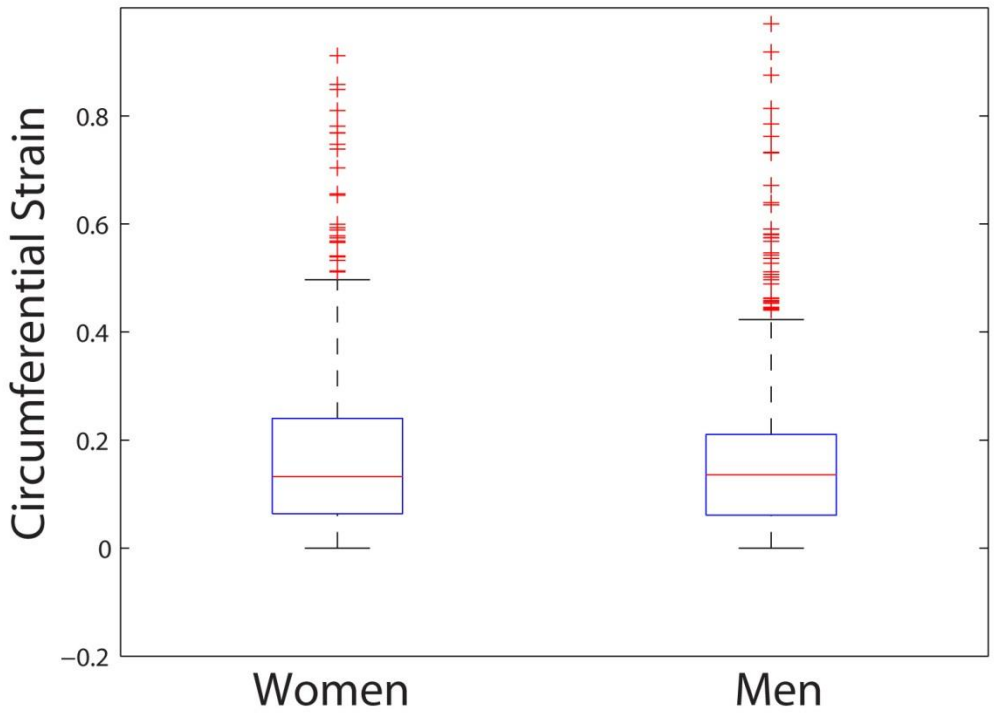

Figure 6.14 Spread of Strain Data in Men and Women. The circumferential strain values measured for each of our populations. As with our displacement values the overall spread of the data is similar. Again we note some outliers in both the populations and do not expect that these very high strain values are true values but rather errors in our method.

We averaged the strain values in each of the sectors for our female volunteers to compare with equivalently averaged values for our male volunteers. Using a two tailed t-test, we found significant difference in the circumferential strain between men and women in sectors 1, 2, and 6. In Sectors 2 & 6 women exhibit a higher degree of strain, while in sector 1 there is an increase in strain for men over women.

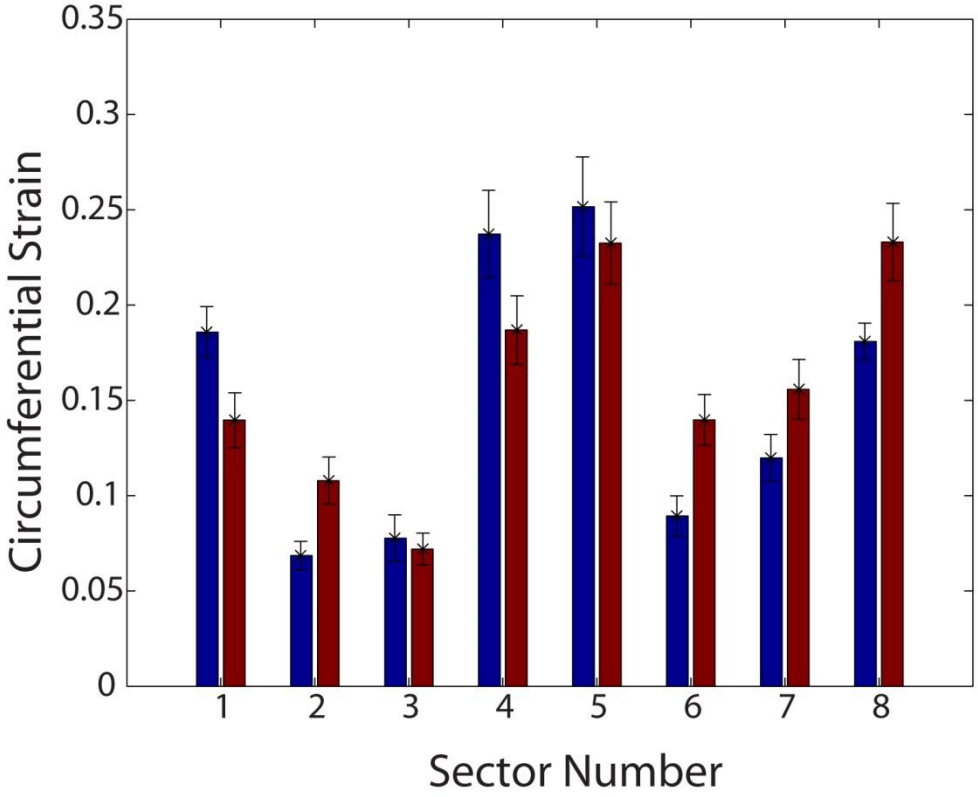

Figure 6.15 Comparison of Circumferential Strain between Men and Women by Sector. Similar to our displacement results, both sexes' strain measurements follow a similar trend to the population as a whole. However, within the sectors on the right side and right posterior of the vessel, we noted significantly higher strain values in women than in men.

6.3.4 Influence of Displacement on Hemodynamics

Using the calculated displacement and strain averages from each of the sectors as described above, we explored the relationship between these values and local hemodynamics. Using the PCMR images and subsequent WSS measurements made at the same locations as the DENSE and displacement measurements, we computed the average OSI values for each of these same sectors. Figure 6.16 shows the results of the average peak radial displacement, circumferential displacement, and circumferential strain for all volunteers and divided across men and women as well.

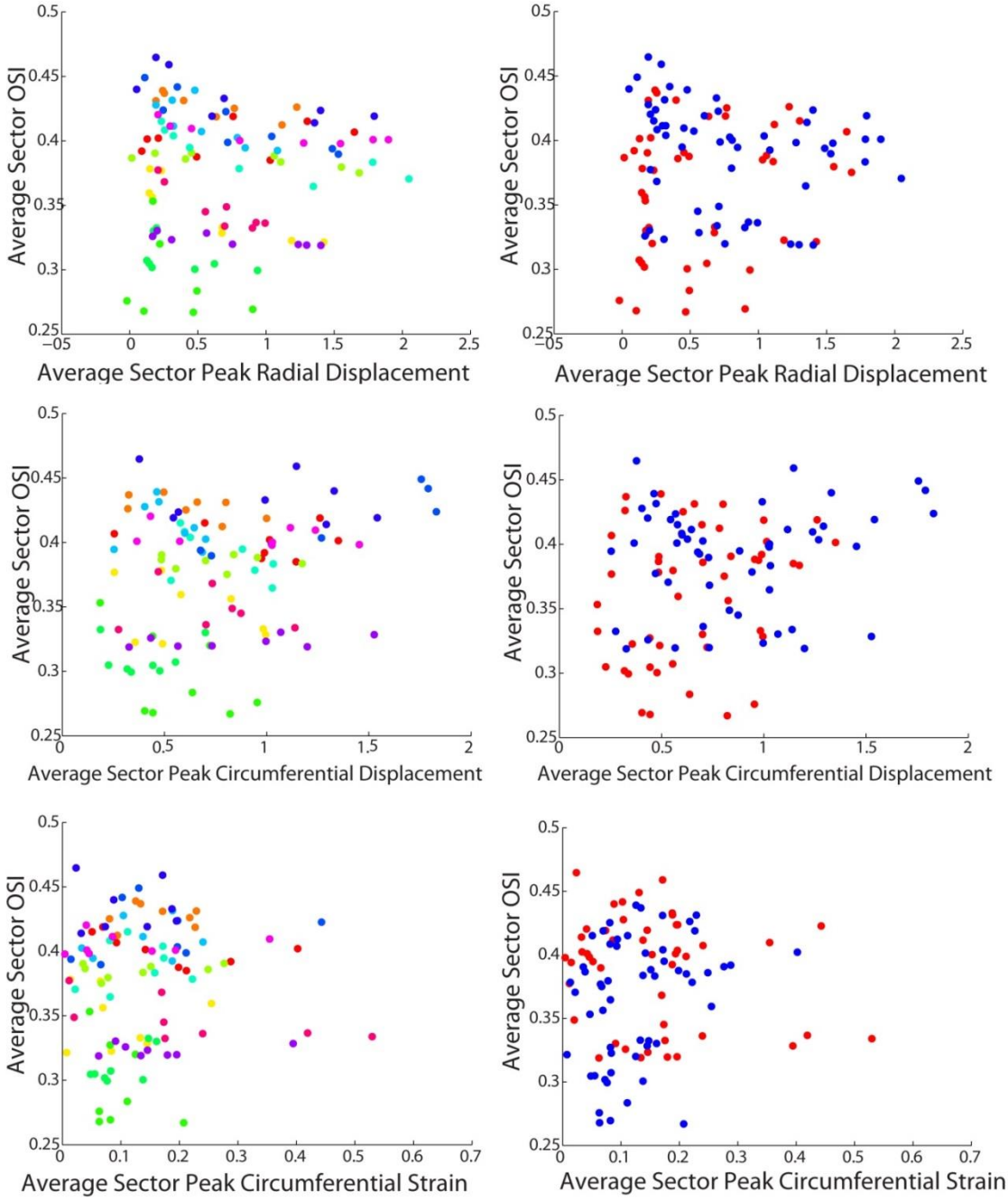

Figure 6.16 Comparison of Displacement and Strain with Oscillatory Shear. From top to bottom, we compared the average local OSI with average radial displacement, circumferential displacement, and circumferential strain. The hand of the figure shows the plots for each volunteer as individual colors while the right shows the relationships grouped by sex. Overall, there was not obvious correlation noted between the measurements of tissue movement and local hemodynamics.

6.4 DISCUSSION

This study is the first to utilize DENSE MRI to quantify time resolved displacement of the abdominal aortic wall. The major findings of this study include the demonstration of a positional dependence on the radial and circumferential contributions to the peak displacement vector in the aortic wall. In quantifying circumferential strain from displacement fields, we demonstrated that there is as an increase in circumferential strain on the lateral walls. Finally, this study showed that there may be modest differences in the displacement and strain maps of healthy male and female volunteers.

6.4.1 Circumferential position in aortic wall predicts principal displacement direction

In this aim, we demonstrated a dependence of the aortic wall's displacement magnitude and directionality on circumferential position. The location of lowest magnitude displacement for all our volunteers was on the posterior aorta where the vessel is bounded by the spine. When comparing the radial and circumferential direction contributions to the displacement, we noted the highest degree of radial displacement on the anterior of the vessel and the highest degree of circumferential displacement on the lateral aspects of the vessel. This observation reveals that the vessel does not expand uniformly around the circumference but rather pushes out anteriorly while remaining fixed to the spine. This finding is consistent with a previous report showing an increase in anterior motion compared with posterior using ultrasound (US) imaging.[180] Because this study used a single B-mode acquisition however, the authors were unable to explore the radial and circumferential contributions to the displacement vector as well as to compare the lateral components of the vessel wall. The asymmetry in displacement revealed in our study appears to be due partly to the anatomy around the vessel physically restricting the motion of the vessel. In comparing the lateral walls, we noted that the contribution of circumferential displacement on the right side was greater than that on the left. This could be explained by the presence of the inferior vena cava (IVC) limiting the

direct outward expansion of the aorta and forcing the vessel to displace along its circumference.

6.4.2 Peak Circumferential Strain in the Aorta in the Postero-lateral Wall

Because the resolution of our DENSE imaging sequence limited the number of transmural pixels to between 2-3 in most positions around the vessel, we elected to only evaluate and analyze the circumferential strain measurement from our interpolant method. Utilization of DENSE MR and displacement fields still presented an advantage over previous MR techniques using PCMR to quantify strain, however, because it allowed for differentiation of strain around the circumference of the vessel instead of a global estimate using changes in radius and strongly depend on the resolution of the image.[181, 182] Our results indicated that on average, the circumferential strain was highest on the lateral vessel. Prior histological studies evaluating abdominal aortic aneurysms have shown that the postero-lateral vessel specimens had microstructural changes that elevated this site's risk of rupture including a decrease in collagen content and an increase in lipid deposition.[183] This fits with post-mortem studies showing that ruptures happen most frequently on the lateral wall of the vessel.[184] While our study evaluated the strain in normal healthy aortas, its application in AAA patients could provide insight to improve identification of aneurysms at risk for rupture.

6.4.3 Potential Differences Between Sexes in Tissue Mechanics as Measured by DENSE MRI

To assess how sex may influence these measurements, we separated our divided our volunteers by sex and assessed how displacement values may differ globally. Figure 6.12 shows that, overall, the peak displacement values throughout the vessel are very similar for both men and women. However, when grouped by sector, a few differences between the populations were noted. Our male population showed a higher degree of radial displacement in the posterior aspect of the vessel, however the displacement values

were so small in this region it is difficult to interpret this result with clinically appreciable meaning. It is unlikely that the observed differences in radial displacement have much significance as these values are the smallest among all the sectors (to be expected as a result of the restriction of movement by the spine). With respect to circumferential displacement, we observed a more displacement in men on the right of the vessel where the aorta abuts the IVC. Previous studies using MRI to evaluate possible differences in aortic mechanics between men and women were limited to measuring distensibility and estimates of compliance. A recent study of 777 subjects showed a steeper decline in aortic distensibility and compliance in women with aging, however, no difference was observed in the age group looked at in this study.[185]

Additionally, it is interesting to note that our results summarized in Chapter 4 show that the women in our population have significantly smaller abdominal aortic radii (Figure 4.4). If the aortic radius is smaller in our female population and the displacements are similar, we would expect strain fields to be different between the sexes as we observed. When comparing the circumferential strain within each of the vessels we observed higher circumferential strain in women on the posterior-left of the vessels.

It is worth noting, however, that the sectors were created based on primary anatomic directions (anterior-posterior-left-right) while our methods allow for more finely resolved displacement and strain fields. Sectors were created in order to allow for a more straightforward comparison amongst volunteers and may represent an oversimplification of the data. However, this analysis does provide normal ranges in each of these regions of the vessel that currently do not exist for a healthy population, especially from a sex-based perspective. With a larger cohort, it may be possible to create a normalized vessel allowing for easy identification of vessel segments with abnormal displacement or strain values.

6.4.4 No Observed Relationship Between Regional Displacement Values and Aortic WSS Profiles

Finally we attempted to identify what relationships may exist between hemodynamics and tissue mechanics. For each volunteer, we identified matched the WSS data we obtained (as described in Chapter 3) with the measured displacements and strains. Similar to our sector method to compare displacement and strain values, we averaged the OSI values within equivalent sectors. We plotted these averaged OSI values against the respective radial and circumferential displacement and circumferential strain measurements for each of our volunteers as seen in Figure 6.16. We also divided these scatter plots by sex to determine if there may be a differential influence of sex on the relationship between any of these tissue mechanics and the hemodynamics. As is evident from our plots, it is clear there are no easily identifiable relationship between oscillatory shear and either displacement or strain. We know that there is a definite relationship between how the tissue moves and the shear patterns in the vessel. We do not think that our results are indicative of the opposite, but rather that our measurements and analysis were insufficient to demonstrate such a result. The field of fluid-solid interaction (FSI) uses much more complex computational modeling to quantify these relationships.[186] Further, these types of methods and modeling problems are used to evaluate much more complex flow conditions than what we are observing here. With our method we are only able to resolve two dimensional in plane displacement and strain fields as well as unidirectional wall shear stress. It is still possible that differences exist between men and in women in the how the tissue mechanics influence the hemodynamics, however, more advanced computation may be required to identify or explain such differences.

Chapter 7

CONCLUSIONS AND FUTURE DIRECTIONS

7.1 SUMMARY

The goal of this project was to provide understanding for why men are more likely to develop abdominal aortic aneurysms than women. Specifically, we hypothesized that the abdominal aorta of men experiences a more pro-inflammatory biomechanical environment when compared with that in women. To test this hypothesis we developed a new method using MRI to quantify WSS in the abdominal aorta and applied it in a group of healthy men and women. Comparisons of the flow profiles, oscillatory shear index, and time averaged WSS magnitude were made between men and women along the length of the abdominal aorta. We then evaluated three innate vascular parameters that we expected to influence the vessel's hemodynamics and to be different between men and women, namely how curvature and radius of the aorta differed between men and women, how the presence and alteration of uterine artery blood flow might influence aortic hemodynamics, and finally if aortic wall displacement and strain as measured by MRI were significantly different between the sexes.

7.1.2 Development and Validation of 2D PCMR WSS Calculation Method

Our first step in this work was to develop and validate a new method for quantifying WSS from 2D PCMR. There have been many previously proposed methods for this purpose that fit direct velocity measurements to estimate wall shear rate and hence wall shear stress.[135, 136, 142, 187] These methods are known to be unreliable when noise is high or when the resolution of the image sets is poor relative to the size of the vessel. The largest issue with these methods stems from the difficulty of accurately identifying the location of the vessel wall, necessary to calculate the wall shear stress. By comparison, our method utilizes regional flow waves determined by overlapping sectors

and the Womersley solution to the Navier Stokes equations to quantify wall shear stress.[137] Our sensitivity analysis demonstrated that the results from this method were not significantly affected when the wall position was changed by up to 10%. Further, we showed that this method reliably reproduces results from one PCMR acquisition to the next. Finally, we compared our results of this method against a CFD simulation with patient specific geometry and boundary conditions and demonstrated that our method had a mean reduction in wall shear stress of less than 5 dyn/cm^2 which we considered to be clinically non-significant.

7.1.2 Application of WSS Method in Men and Women

We then applied this method in a group of healthy men and women. For each of the 28 volunteers, we acquired multiple PCMR image sets along the length of the aorta oriented perpendicular to the primary axis of the vessel. We quantified the OSI from the WSS waveforms at eighty evenly distributed locations around the vessel for each of these image sets. Using anatomical data from a non-contrast angiogram, we identified the relative location of each slice along the vessel length and were able to make comparisons for equivalent relative positions among all volunteers. *We demonstrated that women have a significant reduction in OSI at all points in the aorta when compared with men. This result is consistent with our overarching hypothesis that men are predisposed to developing an AAA more so than women as a result of these pro-inflammatory biomechanics.* We showed that this difference in OSI is strongly correlated with the extent of regional flow reversal and is highest in both men and women in the distal posterior region of the vessel.

7.1.3 Differences in Aortic Geometry and Relationship to Aortic Hemodynamics

After establishing a difference in the aortic WSS profiles of men and women, we explored what vascular parameters may underlie and explain why these dissimilarities

exist. In our first specific aim, we used reconstructions of non-contrast angiograms to evaluate differences in radius and curvature of the vessel, as both of these geometric features are known to influence WSS and OSI distribution. We found, as others have reported, that men have a larger aortic radius along the entire length of the vessel than women.[107, 122] We also demonstrated that in the distal half of the abdominal aorta, women have a greater degree of curvature when compared with men. We had hypothesized this result, as the lumbar spine in women is more lordotic and the pelvis is tilted to accommodate the birth canal.[188] We then looked to see what impact each of these parameters may have on the local hemodynamics and first noted that in both men and women, a larger radius correlated with a larger in OSI. With an increase in vascular curvature we hypothesized that there would be an increased difference in the OSI between the inner and outer curvature (posterior and anterior, respectively in the aorta).[189] On average, we found that women have an increase in the relative difference between the minimum and maximum OSI compared with men in the distal half of the aorta.

7.1.4 Relationship of Uterine Artery Blood Flow and Abdominal Aortic Hemodynamics

The second vascular parameter we hypothesized to be different between men and women and to exert influence over aortic hemodynamics was peripheral resistance. Because uterine artery flow is only present in women and it is one of the only blood vessels in the peripheral vasculature that exhibits no flow reversal under normal physiological conditions, we proposed that this low resistance vessel may be responsible for the reduction in oscillatory shear we observed in the abdominal aorta. Because the uterine artery is too small to visualize by MRI reliably, we measured flow in the internal iliac arteries (the primary artery to the pelvis in both sexes) of our healthy men and women and found a significant reduction in oscillatory flow in women compared to men.

To confirm that this effect was due to the uterine artery, we identified two patient populations that represented a modulation of uterine artery resistance.

We recruited otherwise healthy women with symptomatic uterine fibroids (highly vascularized non-malignant tumors) and showed an even further reduction in the internal iliac oscillatory flow of this group compared to healthy women. We then recruited women who had undergone a hysterectomy (while retaining ovarian function) and showed no significant differences in internal iliac oscillatory flow. To confirm that the effect in the group of patients with fibroids was isolated to the pelvic blood flow we showed no significant changes in the extent of flow reversal of the external iliac artery which supplies the lower limb. We then wanted to evaluate what influence this change in pelvic flow may contribute to the aortic hemodynamics as there was a significant reduction in OSI in our fibroids group and a moderate (non-significant) increase in our hysterectomy group compared to our healthy female controls. We did not observe a strong relationship when we compared the internal iliac flow with the OSI. However, if we compared the total iliac flow oscillations (a combination of both internal and external iliac artery flow waves), we discovered aortic OSI in women was much more sensitive to change in peripheral flow than in men. *This suggests that changes in peripheral flow profiles in women may alter aortic hemodynamics (more so than in men) in a manner that increase risk for developing abdominal aortic aneurysms.*

7.1.5 Implementation of DENSE Imaging and Strain Quantification in the Abdominal Aorta

The last vessel parameter we elected to explore was tissue deformation, as there are histological data showing differences in the elastin and collagen orientation of the aorta between men and women that suggest potential differences in vessel compliance.[171] We utilized DENSE MR imaging to quantify displacement in the vessel wall. This imaging sequence provided an advantage over other speckle or pixel

tracking methods as it allowed us to measure displacements smaller than the resolution of the image itself.[178] We acquired these images in the distal half of the abdominal aorta, oriented perpendicular to the vessel's trajectory, permitting quantification of displacement vectors during the systolic phase of the cardiac cycle. *This is the first reported implementation of the DENSE imaging sequence in the abdominal aorta.*

In comparing the displacement vectors around the vessel we found significant differences in both the magnitude and direction. The anterior and antero-lateral walls of the aorta showed the largest net displacement while the posterior demonstrated the least. This is expected given the restrictions to motion imposed on the vessel by the spine in the posterior region. We also observed a greater degree of circumferentially oriented displacement on the lateral walls of the vessel and radially oriented displacement on anterior wall of the vessel. Using a previously described bi-axial strain interpolation method, we found the highest degree of circumferential strain on the posterior "elbows" of the vessel, where the lateral walls meet the posterior wall. This observation is significant given previous studies which have shown more microstructural changes in the lateral walls of AAA that could increase the risk for rupture at that location.[183] Lateral and dorsal segments of the aorta taken from excised aneurysmal specimens showed increased cholesterol-rich lipid core and decreased collagen quantity compared to the anterior wall. It is possible that this heterogeneity in wall mechanics is not significant in the early stages of disease development but becomes more important as the disease progresses. *Our observations that there is an increase in circumferential strain in the aorta that experiences the highest rate of rupture in an AAA patient implicate the role of underlying tissue properties in the risk of disease mortality.*

7.1.6 Differences Between Men and Women in Aortic Mechanics and the Relationship with Hemodynamics

We next evaluated whether our observations were similar between the sexes or if the tissue deformation were in any way related to the hemodynamics. Overall, we did not

observe any significant differences in the range of measured displacements between men and women. If we looked regionally, we observed that there were significant differences in the circumferential displacement on the right side of the vessel with men demonstrating a higher degree of circumferential displacement. In this same region, however, we observed an increase in circumferential strain in women compared with men. This is most likely a result of both men and women having similar displacement values but with women having a smaller radius. This increase in strain in women at baseline could potentially explain the increased rupture risk for women once disease has developed even in the face of equivalent aneurysm diameter.[190]

We did not observe any significant or meaningful correlation between the hemodynamics and the calculated strain or displacement. It is still certain that tissue mechanics and hemodynamics are related. However, in our population of all healthy individuals the variation in tissue properties may have been too small to reveal a relationship in the hemodynamics.

Figure 7.1 summarizes our findings the potential implications.

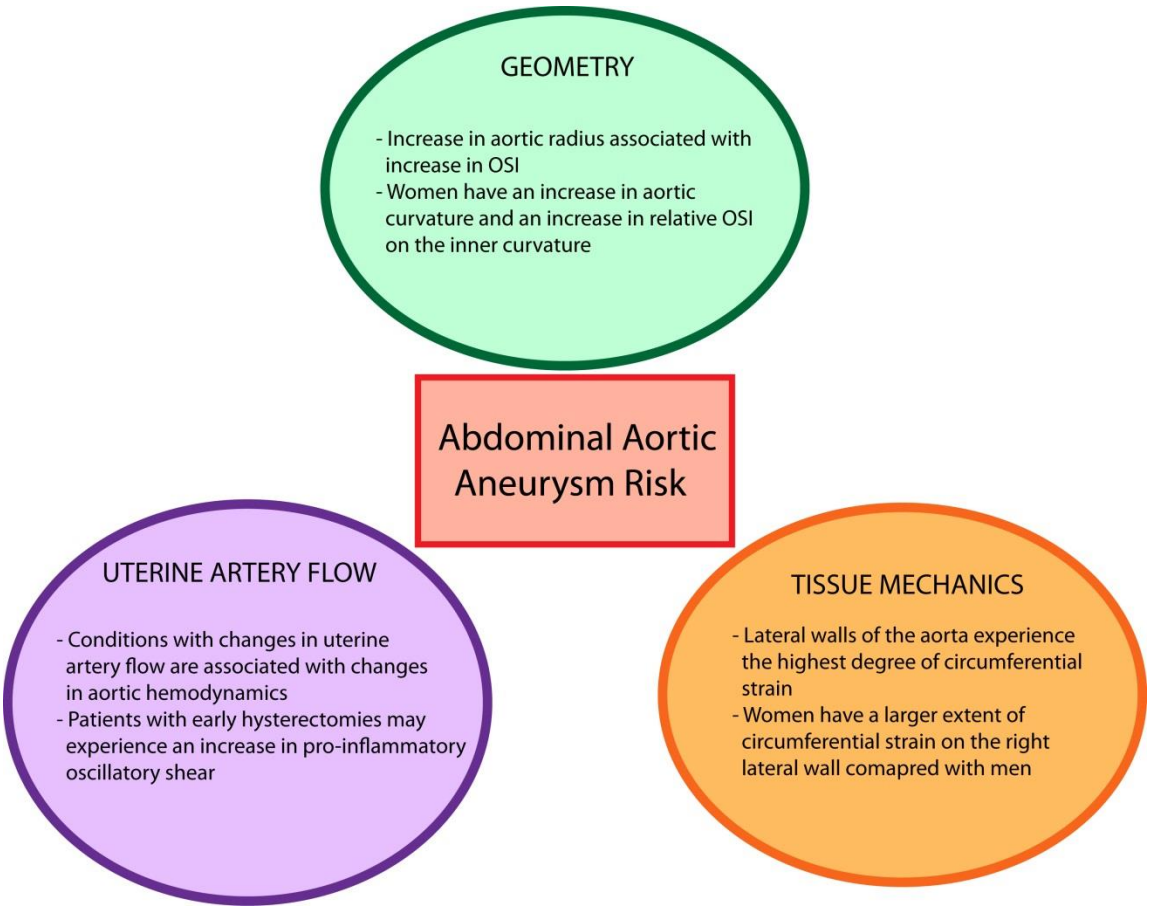

Figure 7.1 Potential New Risk Factors for AAA

7.2 FUTURE WORK

The long-term clinical goal of this research is to aid in the understanding of differences in pathophysiology of abdominal aortic disease between men and women. Currently, screening for AAA is not recommended in women, despite the increased risk in rupture for women who do develop aneurysms.[18, 68] The work laid out here may provide insight into how we could begin to develop selective screening tests for populations of women having a baseline increased risk for developing the disease. More broadly this work attempts to address the pressing need for sex-based research in all cardiovascular disease. [191]

Our work here shows that there are significant differences in the WSS profiles of the sexes, however, the role of WSS in AAA still needs to be clarified. Ideally this would

include a longitudinal study in which WSS measurements are made for a set of the population who would be followed and monitored for development of this disease. However, because of the low incidence of the disease (particularly in women) this approach may be impractical. Further animal model work validating the causal relationship between oscillatory shear and aneurysm is the most appropriate method for confirming this but is outside the scope of this project.[71]

A potentially important follow-up study for our project looking at the role of peripheral resistance, and specifically uterine artery flow, would be to recruit women prior to both uterine artery embolizations and hysterectomies and measure flow before and after treatment. This would allow for a direct intra-volunteer comparison. It would also be beneficial to perform a population study to evaluate the risk of developing an AAA after having had a hysterectomy early in life. Such a study could be performed using some of the currently available databases that are targeted towards women's health such as the Women's Health Initiative or the Nurses' Health Study.

Another worthwhile pursuit is the differences in age related vascular changes in the abdominal aorta between men and women. It has previously been shown that the distensibility of the aorta decreases with age at a different rate between men and women.[115] Specifically, the most significant decreases in compliance in women occur around menopause (as measured by pulse wave velocity) at which point the measured difference in compliance between men and women seems to disappear.[192] In addition to these changes in compliance, uterine artery blood flow declines as a result of loss in hormonal regulation of spiral artery formation.[193] It has not yet been explored however, whether these two change significantly alter either the aortic hemodynamics (as a result of downstream resistance) or the aortic tissue mechanics properties. The ideal experiment would be to measure both tissue displacement and peripheral flow as we described in this experiment and monitor how these values change over time in men and women. However, we would expect that at least 5 to 10 years would be required to

observe any significant differences. Therefore a more feasible alternative would be to compare the peripheral flow and aortic WSS profiles of members of the age population that we have observed here against peri-menopausal and post-menopausal women and age matched men.

An additional experiment that would be of tremendous value is the validation of the strain method used in our work here. Validation of this would require use of an MRI compatible material with known mechanical properties and a mechanism to load the vessel under a known condition. Ideally, a cylindrical tube of this material would be connected to a flow pump for which intra-tube pressures are known. DENSE acquisition could occur using artificial EKG triggering, and both the displacement and strain in the tube material would be calculated using the methods described here. Additional calculations would be made using the tube's material properties and the known loaded pressures and comparisons between the two results would be made.

While MRI was the imaging tool of choice for this study, previous work has utilized ultrasound to quantify displacement and strain in the abdominal aorta. [180] With advances in 3D U/S, quantification of tissue mechanics at multiple locations around the circumference could be performed and compared with results obtained using the methods described here. This would provide an additional level of validation for our methods as well as potential easily accessible imaging tool to be utilized in screening.

7.3 CLINICAL IMPLICATIONS

The purpose of this work was to provide a biomechanical basis for the disparity in risk of AAA development between men and women. We tested the hypothesis that men would exhibit a higher degree of oscillatory shear than women, with the underlying assumption that oscillatory shear plays a role in the development of AAA. We further hypothesized that there would be sex-specific differences in geometry, peripheral resistance and tissue mechanics that would be related to and causal of these differences in

oscillatory shear. *Our foremost conclusion that women exhibit less pro-inflammatory WSS than men is important for how we should consider sex differences in pathophysiology of cardiovascular disease beyond just what we observe in the aorta.* It is likely that in other regions of significant cardiovascular burden, such as the carotid and the coronary arteries, there may be additional vascular parameters that differ between men and women and affect the course of the disease. This body of work furthers the case for sex-specific research in cardiovascular disease, with a special focus on biomechanics.

REFERENCES

1. Organization, W.H. *Leading Causes of Death in Females United States, 2013(current listing).* 2015 [cited 2015.
2. Go AS, M.D., Roger VL, Benjamin EJ, Berry JD, Borden WB, Bravata DM, Dai S, Ford ES, Fox CS, Franco S, Fullerton HJ, Gillespie C, Hailpern SM, Heit JA, Howard VJ, Huffman MD, Kissela BM, Kittner SJ, Lackland DT, Lichtman JH, Lisabeth LD, Magid D, Marcus GM, Marelli A, Matchar DB, McGuire DK, Mohler ER, Moy CS, Mussolino ME, Nichol G, Paynter NP, Schreiner PJ, Sorlie PD, Stein J, Turan TN, Virani SS, Wong ND, Woo D, Turner MB, *Heart disease and stroke statistics-2013 update: a report from the American Heart Association.* Circulation, 2013. **127**: p. e6-e245.
3. Mosca L, J.W., King KB, Ouyang P, Redberg RF, Hill MN, *Awareness, Perception and knowledge of heart disease risk and prevention among women in the US: American Heart Association Women's Heart Disease and Stroke Campaign Task Force.* Arch Game Med, 2000. **9**: p. 506-515.
4. Mosca L, H.G., Mochari-Greenberger H, Towfighi A, Albert MA *Fifteen-Year Trends in Awareness of Heart Disease in Women: Results of a 2012 American Heart Association National Survey.* Circulation, 2013. **127**: p. 1254-1263.
5. Maas A HEM, v.d.S.Y., Reigtz-Zagrosek V, Swahn E, Appelman YE, Pasterkamp G, ten Cate H, Nilsson PM, Huisman MV, Stam HCG, Eizema K, Stramba-Badiale M, *Red alert for women's heart: the urgent need for more research and knowledge on cardiovascular disease in women.* European Heart Journal, 2011. **32**: p. 7.
6. Salerni S, D.F.S., Cadeddu C, Acquistapace F, Maffei S, Gallina S, *The different role of sex hormones on female cardiovascular physiology and function: not only oestrogens.* European Journal of Clinical Investigation, 2015. **45**(6): p. 634-645.
7. SM, H., *Menopausal hormone treatment cardiovascular disease: another look at an unresolved conundrum.* Fertility and Sterility, 2014. **101**(4).
8. Harman SM, V.E., Brinton EA, Budoff MJ, Cedars MI, Lobo RA, Merriam GR, Miller VM, Naftolin F, Pal L, Santoro N, Taylor HS, Black DM, *Timing and Duration of Menopausal Hormone Treatment May Affect Cardiovascular Outcomes* The American Journal of Medicine, 2011. **124**: p. 199-205.
9. Toh S, H.-D.S., Logan R, Rossouw JE, Hernan MA, *Coronary Heart Disease in Postmenopausal Recipients of Estrogen Plus Progestin Therapy: Does the Increase Risk Ever Disappeared.* Annals of Internal Medicine, 2010. **152**: p. 211-217.
10. Giordano S, H.F., Xing D, Chen Y, Allon S, Chen C, Oparil S, *Estrogen and Cardiovascular Disease: Is Timing Everything?* American Journal of Medical Science, 2015. **350**(1): p. 27-35.
11. Harthun, N.L., *Current Issues in the Treatment of Women with Abdominal Aortic Aneurysm.* Gender Medicine, 2008. **5**(1): p. 36-43.
12. Starr JE, H.V., *Abdominal Aortic Aneurysms in women.* Journal of Vascular Surgery, 2013. **57**: p. 7.

13. Grootenboer N, v.S.M., Arends LR, Hendricks JM, Hunink MGM, Bosch JL, *Systematic review and matea-analysis of sex differences in outcome after intervention for abdominal aortic aneurysm.* The British Journal of Surgery, 2010. **97**(8): p. 10.
14. N. Grootenboer, J.L.B., J.M. Hendriks, M. R. H. M. van Sambeek, *Epidemiology, Aetoilogy, Risk of Rupture and Treatment of Abdominal Aortic Aneurysms: Does Sex Matter?* European Journal of Vascular and Endovascular Surgery, 2009. **38**: p. 278-284.
15. FA, L., *Should Abdominal Aortic Aneurysm Be Managed Differently in Women?* Scandinavian Journal of Surgery, 2008. **97**: p. 3.
16. Bart S. Ferket, N.G., Ersen B. Colkesen, Jacob J. Visser, Marc R. H. M. van Sambeek, Sandra Sprink, Ewout W. Steyerber, and M. G. Myriam Hunink, *Systematic review of guiedlines on abdominal aortic aneurysm screening.* Journal of Vascular Surgery, 2012. **55**(5): p. 1296-1304.
17. Norman PE, P.J., *Abdominal Aortic Aneurysm: The Prognosis in Women Is Worse Than in Men.* Circulation, 2007. **115**: p. 2865-2869.
18. Wanhainen A, S.S., Mani K, *Screening for AAA -- Areas Where Information is Still Inadequate.* Scandinavian Journal of Surgery, 2008. **97**: p. 4.
19. Deborah Grady, D.H., Vera Bittner, Roger Blumenthal, Michael Davidson, Mark Hlatky, Judith Hsia, Stephen Hulley, Alan Herd, Steven Khan, L. Kristin Newby, David Waters, Eric Vittinghoff, Vamette Wenger, *Cardiovascular Disease Outcomes During 6.8 Years of Hormone Therapy: Heart and Estrogen/Progestin Replacement Study Follow-up (HERS II).* JAMA, 2002. **288**(1): p. 49/58.
20. Main, C., et al. *Hormone therapy for preventing cardiovascular disease in post-menopausal women*. Cochrane Database of Systematic Reviews, 2013. DOI: 10.1002/14651858.CD002229.pub3.
21. Emma Larsson, F.L., T. Christian Gasser, Jesper Swedenborg, Rebecka Hultgreen, *Analysis of aortic wall stress and rupture risk in patients with abdominal aortic aneurysm with a gender perspective.* Journal of Vascular Surgery, 2011. **54**: p. 295-299.
22. Christina Villard, J.S., Per Eriksson, Rebecka Hultgreen, *Reproductive history in women with abdominal aortic aneurysms.* Journal of Vascular Surgery, 2011. **54**(2): p. 341-345.
23. Sanghavi M, R.J., *Cardiovascular Physiology of Pregnancy.* Circulation, 2014. **130**: p. 1003-1008.
24. GS, K., *Biomechanics of the cardiovascular system: the aorta as an illustratory example.* Journal of the Royal Society Interface, 2006. **3**: p. 719-740.
25. LA, T., *Biomechanics of Cardiovascular Development.* Annual Review of Biomedical Engineering, 2001. **3**: p. 1-25.
26. Topper JN, G.J.M., *Blood flow and vascular gene expression: fluid shear stress as a modulator of endothelial phenotype.* Molecular Medicine Today, 1999: p. 7.
27. Matsumoto T, H.K., *Mechanical and dimensional adaptation of rat aorta to hypertension.* Journal of Biomechanical Engineering, 1994. **116**(3): p. 278-283.
28. Lu X, Z.J., Wang GR, Gregersen H, Kassab GS, *Remodeling of the zero-stress state of femoral arteries in response to flow overload.* American Journal of Physiology Heat Circulation Physiology, 2001. **280**: p. H1547-H1559.

29. CG, C., *Discovery of the Role of Wall Shear in Atherosclerosis.* Arteriosclerosis, Thrombosis, and Vascular Biology, 2008. **29**: p. 4.
30. Haque, N.D.N.a.A.K., *Effect of hemodynamics factors on atherosclerosis in the abdominal aorta.* Atheroscelerosis, 1990. **84**: p. 6.
31. Malek A, A.S., Izumo S, *Hemodynamic shear stress and its role in atherosclerosis.* JAMA, 1999. **282**.
32. Li YJ, H.J., Chien S, *Molecular Basis of the Effects of Shear Stress on Vascular Endothelial Cells.* Journal of Biomechanics, 2005. **38**: p. 22.
33. Davies PF, S.J., Krams R, *Shear Stress of the Endothelium.* Annals of Biomedical Engineering, 2005. **33**(12): p. 1714-1718.
34. Resnick N, Y.H., Shay-Salit A, Shushy M, Schubert S, Zilberman LCM, Wofovitz E, *Fluid shear strss and the vascular endothelium: for better and for worse.* Biophysics & Molecular Biology, 2003. **81**: p. 177-199.
35. Brooks AR, L.P., Rubanyi GM, *Gene Expression profiling of human aortic endothelial cells exposed to disturbed flow and steady laminar flow.* Phyisol Genom, 2002. **9**(27).
36. Ku DN, G.D., Zarins CK, Glagov S, *Pulsatile flow and atherosclerosis in the human carotid bifurcation. Positive correlation between plaque location and low oscilllating shear stress.* Arteriosclerosis, 1985. **5**(3): p. 10.
37. Markl, M., et al., *Co-registration of the distribution of wall shear stress and 140 complex plaques of the aorta.* Magnetic Resonance Imaging, 2013. **31**(7): p. 1156-1162.
38. E.M. Pedersen, S.O., M. Agerbaek, I.B. Kristensen, S. Rnggaard, P. Boesinger, and W.P. Paaske, *Distribution of Early Atherosclerotic Lesions in the Human Abdominal Aorta Correlates with Wall Shear Stresses Measured In Vivo.* European Journal of Vascular Surgery, 1999. **18**: p. 5.
39. Markl M, W.F., Zrch T, Bauer S, Stecker C, Schumacher M, Weiller C, Hennig J, Harloff A, *In Vivo Wall Shear Stress Distribution in the Carotid Artery: Effect of Bifurcation Geometry, Internal Carotid Artery Stenosis, and Recanalization Therapy.* Circulation Cardiovascular Imaging, 2010. **3**(6).
40. Peiffer V, S.S., Weinberg PD, *Does low and oscillatory wall shear stress correlate spatially with early atherosclerosis? A systematic review.* Cardiovascular Research, 2013. **99**: p. 242-250.
41. Haskett D, J.G., Zhou A, Utzinger U, Vande Deest JV, *Microstructural and biomechanical alterations of the human aorta as a function of age and location.* Biomechanical Modeling in Mechanobiology, 2010. **9**: p. 725-736.
42. Zeinali-Davarani S, R.L., Vorp DA, Baek S, *Identification of in vivo material and geometric parameters of a human aorta: toward patient-specific modeling of abdominal aortic aneurysm.* Biomechanical Modeling in Mechanobiology, 2011. **10**: p. 689-699.
43. Vande Geest JP, S.M., Vorp DA, *Age dependency of the biaxial biomechanical behavior of human abdominal aorta.* Journal of Biomechanical Engineering, 2004. **126**(6): p. 815-822.
44. Kassab GS, G.H., Nielsen SL, Lu Z, Tanko LBm Falk E, *Remodelling of the left anterior descending artery in a porcine model of supravalvular aortic stenosis.* Journal of Hypertension, 2002. **20**: p. 2429-2437.

45. Freestone, T., et al., *Inflammation and Matrix Metalloproteinases in the Enlarging Abdominal Aortic Aneurysm.* Arteriosclerosis, Thrombosis, and Vascular Biology, 1995. **15**(8): p. 1145-1151.
46. Baaijens F, B.C., Driessen N, *Modeling collagen remodeling.* Journal of Biomechanics, 2010. **43**: p. 166-175.
47. Gleason RL, H.J., *A 2D constrained mixture model for arterial adaptations to large changes in flow, pressure and axial stretch.* Mathematical Medicine and Biology, 2005. **22**: p. 347-369.
48. YC, F., *Biomechanics: motion, flow, stress and growth*. 1990, New York, NY: Spring.
49. Guo Z, L.X., Kassab S, *Transmural strain distribution in the blood vessel wall.* American Journal of Physiology Heat Circulation Physiology, 2005. **288**: p. H881_H886.
50. Wilkinson IB, F.S., Jansen IM, Spratt JC, Murray GD, Cockcroft JR, Webb DJ, *Reproducibility of pulse wave velocity and augmentation index measured by pulse wave analysis.* Journal of Hypertension, 1998. **16**: p. 2079-2084.
51. *Transesophageal echocardiographic assessment of the effects of age, gender, and hypertension on thoracic arotic wall size, thickness, and stiffness.* American Heart Journl, 1994. **128**(2): p. 344-351.
52. Soljanlahti S, A.T., Hyttinen L, Vuorio AF, Keto P, Lauerma K, *Compliance of the aorta in two disease affecting vascular elasticity, familial hypercholesterolemia, and diabetes: a MRI study.* Vascular Health and Risk Management, 2008. **4**(5): p. 1103-1109.
53. Bargiotas I, M.E., Yu W, Venkatesh BA, Bollache E, de Cesare A, Lima J AC, Redheuil A, Kachenoura N *Estimation of aortic pulse wave transit time in cardiovascular magnetic resonance using complex wavelet cross-spectrum analysis.* Journal of Cardiovascular Magnetic Resonance, 2015. **17**.
54. Davies PF, T.S., *Mechanical stress mechanisms in cells: an endothelial paradigm.* Circulation Research, 1993. **72**: p. 239-245.
55. Stamenovic D, F.J., Wang N, Butler JP, Ingber DE, *A Microstructural Approach to Cytoskeletal Mechanics based on Tensegrity.* Journal of Theoretical Biology, 1996. **181**: p. 125-136.
56. Chiu JJ, U.S., Chien S, *Vascular endothelial responses to altered shear stress: Pathologic implications for atherosclerosis.* Annals of Medicine, 2009. **41**: p. 19*28.
57. PF, D., *Hemodynamic shear stress and the endothelium in cardiovascular pathophysiology.* Nature Clincal Practice Cardiovascular Medicine, 2009. **6**(1): p. 16-26.
58. Zhou J, L.Y., Chien S, *Shear Stress - Initiated Signaling and Its Regulation of Endothelial Function.* Arteriosclerosis Thrombosis and Vascular Biology, 2014. **34**: p. 2191-2198.
59. Davies PF, C.M., Fang Y, Fleming I, *The atherosusceptible endothelium: endothelial phenotypes in complex haemodynamic shear stress regions in vivo.* Cardiovascular Research, 2013. **99**: p. 315-327.

60. Dhawan SS, N.R., Branch JR, Taylor WR, Quyyumi AA, Jo H, McDaniel MC, Suo J, Giddens D, Samady H, *Shear stress and plaque development.* Expert Rev. Cardiovascular Ther., 2010. **8**(4): p. 545-556.
61. Cecchi R, G.C., Valente S, Lazzeri C, Gensini GF, Abbate R, Mannini L, *Role of hemodynamic shear stress in cardiovascular disease.* Atherosclerosis, 2011. **214**: p. 249-265.
62. McNally JS, D.M., Giddens DP, Saha A, Hwang J, Dikalov S, Jo H, Harrison DG, *Role of xanthine oxidoreductase and NAD(P)H oxidase in endothelial superoxide production in response to oscillatory shear stress.* American Journal of Physiology Heat Circulation Physiology, 2003. **285**: p. H2290-H2297.
63. Cai H, H.D., *Endothelial dysfunction in cardiovascular diseases: the role of oxidant stress.* Circulation Research, 2000. **87**(10): p. 840-844.
64. Bentzon JF, W.C., Sondergaard CS, Hindkjaer J, Kassem M, Falk E, *Smooth Muscle Cells in Atherosclerosis Originate From the Local Vessel Wall and Not Circulating Progenitor Cells in ApoE Knockout Mice.* Arteriosclerosis Thrombosis and Vascular Biology, 2006. **26**: p. 2696-2702.
65. Galis ZS, K.J., *Matrix Metalloproteinases in Vascular Remodeling and Atherogenesis: The Good, the Bad, and the Ugly.* Circulation Research, 2002. **90**: p. 251-262.
66. Liu J, S.G., Sun J, Xu W, Libby P, Shi G, *Lysosomal Cysteine Proteases in Atherosclerosis.* Arteriosclerosis Thrombosis and Vascular Biology, 2004. **24**: p. 1359-1366.
67. Chatzizisis YS, C.A., Jonas M, Edelman ER, Feldman CL, Stone PH, *Role of Endothelial Shear Stress in the Natural History of Coronary Athersclerosis and Vascular Remodeling: Molecular Cellular and Vascular Behavior.* Journal of the American College of Cardiology 2007. **49**(25): p. 15.
68. FF, M., *Screening for abdominal aortic aneurysm.* Journal of Vascular Surgery, 2015. **62**(3): p. 774-778.
69. Kuivaniemi H, E.D., *Opportunities in Abdominal Aortic Aneurysm Research: Epidemiology, Genetics, and Pathophysiology.* Annals of Vascular Surgery, 2012. **26**: p. 862-870.
70. Moore JE, M.S.K.D., Boesinger P, *Hemodynamics in the abdominal aorta: a comparison of in vitro and in vivo measurements.* Journal of Applied Physiology, 1994. **76**(4): p. 1520-1527.
71. Amirbekian S, L.R., Consolini MA, Suo J, Willett NJ, Fielden SW, Giddens DP, Taylor WR, Oshinski JN, *In vivo assessment of blood flow patterns in abdominal aorta of mice with MRI: implications for AAA localization.* American Journal of Physiology Heat Circulation Physiology, 2009. **297**(4).
72. Sonesson B, H.F., Lanne T, *Abdominal aortic aneurysm: A general defect in the vasculature with focal manifestations in the abdominal aorta?* Journal of Vascular Surgery, 1997. **26**(2): p. 247-254.
73. Huffman MD, C.J., Moore G, Kerns DB, Starcher BC, Thompson RW, *Functional importance of connective tissue repair during the development of experimental abdominal aortic aneurysms.* Surgery, 2000. **128**: p. 429-438.
74. Satta J, J.T., Haukipuro K, Juvonen M, Kairaluoma MI, *Increased turnover of collagen in abdominal aortic aneurysms, demonstrated by measuring the*

concentration of the aminoterminal propeptide of type III procollagen in peripheral and aortal blood samples. Journal of Vascular Surgery, 1995. **22**: p. 155-160.
75. Holmes DR, L.S., Parks WX, Thompson RW, *Medial neovascularization in abdominal aortic aneurysms: a histopathologic marker of aneurysmal degeneration with pathophysiologic implications.* Journal of Vascular Surgery, 1995. **21**(5): p. 761-772.
76. Herron GS, U.E., Wong M, Rapp JH, Hibbs MH, Stoney RJ, *Connective Tissue Proteinases and Inhibitors in Abdominal Aortic Aneuryms: Involvement of the Vasa Vasorum in the Pathogenesis of Aortic Aneurysms.* Arteriosclerosis and Thrombosis, 1991. **11**: p. 1667-1677.
77. Longo GM, X.W., Greiner TC, Zhao Y, Fiotti N, Baxter BT, *Matrix metalloproteinases 2 and 9 work in concert to produce aortic aneurysms.* The Journal of Clinical Investigation, 2002. **110**(5): p. 625-632.
78. JHN, L., *The pathophysiologic basis of abdominal aortic aneurysm progression: a critical appraisal.* Expert Review of Cardiovascular Therapy, 2015. **13**(7): p. 839-851.
79. Zankl AR, S.H., Krumsdorf U, Katus HA, Jahn L, Tiefenbacher CP, *Pathology, natural history and treatment of abdominal aortic aneurysms.* Clinical Research in Cardiology, 2007. **96**: p. 140-151.
80. Singh K, B.K.J.B., Bjork L, Solber S, *Prevalence of and Risk Factors for Abdominal Aortic Aneurysms in a Population-based Study.* American Journal of Epidemiology, 2001. **154**(3): p. 236-244.
81. Lederle FA, J.G., Wilson SE, Chute EP, Littooy FN, Bandyk D, Krupski WC, Barone GW, Acher CW, Ballard DJ, *Prevalence and Associations of Abdominal Aortic Aneurysm Detected through Screening.* Annals of Internal Medicine, 1997. **126**: p. 441-449.
82. Lindholt JS, H.N., Vammen S, Fasting H, Henneberg EW, Heichendorff L, *Smoking, but not Lipids, Lipoprotein (a) and Antibodies Against Oxidised LDL, is Correlated to the Expansion of Abdominal Aortic Aneurysms.* European Journal of Endovascular Surgery, 2001. **21**: p. 51-56.
83. Powell JT, G.R., *Small Abdominal Aortic Aneurysms.* The New England Journal of Medicine, 2003. **348**: p. 1895-1901.
84. Xie X, L.H., Moorleghen JJ, Howatt DA, Rateri DL, Cassis LA, Daugherty, *Doxycycline Does Not Influence Established Abdominal Aortic Aneurysms in Angiotensin II-Infused Mice.* PLoS One, 2012. **7**(9): p. 1-6.
85. Curci JA, M.D., Bohner DG, Allen BT, Rubin BG, Reilly JM, Sicard GA, Thompson RW, *Preoperative treatment with doxycycline reduces aortic wall expression and activation of matrix metalloproteinases in patients with abdominal aortic aneurysms.* Journal of Vascular Surgery, 2000. **31**: p. 325-342.
86. Greenhalgh RM, B.L., Kwong GP, Powell JT, Thompson SG; EVAR trial participants, *Comparison of endovascular aneurysm repair with open repair in patients with abdominal aortic aneurysm (EVAR trial 1), 30-day operative mortality results: randomised controlled trial.* Lancet, 2004. **364**: p. 843-848.

87. Prinssen M, V.E., Buth J et al, *A randomized trial comparing conventional and endovascular repair of abdominal aortic aneurysms.* The New England Journal of Medicine, 2004. **351**: p. 1607-1618.
88. Participants, T.U.K.S.A.T., *Longterm outcomes of immediate repair compared with surveillance for small abdominal aortic aneurysm.* The New England Journal of Medicine, 2002. **346**: p. 1445-1452.
89. Participants, T.U.S.A.T., *Mortality results for randomised controlled trial of early elective surgery or ultrasonographic surveillance for small abdominal aortic aneurysms.* Lancet, 1998. **352**: p. 1649-1655.
90. VanderLaan PA, R.C., Getz GS, *Site Specificity of Atherosclerosis: Site-Selective Responses to Atherosclerotic Modulators.* Arteriosclerosis Thrombosis and Vascular Biology, 2004. **24**: p. 12-22.
91. Bourantas CV, L.H., Sherwi N, Tweddel AC, de Silva R, Lukaschuk EI, Nicholson A, Rigby AS, Thackray SD, Ettles DF, Nikitin NP, Clark AL, Cleland JGF, *Atherosclerotic disease of the abdominal aorta and its branches: prognostic implications in patients with heart failure.* Heart Failure Review, 2012. **17**: p. 229-239.
92. Gallino A, A.V., Diehm C, Cosentino F, Stricker H, Falk E, Schouten P, Lekakis J, Amann-Vesti B, Siclari F, Poredo P, Novo S, Brodmann M, Schulte KL, Vlachopoulos C, De Caterina R, Libby P, Baumgartner I, *Non-coronary atherosclerosis.* European Heart Journal, 2014. **35**: p. 1112-1119.
93. Bijar PB, W.B., Steinman DA, *Carotid Bifurcation Geometry Is an Independent Predictor of Early Wall Thickening at the Carotid Bulb.* Stroke, 2013.
94. Motomiya M, K.T., *Flow patterns in the human carotid artery bifurcation.* Stroke, 1984. **15**(1): p. 50-56.
95. Augst AD, A.B., Thom SAG, Xu XY, Hughes AD, *Analysis of complex flow and the relationship between blood pressure, wall shear stress, and intima-media thickness in the human carotid artery.* American Journal of Physiology Heat Circulation Physiology, 2007. **293**: p. H1031-H1037.
96. Endo S, G.H., Karino T, *Flow patterns and preferred sites of atherosclerotic lesions in the human aorta -- I. Aortic Arch.* Biorheology, 2014. **51**: p. 239-255.
97. James E. Moore Jr., C.X., Seymour Glagov, Christopher K. Zarins, David N. Ku, *Fluid wall shear stress measurements in a model of the human abdominal aorta: oscillatory behavior and relationship to atherosclerosis.* Atheroscelerosis, 1994. **110**: p. 15.
98. E.M. Pedersen, M.A., I.B. Kristensen, and A.P. Yoganathan, *Wall Shear Stress and Early Atherosclerotic Lesions in the Abdominal Aorta in Young Adults.* European Journal of Vascular Surgery, 1997. **13**: p. 8.
99. Vollmar JR, P.E., Pauschinger P, Gross P, *[Aneurysm of the abdominal aorta and leg amputation. A chance coincidence or a pathogenetic correlation?]*. Deutsche medizinische Wochenschrift, 1988. **113**(46): p. 5.
100. Smolensky AV, C.-G.S., Taylor RW, Oshinski JN, *Lower extremity amputation increases oscillatory flow in the infrrenal aorta: A new potential risk factor for abdominal aortic aneurysm development.* Journal of Cardiovascular Magnetic Resonance, 2012. **14**: p. 2.

101. Barba A, E.L., Rodriguez L, Baquer M, & Vega de Ceniga M, *Detection of Abdominal Aorta Aneurysm in Patients with Peripheral Artery Disease.* European Journal of Vascular Surgery, 2005. **30**: p. 5.
102. Shamoun FE, F.G., Mookadam M, *Vascular Medicine: aortic and peripheral arterial disease.* Primary Care, 2013. **40**(1): p. 9.
103. Yeung JJ, J.H., Abbruzzese TA, Vignon-Clementel EI, Draney-Blomme MT, Yeung KK, Perkash I, Herfkens RJ, Talor CA, Dalman RL, *Aortoiliac hemodynamic and morphologic adaptation to chronic spinal cord injury.* Journal of Vascular Surgery, 2006. **44**: p. 1254-1265.
104. Dua MM, D.R., *Hemodynamic influences on abdominal aortic aneurysm disease: Application to aneurysm pathophysiology.* Vascular Pharmacology, 2010. **53**: p. 11-21.
105. Guedes-Martins L, e.a., *Internal iliac and uterine arteries Dopple ultrasound in the assessment of normotensive and chronic hypertensive pregnant women.* Scientific Reports, 2014. **4**.
106. Jinno M, O.T., Iwashita M, Nakamura Y, Kudo A, Hirano H, *Measurement of endometrial tissue blood flow: a novel way to assess uterine receptivity for implantation.* Fertility and Sterility, 2001. **76**(6): p. 1168-1174.
107. Pearson AC, G.R., Orsinelli DA, Binkley PF, Pasierski TJ, *Transesophageal echocardiographic assessment of the effects of age, gender, and hypertension on thoracic aortic wall size, thickness, and stiffness.* American Heart Journl, 1994. **128**: p. 344-351.
108. Nanna B. Johansen, D.V., Eric J. Brunner, Adam G. Tabak, Martin J Shipley, Ian b. Wilkinson, Carmel M. McEniery, Michael Roden, Christian Herder, Mike Kivimaki, Daniel R. Witte, *Determinants of Aortic Stiffness: 16-Year Follow-up of the Whitehall II Study.* PLoS One, 2012. **7**(5): p. 1-8.
109. Safar ME, B.H., *Vascular Development, Pulse Pressure, and the Mechanisms of Hypertensions.* Hypertension, 2005. **46**: p. 205-209.
110. Gatehouse PD, K.J., Crowe LA, Masood S, Modiaddin RH, Kreitner KF, Firmin DN, *Applications of phase-contrast flow and velocity imaging in cardiovascular MRI.* European Radiology, 2005. **15**: p. 20172-2184.
111. Lotz J, M.C., Leppert A, Galanski M, *Cardiovascular flow measuremnt with phase-contrast MR imaging: basic facts and implementation.* Radiographics, 2002. **22**(3): p. 651-671.
112. Jiang J, K.P., Ying W, Magnano C, Zivadinov R, Haacke, *Quantifying errors in flow measurement using phase contrast magnetic resonance imaging: comparison of several boundary detection methods.* Magnetic Resonance Imaging, 2015. **33**: p. 185-193.
113. Nayler GL, F.D., Longmore DB, *Blood flow imaging by cine magnetic resonance.* Journal of Computer Assisted Tomography, 1986. **10**: p. 715-722.
114. Markl M Schnell S, W.C., Bollache E, Jarvis K, Barker AJ, Robinson JD, Rigsby CK, *Advanced flow MRI: emerging techniques and applications.* Clinical Radiology, 2016.
115. Rose JL, L.A., Bouchot O, Bourennane EB, Walker PM, Ugolini P, Revol-Muller C, Cartier R, Brunote F, *Influence of age and sex on aortic distensibility assessed by MRI in healthy subjects.* Magnetic Resonance Imaging, 2010. **28**.

116. RH Mohiaddin, S.U., HG Brogran, DN Firmin, RH Klipstein, RSO Rees, DB Longmore, *Regional aortic compliance studied by magnetic resonance imaging: the effects of age, training, and coronary artery disease.* British Heart Journal, 1989. **62**(2): p. 90-96.
117. T. Lanne, B.S., D. Bergqvist, H Bengtsson, D. Gustafsson, *Diameter and compliance in the male human abdominal aorta: Influence of age and aortic aneurysm.* European Journal of Vascular Surgery, 1991. **6**(2): p. 178-184.
118. Anne Long, L.R., Alvine Bissery, Patrick Rossignol, Dikran Mouradian, Marc Sapovall, *Compliance of abdominal aortic aneurysms evaluated by tissue Doppler imaging: Correlation with aneurysm size.* Journal of Vascular Surgery, 2005. **42**(1): p. 18-26.
119. Jonathan D. Suever, J.O., Enrique Rojaas-Campos, David Huneycutt, Francesca Cardarelli, Arthur E. Stillman, Paolo Raggi, *Reproducibility of pulse wave velocity measurements with phase contrast magnetic resonance and applanation tonometry.* Internation Journal of Cardiovascular Imaging, 2011.
120. Samuel W. Fielden, B.K.F., Michael Jerosch-Herold, Robert L. Eisner, Arthur E. Stillman, John N. Oshinski, *A New Method for the Determination of Aortic Pulse Wave Velocity Using Cross-Correlation on 2D PCMR Velocity Data.* Journal of Magnetic Resonance Imaging, 2008. **27**(6): p. 1382-1387.
121. Ben-Shlomo Y, S.M., Boustred C, May M, Anderson SG, Benjamin EJ, Boutouyrie P, Cameron J, Chen C, Cruickshank JK, Hwang S, Lakatta EG, Laurent S, Maldonado J, Mitchell GF, Najjar SS, Newman AB, Ohishi M, Pannier B, Pereira T, Vasan RS, Shokawa T, Sutton-Tyrell K, Verbeke F, Wang K, Webb DJ, Hansen TW, Zoungas S, McEniery CM, Cockcroft JR, Wilkinson IB, *Aortic Pulse Wave Velocity Improves Cardiovascular Event Prediction.* Journal of the American College of Cardiology, 2014. **63**(7): p. 636-646.
122. Voges I, J.-H.M., Hedderhc J, Pardun E, Hart C, Gabbert DD, Hansen JH, Petko C, Kramer HH, Rickers C, *Normal values of aortic dimensions, distensibility, and pulse wave velocity in children and young adults: a cross-sectional study.* Journal of Cardiovascular Magnetic Resonance, 2012. **14**(77).
123. Kar J, K.A., Cupps BP, Pasque MK, *A Validation of Two-Dimensional In Vivo Regional Strain Computed from Displacement Encoding with Stimulated Echoes (DENSE), in Reference to Tagged Magnetic Resonance Imaging and Studies in Repeatability.* Annals of Biomedical Engineering, 2013.
124. Haraldsson H, H.M., Acevedo-Bolton G, Tseng E, Zhong X, Epstein FH, Ge L, Saloner D, *Feasibility of assymetric stretch assessment in the ascending aortic wall with DENSE cardiovascular magnetic resonance.* Journal of Cardiovascular Magnetic Resonance, 2014. **16**(1): p. 8.
125. Kar J, K.A., Cupps BP, Zhong X, Pasque MK, *A Three-Dimensional Regional Strain Computation Method with Displacement ENcoding with Stimulated Echoes (DENSE) in Non-Ischemic, Non-Valvular Dilated Cardiomyopathy Patients and Healthy Subjects Validated by Tagged MRI.* Journal of Magnetic Resonance Imaging, 2015. **41**(2): p. 386-396.
126. Zhong X, S.B., Meyer CH, Kramer CM, Epstein FH, *Imaging three-dimensional myocardial mechanics using navigator gated volumetric spiral cine DENSE MRI.* Magnetic Resonance in Medicine, 2010. **64**: p. 1089-1097.

127. Zhong X, G.L., Spottiswoode BS, Gilliam AD, Meyer CH, French BA, Epstein FH, *Comprehensive cardiovascular magnetic resonance of myocardial mechanics in mice using three-dimensional cine DENSE.* . Journal of Cardiovascular Magnetic Resonance, 2011. **13**(83).
128. Feng L, D.R., Babb J, Axel L, Kim D, *Numerical and In Vivo Validation of Fast Cine DENSE MRI for Quantification of Regional Cardiac Function.* Magnetic Resonance Medicine, 2009. **62**(3): p. 682-690.
129. Grandas OH, M.D., Kirkpatrick SS, Cassada DC, Stevens SL, Freeman MB, Goldman MH, *Regulation of vascular smooth muscle cell expression and function of matrix metalloproteinases is mediated by estrogen and progesterone exposure.* Journal of Vascular Surgery, 2009. **49**(1): p. 185-191.
130. Fischer GM, S.M., *Influence of contraceptive and other sex steroids on aortic collagen and elastin.* Experimental Molecular Pathology, 1980. **33**(1): p. 15-24.
131. Cheng C, T.D., van Haperen R, et al, *Atherosclerotic lesion size and vulnerability are determined by patterns of fluid shear stress.* Circulation, 2006. **113**(2744).
132. Shaaban A, D.A., *Wall shear stress and early atherosclerosis: a review.* AJR Am J Roentgenol, 2000. **174**: p. 1657-1665.
133. Ptersson S, D.P., Ebbers T, *Assessment of the Accuracy of MRI Wall Shear Strss Estimation Using Numerical Simulations.* Journal of Magnetic Resonance Imaging, 2012. **36**: p. 128-138.
134. Pipe, J., *A Simple Measure of Flow Disorder and Wall Shear Stress in Phase Contrast MRI.* Magnetic Resonance in Medicine, 2003. **49**: p. 543-550.
135. Oshinski J, K.D., Mukundan S Jr, Loth F, Pettigrew R, *Determination of wall shear stress in the aorta with the use of MR phase velocity mapping.* JMRI, 1995. **5**: p. 640-647.
136. Pantos I, P.G., Efstathopoulos EP, Katrisis D, *In vivo wall shear stress measurements using phase-contrast MRI.* Expert Rev. Cardiovascular Ther., 2007. **5**(5): p. 927-938.
137. Womersley, J., *Method for the Calculation of Velocity, Rate of Flow, and Viscous Drag in Arteries when the Pressure Gradient is Known.* Journal of Physiology, 1955. **127**: p. 10.
138. Edelman RR , S.J., Dunkle E , Schindler N , Carr J , Koktzoglou I *Quiescent-interval single-shot unenhanced magnetic resonance angiography of peripheral vascular disease: technical considerations and clinical feasibility* Magnetic Resonance Imaging, 2010. **63**(4): p. 951-958.
139. S. Bidhult, M.C., K. Steding-Ehrenborg, H. Arheden, and E. Heiberg. *A new method for vessel segmentation bsaed on a priori input from medical expertise in cine phase-contrast Magnetic Resonance Imaging*. in *Proceddings of Seventeen Annual SCMR Scientific Sessions*. 2014. New Orleans, USA.
140. Timmins LH, M.D., Eshtehardi P, McDaniel MC, Oshinski JN, Samady H, Giddens DP, *Focal Association Between Wall Shear Stress and Clinical Coronary Artery Disease Progression.* Annals of Biomedical Engineering, 2015. **43**: p. 94-106.
141. GB, M., *A proposal for strength-of-agreement criteria for Lin's Concordance Correlation Coefficient*, 2005, NIWA.

142. Oyre S, R., Kozerke S, Paaske WP, Scheidegger MB, Booesiger P, Pedersen EM *Quantitation of Circumferential Subpixel Vessel Wall Position and Wall Shear Stress by Multiple Sectored Three-Dimensional Paraboloid Modeling of Velocity Encoded Cine MR.* Magnetic Resonance in Medicine, 1998. **40**: p. 645-655.
143. Dyverfeldt P, B.M., Barker AJ, Bolger AF, Carlhall C. Ebbers T, Francios CJ, Frydrychowicz A, Geiger J, Giese D, Hope MD, Kilber PJ, Kozerke S, Myerson S, Neubauer S, Wieban O, Markl M, *4D flow cardiovascular magnetic resonance consensus statement.* Journal of Cardiovascular Magnetic Resonance, 2015. **17**.
144. Cecchi E, G.C., Valente S, Lazzeri C, Gensini GF, Abbate R, Mannini L, *Role of hemodynamic shear strss in cardiovascular disease.* Atheroscelerosis, 2011. **214**: p. 249-256.
145. Morris PD, N.A., von Tengg-Kobligk H, Silva Sota DA, Hsiao S, Lungu A, Evans P, Bressloff NW, Lawford PV, Hose DR, Gunn JP, *Computation fluid dynamics modelling in cardiovascualr medicine.* Heart, 2016. **102**: p. 18-28.
146. Hodnett PA, K.I., Davarpanah AH, Scanlon TG, Collins JD, Sheehan JJ, Dunkle EE, Gupta N, Carr JC, Edelman RR, *Evaluation of Peripheral Arterial Disease with Nonenhanced Quiescent-Interval Single-Shot MR Angiography.* Radiology, 2011. **260**(1): p. 12.
147. Steinman DA, V.D., Ethier CR, *Computational modeling of arterial biomechanics: Insights into pathogenesis and treatment of vascular disease.* Journal of Vascular Surgery, 2003. **37**: p. 1118-1128.
148. Pedersen EM, O.S., Agerbaek M, Kristensen IB, Ringgaard S, Boesiger P, Paaske WP, *Distribution of Early Atherosclerotic Lesions in the Human Abdominal Aorta Correlates with Wall Shear Stresses Measured In Vivo.* European Journal of Vascular Surgery, 1999. **18**: p. 6.
149. Wells DR, A.J.J., Kleinstreuer C, *Effect of carotid artery geometry on the magnitude and distribution of wall shear stress gradients.* Journal of Vascular Surgery, 1996. **23**(4).
150. Burk J, B.P., Stankovic Z, Barker A, Russe M, Geiger J, Frydrychowicz A, Langer M, Markl M, *Evaluation of 3D blood flow patters and wall shear strss in the normal and dilated thoracic aorta using flow-sensitive 4D CMR.* Journal of Cardiovascular Magnetic Resonance, 2012. **14**(84).
151. Ward EV, G.M., Usman A, Popescu AR, Dunkle E, Edelman RR, *Comparison of quiescent inflow single-shot and native space for nonenhanced periperhal MR angiography.* Journal of Magnetic Resonance Imaging, 2013.
152. Gao X, S.J., and Martin ER, *A Multiple Testing Correction Method for Genetic Association Studies Using Correlated Single Nucleotide Polymorphisms.* Genetic Epidemiology, 2008. **32**: p. 361-369.
153. Eric B. Rosero, R.P., Amit Khera, Patrick Clagett, Hao Lo, Carlos H. Timaran, *Sex, race, and age distributions of mean aortic wall thickness in a multiethnic population-based sample.* Journal of Vascular Surgery, 2011. **53**(4): p. 950-957.
154. O'Flynn PM, O.S.G., Pandit AS, *Geometric variability of the abdominal aorta and its major peripheral branches.* Annals of Biomedical Engineering, 2010. **38**(3): p. 16.
155. Sweeting MJ, B.R., Desgranges P. Ulus P, Powell JT, *Individual-patient meta-analysis of three randomized trials comparing endovascular versus open repair*

for ruptured abdominal aortic aneurysm. British Journal of Surgery, 2015. **102**: p. 1229-1239.
156. Austin GE, M.T., *Gender and pre-atherosclerotic lesions. Effects on prevalence in human abdominal aortas.* Archives of pathology & laboratory medicine, 1984. **108**(10): p. 811-813.
157. Erhart P, H.-D.A., Geisbusch P, Kotelis D, Muller-Eschner M, Gasser TC, von Tengg-Kobligk H, Bockler D, *Finite Element Analysis in Asymptomatic, Symptomatic and Ruptured Abdominal Aortic Aneurysms: In Search of New Rupture Risk Predictors.* European Journal of Endovascular Surgery, 2015. **49**: p. 239-245.
158. Khosla S, M.D., Moxon JV, Walker PJ, Gasser TC, Golledge J, *Meta-analysis of peak wall stress in ruptured, symptomatic and intact abdominal aortic aneurysms.* British Journal of Surgery, 2014. **101**: p. 1350-1357.
159. Kelly S, O.R.M., *Fluid, solid and fluid-structure interaction on patient based abdominal aortic aneurysm models.* Proceedings of the Institute of Mechanical Engineers, 2012. **226**(4): p. 16.
160. Devereux RB, P.T., Alderman MH, Chien S, Borer JS, Laragh JH, *Left Ventricular Hypertrophy in Hypertension: Prevalence and Relationship to Pathophysiologic Variables.* Hypertension, 1987. **9**.
161. Palevsky HI, F.A., *Chronic Cor Pulmonale: Etiology and Management.* Journal of American Medical Association, 1990. **263**: p. 2347-2353.
162. Vollmar JF, P.E., Pauschinger P, Henze E, Friesch A, *Aortic aneurysms as late sequelae of above-knee amputation.* Lancet, 1989. **2**(8667): p. 2.
163. Gordon IL, K.C., Arefi M, Complin RA, Vulpe M., *Spinal cord injury increases the risk of abdominal aortic aneurysm.* The American Surgeon, 1996. **62**(3): p. 249-252.
164. Carter EB, G.K., Tuuli MG, Odibo L, Cahill AG, Macones GA, Odibo AO, *Evaluating the Optimal Definition of Abnormal First-Trimester Uterine Artery Dopple Parameters to Predict Adverse Pregnancy Outcomes.* Journal of Ultrasound in Medicine, 2015. **34**(7): p. 1265-1269.
165. CR, R., *Distribution of cardiac ouput in ovine pregnancy.* American Journal of Phyisiology, 1977. **232**(3): p. H231-H235.
166. Versluis B, N.P., Wildberger JE, Schurink GW, Leiner T, Backes WH, *Magnetic resonance imaging-derived arterial peak flow in peripheral arterial disease: towards a standardized measurement.* European Journal of Vascular Endovascular Surgery, 2014. **48**(2): p. 185-192.
167. Exacoustòs C, L.S., Caporale E, Minghetti MC, Angelozzi D, Arduini D, Romanini C., *Monitoring of hormone therapy in postmenopausal women by trasvaginal sonography and color flow doppler: study in different phases of sequential therapy.* Fertility and Sterility, 1999. **71**(3): p. 536-543.
168. Villard C, S.J., Eriksson P, Hultgren R., *Reproductive history in women with abdominal aortic aneurysms.* Journal of Vascular Surgery, 2011. **54**(2): p. 341-345.
169. Parker BA, S.S., Pelberg JA, Mishkin AD, Proctor DN., *Sex-specific influence of aging on exercising leg blood flow.* Journal of Applied Physiology, 1985. **104**(3): p. 655-664.

170. Kylintireas I, S.C., Le JMS, Cunningon C, Lindsay A, Francis J, Robson MD, Neubauer S, Channon KM, Choudhury R, *Multimodal cardiovascular magnetic resonance quantifies regional variation in vascular structure and function in patients with coronary artery disease: Relationships with coronary disease severity.* Journal of Cardiovascular Magnetic Resonance, 2011. **13**(61).
171. H. Astrand, J.S., J. Karlsson, M. Karlsson, B. Sonesson, T. Lanne, *In vivo estimation of the contribution of elastin and collagen to the mechanical properties in the human abdominal aorta: effect of age and sex.* 2011.
172. Reeps C, M.A., Pellsek J, Harti F, Grabhar-Meier V, Wall WA, Essler M, Eckstein HH, Gee MW, *Measuring and modeling patient-specific distributions of material properties in abdominal aortic aneurysm wall.* Biomechanical Modeling in Mechanobiology, 2013. **12**: p. 717-733.
173. Hellenthal FAMVI, B.W., Hodzig WKWH, Schurink GWH, *Biomarkers of AAA progression. Part 1: extracellular matrix degeneration.* Nature Review Cardiology, 2009. **6**: p. 464-474.
174. Humphrey JD, H.G., *Mechanics, mechanobiology, and modeling of human abdominal aorta and aneurysms.* Journal of Biomechanics, 2012. **45**: p. 805-814.
175. He CM, R.M., *The composition and mechanical properties of abdominal aortic aneurysms.* Journal of Vascular Surgery, 1994. **20**(1): p. 6-13.
176. Abdul-Hussein H, S.R., Weber E, von der Thusen JH, Kleemann R, Mulder A, van Bockel JH, Hanemaaijer R, Lindeman JHN, *Collagen Degradation in the Abdominal Aneurysm.* The American Journal of Pathology, 2007. **170**(3): p. 809-817.
177. Jensen-Urstad K, J.J., *Gender difference in age-related changes in vascular function.* Journal of Internal Medicine, 2001. **250**(1): p. 5.
178. Aletras AH, D.S., Balaban RS, Wen H, *DENSE: Displacement Encoding with Stimulated Echoes in Cardiac Functional MRI.* Journal of Magnetic Resonance 1999. **137**: p. 247-252.
179. JD, H., *Cardiovascular Solid Mechanics: Cells, Tissues, and Organs*. 2002, New York, NY: Springer.
180. Goergen CJ, J.B., Greve JM, Taylor CA, Zarins CK., *Increased anterior abdominal aortic wall motion: possible role in aneurysm pathogenesis and design of endovascular devices.* Journal of Endovascular Therapy, 2007. **14**(4): p. 574-584.
181. Wedding KL, D.M., Herfkens RJ, Zarins CK, Taylor CA, Pelc NJ, *Measurement of vessel wall strain using cine phase contrast MRI.* Journal of Magnetic Resonance Imaging, 2002. **15**(4): p. 418-428.
182. Draney MT, H.R., Hughes TJ, Pelc NJ, Wedding KL, Zarins CK, Taylor CA., *Quantification of vessel wall cyclic strain using cine phase contrast magnetic resonance imaging.* Annals of Biomedical Engineering, 2002. **30**(8): p. 1033-1045.
183. Hurks R, P.G., Vink A, Hoefer IE, Bots ML, van de Pavoordt H, de Vries JP, Moll FL, *Circumferential heterogeneity in the abdominal aortic aneurysm wall composition suggests lateral sides to be more rupture prone.* Journal of Vascular Surgery, 2012. **55**(1): p. 203-209.

184. Assar AN, Z.C., *Ruptured abdominal aortic aneurysm: a surgical emergency with many clinical presentations.* Postgraduate Medical Journal, 2009. **85**: p. 268-273.
185. Nethononda RM, L.A., Stewart R, Kylinterias I, Whitworth P, Francis J, Leeson P, Watkins H, Neubauer S, Rider OJ, *Gender specific patterns of age-related decline in aortic stiffness: a cardiovascular magnetic resonance study including normal ranges.* Journal of Cardiovascular Magnetic Resonance, 2015.
186. Simsek FG, K.Y., *Investigation of material modeling in fluid-structure interaction analysis of an idealized three-layered abdominal aorta: aneurysm initiation and fully developed aneurysms.* Journal of Biological Physics, 2015. **41**(2): p. 173-201.
187. Cheng CP, P.D., Taylor CA, *Quantification of Wall Shear Stress in Large Bloof Vessels Using Langrangian Interpolation Functions with Cine Phase-Contrast Magnetic Resonance Imaging.* Annals of Biomedical Engineering, 2002. **30**: p. 12.
188. Hay O, D.G., Abbas J, Stein D, May G, Masharawi T, et al, *The Lumbar Lordosis in Males and Females, Revisited.* PLoS One, 2015. **10**(8).
189. Gitsioudis G, C.Y., Wolf P, Missiou A, Antoniadis AP, Mitsouras D, Bartling S, Arica Z, Stuber M, Rybicki FJ, Nunninger M, Erbel C, Libby P, Giannoglou GD, Katus HA, Korosoglou, *Combined non-invasive assessment of endothelial shear stress and molecular imaging of inflammation for the prediction of inflamed plaque in hyperlipidaemic rabbit aortas.* European Heart Journal - Cardiovascular Imaging, 2015.
190. Brown PM, Z.D., Sobolev B., *The risk of rupture in untreated aneurysms: the impact of size, gender, and expansion rate.* Journal of Vascular Surgery, 2003. **37**: p. 280-284.
191. VM, M., *Sex-based differences in vascular function.* Women's Health, 2010. **6**(5): p. 737-752.
192. Staessen JA, v.d.H.-S.J., Safar ME, Den Hond E, Gasowski J, Fadard RH, Wang JG, Struijker Boudier HA, Van Bortel LM, *Menopause and the characteristics of the large arteries in a population study.* Journal of Juman Hypertension, 2001. **15**: p. 511-518.
193. Luzi G, C.G., Cosmi EV, Di Renzo GC, *Doppler studies of uterine arteries in spontaneous and artificially induced menopausal women.* Ultrasound Obstetrics and Gynecology, 1993. **3**: p. 354-356.